Department of Electrical and Computer Engineering

Improving Small Signal Stability of Power Systems in the Presence of Harmonics

Marjan Ladjavardi

This thesis is presented for the Degree of
Doctor of Philosophy
of
Curtin University of Technology

July 2008

Declaration

To the best of my knowledge and belief this thesis contains no material previously published by any other person except where due acknowledgment has been made.

This thesis contains no material which has been accepted for the award of any other degree or diploma in any university.

Signature: …….

Date: ……...

ABSTRACT

This thesis investigates the impact of harmonics as a power quality issue on the dynamic behaviour of the power systems. The effectiveness of the power system stabilizers in distorted conditions is also investigated. This thesis consists of three parts as follows:

The first part focuses on the operation of the power system under distorted conditions. The conventional model of a synchronous generator in the *dq*-frame of reference is modified to include the impact of time and space harmonics. To do this, the synchronous generator is first modelled in the harmonic domain. This model helps in calculating the additional parts of the generator fundamental components due to the harmonics. Then the Park transformation is used for calculating the modified fundamental components of the synchronous generator in *dq* axes. The modified generator rotor angle due to the presence of harmonics is calculated and the impact of damper windings under the influence of harmonics is investigated. This model is used to study the small-signal stability of a distorted Single Machine Infinite Bus (SMIB) system. The eigenvalue analysis method is employed and the system state space equations are calculated by linearizing the differential equations around the operating point using an analytical method. The simulation results are presented for a distorted SMIB system under the influence of different harmonic levels. The impact of damper windings and also harmonics phase angles are also investigated.

In the second part of the thesis, the effectiveness of the power system damping controllers under distorted conditions is studied. This investigation is done based on a distorted SMIB system installed with a Static Synchronous Series Compensator (SSSC). In the first step, the system state space equations are derived. A Power Oscillation Damping (POD) controller with a conventional structure is installed on the SSSC to improve the system dynamic behaviour. A genetic-fuzzy algorithm is proposed for tuning the POD parameters. This method along with the observability matrix is employed to design a POD controller under sinusoidal and distorted

conditions. The impact of harmonics on the effectiveness of the POD controller under distorted conditions is investigated.

In the last part, the steady state and dynamic operation of an actual distributed generation system under sinusoidal and distorted conditions are studied. A decoupled harmonic power flow program is employed for steady state analysis. The nonlinear loads are modelled as decoupled harmonic current sources and the nonlinear model of synchronous generator in harmonic domain is used to calculate the injected current harmonics. For the system dynamic stability study, the power system toolbox with the modified model of the synchronous generator is used. The system eigenvalues are calculated and the effectiveness of the installed Power System Stabilisers (PSS) is investigated under sinusoidal and distorted conditions. Simulation results show that in order to guarantee the effectiveness of a PSS in distorted conditions, it is necessary to consider the harmonics in tuning its parameters.

ACKNOWLEDGMENTS

First of all I would like to acknowledge my supervisor, Associate Professor Mohammad Ali Sherkat Masoum, who was abundantly helpful and offered invaluable assistance, support and guidance throughout the period of my study. I also like to thank my co-supervisor, Professor Syed Islam, who always provides support to the whole department of Electrical and Computer Engineering.

I appreciate my International Postgraduate Research Scholarship supported by the Australian Government and Postgraduate Scholarship by Curtin University of Technology which gave me the opportunity to complete the PhD course.

I also wish to express my love and gratitude to my beloved family for their understanding and endless love.

TABLE OF CONTENTS

LIST OF FIGURES

LIST OF TABLES

NOMENCLATURE

ψ_r	Rotor fluxes matrix
ψ_s	Stator fluxes matrix
L	Inductances matrix
R	Rotor windings resistance matrix
i_r	Rotor windings current vector
i_s	Stator windings current vector
v_r	Rotor windings voltage vector
v_s	Stator windings voltage vector.
K_D	Damping factor
H	Inertia constant
ω_r	Rotor speed
T_m	Mechanical torque
δ	Rotor angle
ψ_{Fd}	Field flux
ψ_d	Stator flux component along the d-axis
ψ_q	Stator flux component along the q-axis
$\psi_d^{due\,to\,harm}$	Stator flux component due to interaction between time and space harmonics along d-axis
$\psi_q^{due\,to\,harm}$	Stator flux component due to interaction between time and space harmonics along q-axis

CHAPTER ONE

INTRODUCTION

The power quality and system stability are two important issues of modern power systems.

Stability of the power system has been recognized as an important problem for secure system operation since the 1920s. It has been classified into different categories regarding the duration and type of disturbances. The small-signal (dynamic) behaviour of a power system is one of the important stability categories and is related to the synchronous generator rotor oscillations.

On the other hand, actual power systems contain different types of nonlinear loads that generate harmonic pollution. Examples of these nonlinear loads are power electronic based devices, motor drives, saturated transformers, electrical machines, Flexible AC Transmission System (FACTS) devices and other appliances with nonlinear voltage-current characteristics. It causes concerns with respect to the impact of harmonics and poor power quality on the performance and stability of power systems and synchronous generators (SG). Distributed Generation (DG) and isolated systems in particular are at higher risks due to their typical low inertia features; short-circuit levels, frequency/voltage variations and unbalances. It is shown in literatures that the harmonic distortion level of DG systems in the presence of nonlinear loads can be much higher than the standard and recommended levels. Hence, the operation of the SGs in distorted conditions might be affected by the high level of voltage harmonic distortions at the connected buses.

Therefore, the impact of power quality on performance of the synchronous generators and stability of the power system especially in isolated and DG systems is a new arisen issue and has attracted more attention in the recent years.

The first part of this thesis investigates the impact of harmonics on the steady-state and dynamic behaviour of a synchronous generator connected to a large system.

For this purpose, the initial step is modelling the synchronous generator under distorted conditions. To consider the time and space harmonics, a nonlinear model of the synchronous generator in the Harmonic Domain (HD) is used. Using this model the impact of harmonics on the fundamental parameters of the generator is investigated and used to modify the conventional model in the *dq*-frame of reference.

This modified model is then employed to study the system small-signal stability using eigenvalue analysis under distorted conditions. The formulation of the state equations for small-signal analysis involves the development of linearized equations about an operating point and elimination of all variables other than the state variables. The presence of harmonics makes the analytical methods used for calculation of the state space equations very complex. Therefore, the study is done on a distorted Single Machine Infinite Bus (SMIB) system. This method can be extended to study a large multi-machine system.

As the application of power oscillation damping (POD) controllers is a common approach for improving the system dynamic stability, the impact of harmonics on the effectiveness of a POD controller is investigated in the second part of the thesis. A POD controller based on a Static Synchronous Series Compensator (SSSC) is selected for the investigation.

Flexible AC Transmission Systems (FACTS) are widely used for increasing the utilization of the power systems and applying an axillary controller on these devices can improve the dynamic behaviour of the power system. The SSSCs are one of the most widely used types of series-connected FACTS devices. To investigate the performance of the POD controller, the state space equations of a distorted SMIB system installed with an SSSC are calculated. Various optimization methods have been proposed for tuning the parameters of the POD controller. In this thesis, a genetic-fuzzy method is proposed and used for tuning the SSSC based POD controller under sinusoidal and distorted conditions. The effectiveness of the POD controller designed for sinusoidal conditions is tested under the influence of harmonics. This part concludes with designing a POD controller which remains

effective under both sinusoidal and distorted conditions. This method is applicable for tuning other types of power system stabilizers.

In the last part of the thesis, the steady state and dynamic behaviour of an actual distributed generation system is investigated. This investigation is done under sinusoidal and distorted conditions. A Decoupled Harmonic Power Flow (DHPF) algorithm is used for the steady state studies. The nonlinear loads are modelled as decoupled harmonic current sources and the nonlinear model of the synchronous generators in the harmonic domain is employed to calculate the injected current harmonics by the generators.

As the analytical calculations of the state space equations for a multi-machine system is very complex under the distorted conditions, a power system toolbox is used for the system dynamic study. The model of a synchronous generator is modified to include the impact of time and space harmonics. The system eigenvalues are calculated and used for the stability studies.

To improve the system dynamic behaviour, Power Systems Stabilizers (PSS) are connected in the excitation system of the distributed generators. The conventional phase compensation method is used for tuning these PSSs. The performance of these PSSs under distorted conditions is studied and their gains are adjusted to remain effective under the distorted conditions.

In conclusion, this work presents the impact of harmonics on the synchronous generator steady-state operation, small-signal stability of the system, relocation of the system eigenvalues and optimum POD controller design for improving the system dynamic behaviour.

1.1. Research Objectives

The main objectives of this research can be summarised as follows:

- Finding a proper model of synchronous generators for system small-signal stability studies under distorted conditions.
- Investigating the synchronous generators steady-state operation considering the impact of time and space harmonics.

- Investigating the impact of harmonics and damper windings on the dynamic behaviour of a distorted SMIB system.
- Investigating the impact of harmonics on the performance of a FACTS device based POD controller installed on a SMIB system.
- Finding a proper method for tuning the POD parameters under the influence of harmonics.
- Studying the dynamic behaviour of an actual distributed generation system in sinusoidal and distorted conditions and the effectiveness of the connected power system stabilizers.

1.2. Thesis Structure

This thesis includes seven chapters. Chapter two presents an introduction on power quality and power system stability issues. This chapter also introduces some literatures on nonlinear models of synchronous generators and the usage of FACTS devices for improving the system dynamic stability. A proper model of a synchronous generator for small-signal stability studies considering the presence of time and space harmonics is presented in Chapter three. Chapter four includes the small-signal study of a distorted SMIB system. The eigenvalue analysis method is used and the system state space equations are calculated using an analytical method from the system differential equations. The impact of damper windings is also investigated. The effectiveness of an SSSC based POD controller under distorted conditions is investigated in Chapter five. In the first part of this chapter the state space equations of a distorted SMIB system installed with an SSSC are calculated. In the second part, a POD is installed on the SSSC to improve the system dynamic stability and a genetic-fuzzy method is proposed and used for tuning its parameters. Chapter six presents the impact of harmonics on the operation of an actual distributed generation system under sinusoidal and distorted conditions. Finally, Chapter seven summarises the conclusions of the impact of harmonics on the power systems and their operation.

CHAPTER TWO
LITERATURE REVIEW AND BACKGROUND

2.1. Introduction

This chapter presents an introduction on subject related to this work including the system stability and power quality issues, usage of FACTS devices, design of auxiliary POD controllers and nonlinear models of synchronous generators.

Different classifications of power quality and power system stability are introduced and it is shown that different type of FACTS devices with axillary POD controllers are proposed for improving the system dynamic behaviour.

Finding a proper model of the synchronous generator including the impact of space harmonics is essential for this work. The modelling of a synchronous generator, as one of the most essential parts of the power systems, has attracted the attention of many researchers. Some nonlinear models of synchronous generators are introduced in this chapter.

2.2. Power System Stability

For practical analysis and resolution of power system instability, it is essential to have proper classification of stability problems. Figure 2.1 gives the overall picture of power system stability problem and identifies its categories and subcategories [1].

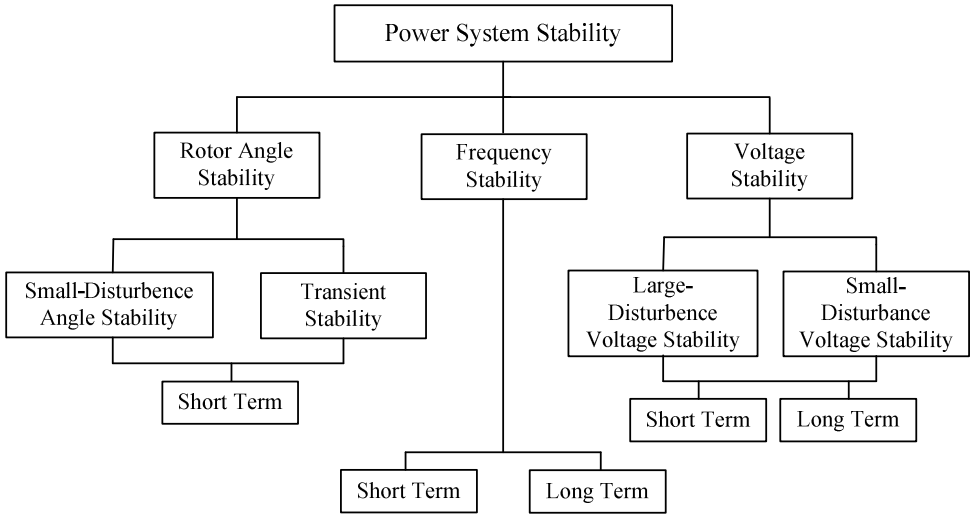

Figure 2.1 Classification of power system stability [1]

The description of the corresponding forms of stability phenomena are as follows:

a- Rotor Angle Stability:

Rotor angle stability refers to the ability of synchronous machines of an interconnected power system to remain in synchronism after being subjected to a disturbance. It depends on the ability to maintain equilibrium between electromagnetic torque and mechanical torque of each synchronous machine in the system. The change in electromagnetic torque of a synchronous machine following perturbation can be resolved into two components: synchronizing torque (in phase with rotor angle deviation) and damping torque (in phase with the speed deviation). Instability may occur in the form of increasing angular swings of some generators leading to their loss of synchronism with other generators. System stability depends on the existence of both components of torque for each of the synchronous machines. Rotor angle stability can be characterized into two subcategories:

- Small-disturbance or small-signal rotor angle stability is defined as the ability of the power system to remain stable in the presence of small disturbances. These disturbances could be minor variations in load or generation on the system which results in low power frequency oscillations in the system. The disturbances are considered to be sufficiently small that linearization of system equations is

permissible for analysis purposes [2]. The term *dynamic stability* is also used in literature for this class of rotor angle stability.

Three types of oscillations that have been experienced with large interconnected generators and transmission networks include [3]:

Inter-unit oscillations: These oscillations involve two or more synchronous machines at a power plant or nearby power plants. The machines swing against each other, with the frequency of the power oscillation ranging between 1.5Hz to 3Hz.

Local mode oscillations: These oscillations involve one or more synchronous machines on a power station swinging together against a comparatively large power system or load centre. The frequency of oscillation is in the range if 0.7Hz to 2Hz.
Inter-area oscillations: These oscillations usually involve combinations of many machines on one part of a power system swinging against machines on another part of the power system. Inter-area oscillations are normally in the frequency range of less than 0.5Hz.

- Large-disturbance rotor angle stability or transient stability is concerned with the ability of the power system to maintain synchronism when subject to a sever disturbance, such as a short circuit on a transmission line. The system response involves large excursion of generator rotor angles and is influenced by the nonlinear power-angle relationship.

b- Frequency Stability:

Frequency stability refers to the ability of a power system to maintain steady frequency following a severe system upset resulting in a significant imbalance between generation and load. Instability may occur in the form of sustained frequency swings leading to tripping of generating units and/or loads.

c- Voltage Stability:

Voltage stability refers to the ability of a power system to maintain steady voltages at all buses in the system after being subjected to a disturbance from a given initial condition. Instability may occur in the form of a progressive fall or rise of voltage of some buses. It might lead to loss of load in an area or tripping off transmission lines or other elements by their protective systems.

This PhD thesis focuses on small-signal stability of the power systems in the presence of time and space harmonics. Hence, the following section presents more details on this category.

2.2.1. Small-Signal Stability Analysis of a Power System

The small-signal stability of a nonlinear system can be investigated using Lyapunov's first method [4]. In this method which is also known as eigenvalue analysis, the system stability is given by roots of the characteristic equation of the system of first approximation, for example eigenvalues of the state matrix A [2].

It should be noticed that matrix A is the Jacobian matrix whose elements a_{ij} are given by the partial derivatives $\frac{\partial f_i}{\partial x_j}$ evaluated at the equilibrium point about which the small disturbance is being analysed. This matrix is referred to as state matrix. By calculating eigenvalues of this matrix, A, the stability of the system is determined. A real eigenvalue corresponds to a non-oscillatory mode. A negative real eigenvalue represents a decaying mode. A positive real eigenvalue represents aperiodic instability. Complex eigenvalues occur in conjugate pairs and each pair corresponds to an oscillatory mode. In summary:

- When all of the system eigenvalues have negative real parts, the system is asymptotically stable.
- Having at least one eigenvalue with positive real part means the system is unstable.
- If the eigenvalues have real parts equal to zero, it is not possible to say anything based on the first approximation.

The eigenvalue analysis method has been widely used to study the small-disturbance rotor angle stability of power systems. This method does not require the explicit solution of system differential equations. However, the large-disturbance stability may be studied by explicit solution of the nonlinear differential equations or the direct method of Lyapunov (Lyapunov's second method) [4].

The traditional approach to damp the system oscillation is through the installation of PSS devices that provides supplementary control action through the excitation system of generators. The conventional PSS uses phase compensation to adjust the timing of its correction signal to oppose the oscillations it detects in the generator rotor. This conventional PSS [3, 5] is widely used in single machine systems by power system utilities.

Recently, several approaches based on modern control theory have been applied to PSS design problem. These include optimal, adaptive, variable structure, intelligent control [6-8], simulated annealing [9] and sensitivity analysis [10]. These methods are more effective for damping the critical modes of multi machine systems.

Another approach for improving the system small-signal stability is through adding an auxiliary POD controller to the installed FACTS devices on the system.

Next section focuses on the utilization of FACTS devices in power systems and design of the POD controllers for improving their stability.

2.3. FACTS Devices

In recent years, the implementation of FACTS devices has become a common practice to make full utilization of the existing transmission capacities instead of adding new lines which are often restricted for economic and environmental reasons [11].

In addition to enhancing the available transfer capacity (ATC) of the transmission system, applying FACTS devices may affect the system stability [12, 13]. For example, the small-signal stability analysis in reference [12] reveals that some system modes may be significantly affected by Static Var Compensators.

Furthermore, a supplementary control is being added to the FACTS device to damp out the rotor angle oscillations and have been widely used for improving the dynamic stability of the power systems [12-23].

As the number of swing modes in a system is usually larger than the number of available control devices, designing new control structures which can improve the damping of multiple swing modes is of high concern. There are a number of

proposed control methods including: fuzzy-logic [18], robust control [19], fuzzy sliding mode [20] and genetic algorithm [22]. A multivariable control design methodology for robust damping of power oscillations is proposed in [24]. This method employs the local as well as the remote stabilizing signals.

Numerous papers have been published to discuss and find ways to answer the question of which location and feedback signal could result in the power system stabilizer (PSS) and the FACTS devices having the maximum effect on the system [14, 25]. Usually selection of the most suitable location and stabilizing signal is based on controllability and observability indexes [25].

Reference [15] presents a detailed study on the use of a SVC for damping system oscillations. Having considered several factors including observability and controllability, it was concluded that the most suitable auxiliary input signal for the SVC for damping improvement is the locally measured transmission line current magnitude. Other studies, however, select locally measured active power [16], or generator angular speed [17] as a stabilizing signal.

In this thesis, a series FACTS device is connected on a distorted SMIB system and a genetic-fuzzy auxiliary controller is designed to shift the system eigenvalues toward the permissible region of the *s*-plane. The POD control signal is selected based on the controllability method.

2.4. Power Quality

Power quality is an important aspect of power system that affects the system efficiency, stability, security and reliability. This is a very broad subject and covers different aspects of power engineering from transmission and distribution level to customers' problems. Investigating the impact of power quality disturbances on the power system operation, the equipments and also the methods of power quality improvement has attracted the attention of many researchers. This subject has become an important part of power systems and electric machines and a number of books have been published in this area [26-29].

The causes of power quality problems can be put into two categories [30]:

- Disturbances arising in power system due to faults and the operation of power system equipments such as capacitor switching, transformer saturation, Power electronic based devices.
- Disturbances induced by the operation of customer equipment and nonlinear loads such as phase controlled power supplies and switching power supplies.

There are different classifications of power quality issues [26, 27, 30]. Based on IEEE-1159 [30], categories of electromagnetic phenomena are: transients, short-duration voltage variations, long-duration voltage variations, voltage imbalance, waveform distortion, voltage fluctuation and power-frequency variations.

Presence of current/voltage harmonics in the power system is one of the most common power quality disturbances. Nonlinear current and voltage waveforms occur in power systems due to equipments and loads with nonlinear characteristics such as transformers, rotating electrical machines, FACTS devices, power electronics components (such as rectifiers, triacs, thyristors), switch-mode power supplies, compact florescent lamps, adjustable AC and DC derives, renewable energy sources and HVDC networks.

According to the frequencies of disturbances, harmonics are divided into different groups [29]:

- Triple harmonics: are the odd multiples of the third harmonic
- Sub-harmonics: have frequencies below the fundamental frequency.
- Inter-harmonics: their frequencies are not integer multiplies of fundamental frequency.
- Characteristics and uncharacteristic harmonics: harmonics of order 12k+1 (positive sequence) are called characteristic harmonics and orders 12k-1 (negative sequence) are called uncharacteristic harmonics.
- Positive-, negative- and zero-sequence harmonics: the phasors of harmonics with negative and positive displacement angles rotate clockwise (positive sequence) and counter-clockwise (negative sequence), respectively. Phasors with zero displacement angles are in phase and are called zero-sequence harmonics.

- Time and spatial (space) harmonics: time harmonics are the harmonics in the voltage and current waveforms of electric machines and power systems due to magnetic core saturation, presence of nonlinear loads, and irregular system conditions such as faults and imbalance. Spatial harmonics are referred to the harmonics in the flux linkage of rotating electromagnetic devices such as induction and synchronous machines. The main cause of spatial harmonics is the unsymmetrical physical structure of stator and/or rotor magnetic circuits.

The literatures are rich in investigation of the current/voltage time harmonics in the power system and their influence on the operation of the power system and system equipments [28, 29]. Some effects of harmonics including interfering with control devices, telephone interferences, additional line losses and decreased lifetime and increased losses in utility equipment and customer devices are well investigated.

Reference [29] presents the nonlinear models of transformers, induction machines and synchronous machines. Also the impact of harmonics on power system operation including nonlinear modelling of power system, interaction of harmonics with capacitors, impact of poor power quality on reliability, relaying and security are investigated in this book.

Installation of distributed generation systems within low voltage and medium voltage systems have introduced a number of power quality problems such as voltage variations and fluctuations, harmonics and inter-harmonics distortions and voltage stabilization [31, 32]. Reference [31] calculates the level of voltage harmonic distortion in a distributed generation system operating in grid-connected and stand-alone modes. It is shown that the harmonic distortion in the presence of nonlinear loads can be much higher than the standard and recommended levels. Reference [32] investigates the influence of distributed generation on voltage quality of a medium voltage network and presents the results of a case study showing high level of voltage harmonics.

The impact of power quality disturbances on the system stability is a fairly new subject and has attracted academic and utility attentions. The impact of power quality on dynamic stability of an isolated system is investigated in recent years [33, 34]. In these papers the impact of harmonics on a synchronous generator damping and

synchronizing coefficients is studied. However, the impact of frequency conversion is not considered and the system eigenvalues are not calculated.

In this thesis, the impact of harmonics on the small-signal stability, relocation of the system eigenvalues and optimum controller design for improving the system dynamic behaviour are investigated. To study the system stability, an accurate model of the synchronous generator is essential which is targeted in the next section.

2.5. Non-linear Models of a Synchronous Generator

A synchronous Generator is an essential component of a power system which works in synchronism with the rest of the electrical network. The accurate modelling of SG is needed to analyse its behaviour under different operating conditions such as steady-state, transient, sub-transient, imbalance and under influence of harmonics.

The problem of modelling and analysis of the synchronous generator was primarily investigated in the 1920s and 1930s [35-38], and many classical models were proposed and implemented. With the introduction of distributed generation and renewable energy systems, this subject has drawn more attention and devoted more research in recent years.

The most widely used model of a synchronous generator is based on the two reaction theory proposed by Blondel [35] and extended by Doherty *et. al* [36] and Park [37, 38]. Details of the synchronous generator sinusoidal model in *dq*-frame of reference are expressed in [2]. Defining the transient and sub-transient inductances, this model has been widely used for stability studies of the power system. This conventional model assumes balance operating conditions at the machine terminals and is efficient for steady state solution. It can not be used to model the frequency coupling caused by rotor saliency in the presence of current distortion.

Several nonlinear models of synchronous machine have been developed in frequency domain [39, 40]. A well-known harmonic model of a synchronous generator based on the negative, positive and zero-sequence reactance is presented in [39]. This model is applicable in harmonic power flow analysis. However it does not include the factor of frequency conversion and is inappropriate for harmonic modelling of a

synchronous generator when detailed information such as harmonic torque must be extracted.

Synchronous machine harmonic model based on transient inductances is represented in [41]. In this paper, three cases are considered when SG is fed by: harmonic currents, harmonic voltages and combination of current and voltage harmonics. The proposed harmonic model is based on the *dq*-frame of reference. It is shown that when a synchronous machine is subjected to a harmonic voltage disturbance at frequency $n\omega$, harmonic current components are drawn at $n\omega$ and the associated frequency $(n \pm 2)\omega$. Machine harmonic behaviour is also affected by non-sinusoidal inductance variation with rotor position which is not considered in this paper. Moreover, this paper does not investigate the effect of harmonics on shaft torques.

Several machine models have been proposed for power system harmonic studies [42, 43]. Some of them are too simple and can not deal with the higher harmonics derived by synchronous machines themselves [42], or too complicated [43].

A more sophisticated Park-equation based synchronous machine model used in harmonic power flow study has been proposed in [44]. From the physical interpretation of this model, it is noticed that only if the power network is asymmetrical, synchronous generator should be considered as harmonic sources in power flow study. This model of SG can correctly originate the higher harmonics that are derived by the machine itself and is incorporated with the extended "decoupling-compensation" network model used for harmonic power flow studies. However, this steady-state decoupled harmonic model of synchronous generator does not include the impact of space harmonics.

The explicit time-varying nature of the stator self inductances and the mutual stator-rotor inductances, as well as the space harmonics can be represented in a machine model in the *abc*-frame of reference. This model can naturally reproduce the abnormal conditions since it is based on realistic representation of the machine parameters. The *αβo*-coordinates are used to allow a natural transition between the *abc*- and *dq*-frames [45]. Reference [46] discusses the advantages of a synchronous generator representation in the *abc* domain with respect to the models based on the *dq* and $\alpha\beta 0$ coordinates.

Detailed models of the synchronous machine have also been developed for harmonic analysis [40, 41, 47-49]. Reference [47] has employed the *abc*-coordinates for the dynamic analysis of a synchronous generator connected to a static converter for high-voltage DC.

A frequency domain model including imbalance and saturation effects is introduced in [49]. This model incorporates the frequency conversion and saturation effects under various machine load-flow constraints such as unbalanced operation. To model these effects, a three-phase Norton equivalent circuit of the machine is developed in the *abc*-frame of reference. To incorporate this model into harmonic programs, some reasonable simplifications are made and a *dq0* transformation is used to transfer machine quantities from the *abc*-coordinates into the rotating *dq*-coordinates.

The harmonic domain is a general frame of reference for power system analysis under steady-state conditions that models the coupling between phases and also between harmonics [50, 51]. The harmonic domain has been widely used to represent nonlinear elements of the power system. A synchronous machine in the *abc*-frame represents a linear time periodic system, which can be renovated to a linear time invariant system in the harmonic domain. An appropriate model of a synchronous generator in the harmonic domain and *abc*-frame of reference is proposed and used in [29, 40, 48].

An accurate calculation of the synchronous generator inductances as a function of time is essential for its nonlinear modelling. Having the profile of the machine winding inductances versus the rotor position, the machine performance characteristics can be easily calculated. These include emf and terminal voltages, currents, flux linkages, developed torques, losses of electric or magnetic origins, input and output powers, and efficiency [52].

The inductances can be estimated by calculating flux linkages or they can be determined using the magnetic energy, or co-energy, approach. Escarela-Perez *et. al* [53] have presented the comparison between these two methods for inductance calculation of a 150MVA, 13.8kV synchronous generator. Both definitions lead to equal inductance values for linear systems, but different results are reported for non-

linear conditions. The reason is that co-energy can be accurately calculated by using the actual BH curves of the magnetic materials, while the determination of magnetic flux is generally based on a linearized BH characteristics.

Different numerical computations of electromagnetic fields in electric machinery have been introduced in the past decades. These methods include two-dimensional (2D) and three dimensional (3D) field solution techniques which are based on finite-difference (FD), finite-element (FE), and boundary-element (BE) formulations, as well as other numerical methods.

Demerdash *et. al* have shown the application of energy/current (E/C) perturbation method for computation of machine winding inductances in a couple of publications [54-59]. Application of the method to a 2D magnetic field FE algorithm is presented for different types of electrical machines such as a 1.2 hp induction motor [54], a 733 MVA turbogenerator [57] and several 60 kVA to 75 kVA salient-pole synchronous generators [58]. The energy/current (E/C) perturbation method is also applied to large-scale magnitude of the 3D magnetic field FE algorithm [55], magnetic vector potential (MVP) and magnetic scalar potential (MSP) formulations [56, 59].

Winding function methods have been also used for modelling, simulation and analysis of electrical machines [60]. One of the advantages of these methods is that it is possible to predict transient and steady-state performance of any machine with any type of winding distribution and air-gap length, while taking into account the effect of all spatial and time harmonics. This means that all faults occurring in the stator windings, rotor turns and air-gap eccentricity can be included in the model obtained using this theory.

In this thesis, a synchronous generator model in the harmonic domain and *abc*-frame of reference is used for the investigations.

2.6. Conclusions

It was shown in this chapter that the system stability and power quality can affect different aspects of power system studies. Some standard categories and classifications were presented for the power quality and stability of the systems.

The harmonic distortion is one of the power quality issues that affect the operation of power system and system equipments. The literature is rich in the study of the impact of harmonics on the operation of power system equipments.

A synchronous generator is one of the essential system components that should be modelled accurately for system stability studies. Different models of a synchronous generator in the *abc*-frame of reference, *dq*-frame of reference, time or harmonic domain are proposed in literatures.

The small-signal stability of a power system was introduced as a category of the system stability. It was shown that the application of FACTS devices with an additional auxiliary controller can improve the power system dynamic behaviour.

Although there are some studies on the impact of power quality issues such as the influence of unbalanced voltages on the system stability, this area still needs more investigation and dedicated more research resources.

CHAPTER THREE

SYNCHRONOUS GENERATOR OPERATION UNDER NON-SINUSOIDAL CONDITIONS

3.1. Introduction

A Synchronous generator is a complicated electromagnetic device which is very important in the operation of power systems. Computing the steady-state operating parameters of a synchronous generator is essential for system studies including small-signal analysis of power systems.

Distorted operating conditions can affect the synchronous generator steady-state parameters. Non-sinusoidal conditions can be due to the presence of time and space harmonics. Time harmonics are the harmonics in the voltage and current waveforms of electric machines and power systems. These harmonics may be caused by nonlinear or unbalanced loading conditions due to the introduction of large variable speed drives, large industrial plant, saturated transformers, renewable energy sources, switching devices, FACTS controllers and other nonlinear loads. Space harmonics are the harmonics in the flux linkage of rotating electromagnetic devices such as induction and synchronous machines. The main cause of space harmonics is the unsymmetrical physical structure of the stator and rotor magnetic circuits.

This chapter focuses on calculation of the synchronous generator steady state parameters including the load angle, stator fluxes and voltages in the presence of harmonics. The approach is based on a nonlinear model of the synchronous generator in the harmonic domain and the *abc*-frame of reference. Space harmonics, pole-saliency and damper windings are included. Using this model, the produced stator fluxes are calculated and it is shown that there are additional harmonic components that can generate harmonic magnetic fields. These harmonic fields rotate at different speeds and directions with respect to the rotor. The interaction between time and space harmonics also adds additional terms to the fundamental component of the

stator flux. Considering these terms, the modified fundamental stator fluxes are calculated and the Park transformation is applied to them. Hence, the *dq* components of the stator flux are achieved and used for calculating the synchronous generator steady state operating point in the presence of time and space harmonics. The impact of damper windings and harmonic phase angles are investigated and a general formulation to compute the load angle is proposed. Simulation results are provided for three different operating conditions.

3.2. Synchronous Generator Parameters

The non-sinusoidal distribution of the stator windings, for example the step-like mmf distribution, may be presented by trigonometric series as a function of rotor angle θ for mutual inductances between stator and rotor and also between stator windings. These higher frequency terms present the space harmonic components. The Winding Function Approach (WFA), accounting for all space harmonics, [60] or finite element methods [58] can be used for the calculations of machine winding inductances.

Assuming the rotor speed (ω_r) to be equal to the system base frequency (ω_0), rotor angle is written as a function of time:

$$\theta = \omega_0 t + \theta_0 \tag{3-1}$$

where θ_0 is the initial rotor angle at time zero and can be determined for a constant load using the conventional power flow solutions [2].

Considering space harmonics, the synchronous generator inductances are defined as follows [48]:

(a) Stator Self and Mutual Inductances

Stator self inductances:

$$\begin{cases} L_{aa} = L_s + \sum_h L_m^{(h)} \cosh\theta \\ L_{bb} = L_s + \sum_h L_m^{(h)} \cosh(\theta - 2\pi/3) \\ L_{cc} = L_s + \sum_h L_m^{(h)} \cosh(\theta + 2\pi/3) \end{cases} \quad ; h = 2,4,..$$

$$\text{Stator mutual inductances:} \begin{cases} L_{ab} = L_{ba} = -M_s - \sum_h L_m^{(h)} \cosh(\theta + \pi/6) \\ L_{bc} = L_{cb} = -M_s - \sum_h L_m^{(h)} \cosh(\theta - \pi/2) \quad ; h = 2,4,... \\ L_{ca} = L_{ac} = -M_s - \sum_h L_m^{(h)} \cosh(\theta + 5\pi/6) \end{cases} \tag{3-2}$$

where L_{aa}, L_{bb} and L_{cc} are self inductances of the stator three-phase windings, with L_s and $L_m^{(h)}$ showing the constant term and the magnitude of the h^{th} space harmonic component, respectively. L_{ab}, L_{bc} and L_{ca} are the mutual inductances between the stator windings including the constant term of M_s and harmonic periodic terms with the magnitudes of $L_m^{(h)}$. Ignoring space harmonics, stator self and mutual inductances will only consist of constant terms and the second harmonic order. Figure 3.1 and Figure 3.2 show the stator self and mutual inductances with and without harmonic terms, respectively. Space harmonics are considered up to 10th order with magnitudes of 0.3, 0.2, 0.1 and 0.01 of the second harmonic order [61].

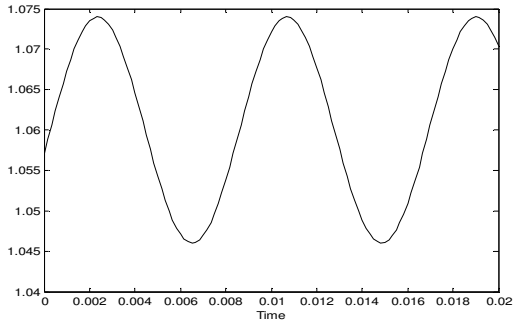

(a)

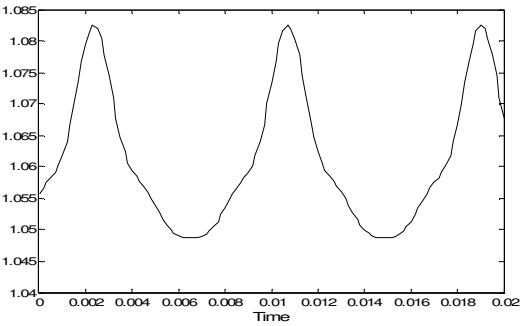

(b)

Figure 3.1. Stator self inductances; (a) sinusoidal conditions (b) in the presence of space harmonics

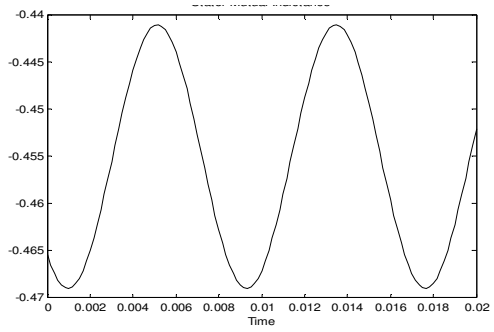

(a)

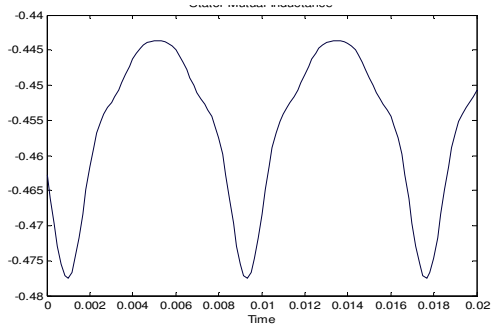

(b)

Figure 3.2. Stator mutual inductances; (a) sinusoidal condition (b) in the presence of space harmonics

b- Rotor Self and Mutual Inductances

Four windings are considered in the rotor circuit, including the field winding (L_F) and three damper windings; two on the *q*-axis (L_G, L_Q) and one on the *d*-axis (L_D). The corresponding rotor inductances are as follows [48]:

Rotor self inductances: $\{L_F, L_D, L_G, L_Q$

Rotor mutual inductances: $\begin{cases} L_{FD} = M_X,\ L_{GQ} = M_Y \\ L_{FG} = L_{FQ} = L_{DG} = L_{DQ} = 0 \end{cases}$ (3-3)

where M_X and M_Y are the mutual inductances along the *d* and *q* axes, respectively.

c- Stator-Rotor Mutual Inductances

Space harmonics influence the stator-rotor mutual inductances as follows [48]:

Mutual inductance between rotor windings and phase "a" of stator windings:

$$\begin{cases} L_{aF} = \sum_h M_F^{(h)} \cosh\theta \\ L_{aD} = \sum_h M_D^{(h)} \cosh\theta \\ L_{aG} = \sum_h M_G^{(h)} \sinh\theta \\ L_{aQ} = \sum_h M_Q^{(h)} \sinh\theta \end{cases} ; h = 1,3,..$$

Mutual inductance between rotor windings and phase "b" of stator windings:

$$\begin{cases} L_{bF} = \sum_h M_F^{(h)} \cosh(\theta - 2\pi/3) \\ L_{bD} = \sum_h M_D^{(h)} \cosh(\theta - 2\pi/3) \\ L_{bG} = \sum_h M_G^{(h)} \sinh(\theta - 2\pi/3) \\ L_{bQ} = \sum_h M_Q^{(h)} \sinh(\theta - 2\pi/3) \end{cases} ; h = 1,3,..$$

Mutual inductance between rotor windings and phase "c" of stator windings:

$$\begin{cases} L_{cF} = \sum_h M_F^{(h)} \cosh(\theta + 2\pi/3) \\ L_{cD} = \sum_h M_D^{(h)} \cosh(\theta + 2\pi/3) \\ L_{cG} = \sum_h M_G^{(h)} \sinh(\theta + 2\pi/3) \\ L_{cQ} = \sum_h M_Q^{(h)} \sinh(\theta + 2\pi/3) \end{cases} ; h = 1,3,..$$

(3-4)

Under sinusoidal conditions, stator-rotor mutual inductances will only contain the fundamental components. Figure 3.3 shows the stator-rotor mutual inductance (between phase "a" of stator windings and the field winding) with and without harmonics. Space harmonics are considered up to 9th order with magnitudes of 0.3, 0.2, 0.1 and 0.01 the fundamental component [61].

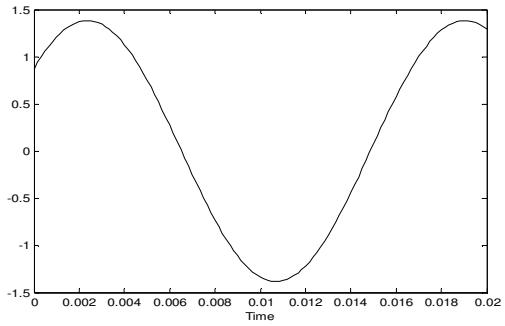

(a)

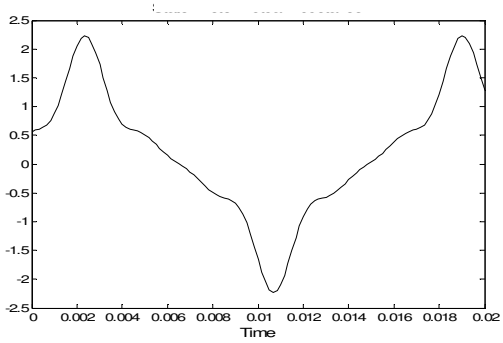

(b)

Figure 3.3. Stator-rotor mutual inductances; (a) sinusoidal condition (b) in the presence of space harmonics

3.3. Non-Linear Model of a Synchronous Generator

Based on the *abc*-frame of reference in the time domain, the main equations of a synchronous generator rotor and stator voltages and fluxes are as follows [2]:

$$\begin{cases} v_r = \dot{\psi}_r(t) + R_r i_r(t) \\ v_s(t) = \dot{\psi}_s(t) - R_s i_s(t) \\ \psi_r(t) = -L_{rs}(t) i_s(t) + L_{rr} i_r(t) \\ \psi_s(t) = -L_{ss}(t) i_s(t) + L_{sr}(t) i_r(t) \end{cases} \tag{3-5a}$$

where:

ψ_r =rotor fluxes matrix

ψ_s = stator fluxes matrix

L_{rr} = rotor-self inductances matrix

L_{ss} = stator-self inductances matrix

L_{rs} = rotor-stator mutual inductances matrix

L_{sr} = stator-rotor mutual inductances matrix

R_r = rotor windings resistance matrix

R_s = stator windings resistance matrix

i_r = rotor windings current vector

i_s = stator windings current vector

v_r = rotor windings voltage vector

v_s = stator windings voltage vector.

The generator inductance matrices are:

Stator inductance matrix: $$L_{ss} = \begin{bmatrix} L_{aa} & L_{ab} & L_{ac} \\ L_{ba} & L_{bb} & L_{bc} \\ L_{ca} & L_{cb} & L_{cc} \end{bmatrix} \quad \text{(3-5b)}$$

Stator windings resistance matrix: $$R_s = \begin{bmatrix} R_a & 0 & 0 \\ 0 & R_b & 0 \\ 0 & 0 & R_c \end{bmatrix} \quad \text{(3-5c)}$$

Rotor inductance matrix: $$L_{rr} = \begin{bmatrix} L_F & M_X & 0 & 0 \\ M_X & L_D & 0 & 0 \\ 0 & 0 & L_G & M_Y \\ 0 & 0 & M_Y & L_Q \end{bmatrix} \quad \text{(3-5d)}$$

Rotor windings resistance matrix: $$R_r = \begin{bmatrix} R_F & 0 & 0 & 0 \\ 0 & R_D & 0 & 0 \\ 0 & 0 & R_G & 0 \\ 0 & 0 & 0 & R_Q \end{bmatrix} \quad \text{(3-5e)}$$

Stator-rotor mutual inductance matrix: $$L_{sr} = \begin{bmatrix} L_{aF} & L_{aD} & L_{aG} & L_{aQ} \\ L_{bF} & L_{bD} & L_{bG} & L_{bQ} \\ L_{cF} & L_{cD} & L_{cG} & L_{cQ} \end{bmatrix} \quad \text{(3-5f)}$$

where:

Rotor-stator mutual inductance matrix: $L_{rs} = (L_{sr})^T$

Stator windings current vector: $i_s(t) = [i_a(t), i_b(t), i_c(t)]^T$

Stator windings voltage vector: $v_s = [v_a(t), v_b(t), v_c(t)]^T$

Rotor windings current vector: $i_r(t) = [i_F(t), i_D(t), i_G(t), i_Q(t)]^T$

Rotor windings voltage vector: $v_r = [v_F, v_D, v_G, v_Q]^T$, $v_F = v_F^{(DC)}$, $v_D = v_G = v_Q = 0$.

Note that currents and voltages of stator and rotor windings contain fundamental and harmonic components. The impacts of space harmonics and rotor saliency are included in the inductance matrices.

Equation 3-5(a) can be rewritten in the following form:

$$\begin{cases} \dot{\psi}_r(t) = \underbrace{(-R_r L_{rr}^{-1})}_{a}\psi_r(t) + \underbrace{[-R_r L_{rr}^{-1} L_{rs}(t) \;\; I]}_{b} u(t) \\ i_r(t) = L_{rr}^{-1}\psi_r(t) + (L_{rr}^{-1} L_{rs}(t))i_s(t) \\ \psi_s(t) = -L_{ss}(t)i_s(t) + L_{sr}(t)i_r(t) \\ v_s(t) = \dot{\psi}_s(t) - R_s i_s(t) \end{cases} \tag{3-6}$$

where, u(t) is the input vector:

$$u(t) = \begin{bmatrix} i_s(t) \\ v_{\mathrm{F}}^{(DC)} \end{bmatrix}, \; I = \begin{bmatrix} 1 \\ 0 \\ 0 \\ 0 \end{bmatrix}$$

Equation 3-6 shows that a synchronous machine can be treated as a linear time periodic (LTP) system. This model of a synchronous generator is useful for understanding effects of time and space harmonics on the nature of stator fluxes and voltages. However, it is difficult to determine the induced stator and rotor harmonic fluxes and their impacts on electromagnetic torque and the steady-state operation of the synchronous generator. Calculation of steady-state parameters will be easier and more convenient if the synchronous generator model is transferred into the harmonic domain.

3.3.1. Synchronous Generator Model in the Harmonic Domain

The main advantage of using the harmonic domain for analysis is that a linear time variant system with time periodic coefficient matrices will be transformed to a linear time invariant system with constant Toeplitz-type matrices [50, 51].

In the harmonic domain, the time periodic variable, *x(t)*, is approximated by the Fourier series in the interval under consideration and can be written as:

$$\begin{aligned} &x(t) = G(t)\,X \\ &G(t) = [e^{-jh\omega_0 t},\ldots,e^{-j\omega_0 t},1,e^{j\omega_0 t},\ldots,e^{jh\omega_0 t}] \\ &X = [X_{-h}(t),\ldots,X_{-1}(t),X_0(t),X_1(t),X_h(t)]^T \end{aligned} \tag{3-7}$$

where X_k is the Fourier coefficient of variable *X* [51].

The derivative of *x(t)* with respect to time (*t*) is:

$$\dot{x}(t) = \dot{G}(t)\,X + G(t)\,\dot{X}\ ;\ \dot{G}(t) = G(t)[D] \tag{3-8}$$

where [D] is the operational matrix of differentiation:

$$[D] = \begin{bmatrix} -jh\omega_0 & & & & & & \\ & \ddots & & & & & \\ & & -j\omega_0 & & & & \\ & & & o & & & \\ & & & & j\omega_0 & & \\ & & & & & \ddots & \\ & & & & & & jh\omega_0 \end{bmatrix} \tag{3-9}$$

Using the above equations, transforming the linear time periodic system of Equation 3-10 to the harmonic domain will result in a linear time invariant system as demonstarted by Equation 3-11:

$$\dot{x}(t) = a(t)\,x(t) + B(t)\,u(t) \tag{3-10}$$

$$\dot{X} = (A - D)\,X + BU \tag{3-11}$$

where, A and B have the Toeplitz form of [M].

$$[M] = \begin{bmatrix} a_0 & a_{-1} & \cdots & a_{-h} & & & \\ a_1 & \ddots & \ddots & \ddots & \ddots & & \\ \vdots & \ddots & a_0 & a_{-1} & \ddots & \ddots & \\ a_h & \ddots & a_1 & a_0 & a_{-1} & \ddots & a_{-h} \\ & \ddots & \ddots & a_1 & a_0 & \ddots & \vdots \\ & & \ddots & \ddots & \ddots & \ddots & a_{-1} \\ & & & a_h & \cdots & a_1 & a_0 \end{bmatrix} \tag{3-12}$$

Now using equations 3-7 to 3-12, the time periodic coefficient matrices of the nonlinear model of a synchronous generator (Equation 3-5) can be converted into the harmonic domain. Further, the Toeplitz form of the mutual stator-rotor matrix $[L_{sr}]$ is calculated as an example.

Mutual stator-rotor inductance in the time domain:

$$L_{sr}(t) = \begin{bmatrix} L_{aF}(t) & L_{aD}(t) & L_{aG}(t) & L_{aQ}(t) \\ L_{bF}(t) & L_{bD}(t) & L_{bG}(t) & L_{bQ}(t) \\ L_{cF}(t) & L_{cD}(t) & L_{cG}(t) & L_{cQ}(t) \end{bmatrix} \tag{3-13}$$

Each element of the above matrix is a summation of cosine waveforms (Equation 3-4) and can be written in the exponential form. For example, considering harmonics up to 3rd order:

$$\begin{aligned} L_{aF}(t) &= M_F^{(1)} \cos\theta + M_F^{(3)} \cos 3\theta \\ &= M_F^{(1)}\left(\frac{1}{2}e^{-j\omega_0 t}\, e^{-j\theta_0} + \frac{1}{2}e^{+j\omega_0 t}\, e^{+j\theta_0}\right) + M_F^{(3)}\left(\frac{1}{2}e^{-j3\omega_0 t}\, e^{-3j\theta_0} + \frac{1}{2}e^{+j3\omega_0 t}\, e^{+3j\theta_0}\right) \\ &= L_{aF}^{-1}\, e^{-j\omega_0 t} + L_{aF}^{+1}\, e^{+j\omega_0 t} + L_{aF}^{-3}\, e^{-j3\omega_0 t} + L_{aF}^{+3}\, e^{+j3\omega_0 t} \end{aligned} \tag{3-14}$$

Hence, $[L_{aF}]$ can be written in Toeplitz form:

$$[L_{aF}]_{7\times 7} = \begin{bmatrix} 0 & L_{aF}^{-1} & 0 & L_{aF}^{-3} & 0 & 0 & 0 \\ L_{aF}^{+1} & 0 & L_{aF}^{11} & 0 & L_{aF}^{-3} & 0 & 0 \\ 0 & L_{aF}^{+1} & 0 & L_{aF}^{-1} & 0 & L_{aF}^{-3} & 0 \\ L_{aF}^{+3} & 0 & L_{aF}^{+1} & 0 & L_{aF}^{-1} & 0 & L_{aF}^{-3} \\ 0 & L_{aF}^{+3} & 0 & L_{aF}^{+1} & 0 & L_{aF}^{-1} & 0 \\ 0 & 0 & L_{aF}^{+3} & 0 & L_{aF}^{+1} & 0 & L_{aF}^{-1} \\ 0 & 0 & 0 & L_{aF}^{+3} & 0 & L_{aF}^{+1} & 0 \end{bmatrix} \tag{3-15}$$

A similar method is followed to convert the other element of $L_{sr}(t)$ to the harmonic domain and $[L_{sr}]$ is derived as:

$$[L_{sr}]_{21\times 28} = \begin{bmatrix} [L_{aF}] & [L_{aD}] & [L_{aG}] & [L_{aQ}] \\ [L_{bF}] & [L_{bD}] & [L_{bG}] & [L_{bQ}] \\ [L_{cF}] & [L_{cD}] & [L_{cG}] & [L_{cQ}] \end{bmatrix} \tag{3-16}$$

Hence, the linear time periodic model of a synchronous generator (Equation 3-6), is amended to an alternative form as Equation 3-17, using the harmonic domain:

$$\begin{cases} \dot{\Psi}_r = ([A]-[D_r])\Psi_r + [B]U \\ I_r = [L_{rr}^{-1}]\Psi_r + [L_{rr}^{-1}L_{rs}]I_s \\ \Psi_s = [-L_{ss}]I_s + [L_{sr}]I_r \\ V_s = [D_s]\Psi_s + \dot{\Psi}_s - [R_s]I_s \end{cases} \tag{3-17}$$

where,

$$U = [I_s^{(-h)}, I_s^{(-h+1)}, \ldots, I_s^{(-1)}, 0, I_s^{(+1)}, \ldots, I_s^{(+h-1)}, I_s^{(+h)}, V_F^{(DC)}]^T$$
$$I_s^{(+h)} = [I_a^{(+h)}, I_b^{(+h)}, I_c^{(+h)}]^T$$

and $[D_r]$ and $[D_s]$ are the operational matrices of differentiation (Equation 3-9) applied to the rotor and stator equations, respectively. Matrices [*A*], [*B*], $[L_{rr}^{-1}]$ and $[L_{rr}^{-1}L_{rs}]$ are of the constant Toeplitz-type with the general form of matrix [*M*] (Equation 3-12).

Fundamental and harmonic components of the stator current ($I_s^{(1)}, I_s^{(h)}$) can be measured at the SG bus or calculated by harmonic power flow algorithms using a nonlinear model of the synchronous generator. The applied DC voltage to the field winding ($V_F^{(DC)}$) can also be measured or computed from the sinusoidal operation. Note that the interaction between space and time harmonics will not induce DC current on the rotor windings. Stator and rotor currents and fluxes are defined by their Fourier coefficients as Equation 3-7.

As an example, the stator winding flux of phase "a", induced by the field winding is obtained as follows:

$$\begin{bmatrix} \psi_a^{(-3)} \\ 0 \\ \psi_a^{(-1)} \\ 0 \\ \psi_a^{(+1)} \\ 0 \\ \psi_a^{(+3)} \end{bmatrix} = \begin{bmatrix} 0 & L_{aF}^{-1} & 0 & L_{aF}^{-3} & 0 & 0 & 0 \\ L_{aF}^{+1} & 0 & L_{aF}^{11} & 0 & L_{aF}^{-3} & 0 & 0 \\ 0 & L_{aF}^{+1} & 0 & L_{aF}^{-1} & 0 & L_{aF}^{-3} & 0 \\ L_{aF}^{+3} & 0 & L_{aF}^{+1} & 0 & L_{aF}^{-1} & 0 & L_{aF}^{-3} \\ 0 & L_{aF}^{+3} & 0 & L_{aF}^{+1} & 0 & L_{aF}^{-1} & 0 \\ 0 & 0 & L_{aF}^{+3} & 0 & L_{aF}^{+1} & 0 & L_{aF}^{-1} \\ 0 & 0 & 0 & L_{aF}^{+3} & 0 & L_{aF}^{+1} & 0 \end{bmatrix} \times \begin{bmatrix} 0 \\ I_F^{(-2)} \\ 0 \\ I_F^{(DC)} \\ 0 \\ I_F^{(+2)} \\ 0 \end{bmatrix} \tag{3-18}$$

In the stator voltage expression (Equation 3-17), the terms of $[D_s]\Psi_s$ and $\dot{\Psi}_s$ represent the speed voltage and transformer voltage respectively. Speed voltage is due to the flux change in space (equivalent to the terms $(\psi_d \dot{\theta})$ and $(\psi_q \dot{\theta})$ in the conventional model using the *dq*-frame of reference) and transformer voltage is due to the flux change in time (equivalent to $(\dot{\psi}_d)$ and $(\dot{\psi}_q)$ in the *dq*-frame of reference). The speed voltage terms are the dominant components of the stator voltage. Hence, transformer voltages can be dropped from the stator voltage equations without causing any significant error.

Considering the steady-state performance of the synchronous generator in the harmonic domain, Equation 3-17 will be simplified as:

$$\begin{cases} \Psi_r = ([D_r] - [A])^{-1}[B]U \\ I_r = [L_{rr}^{-1}]\Psi_r + [L_{rr}^{-1} L_{rs}]I_s \\ \Psi_s = [-L_{ss}]I_s + [L_{sr}]I_r \\ V_s = [D_s]\Psi_s - [R_s]I_s \end{cases} \tag{3-19}$$

Using the above equation, solutions of the rotor flux and current, as well as stator flux is carried out directly with the general form of Equation 3-7.

Figure 3.4 shows the flow of variables for simulation of a synchronous generator in the harmonic domain, using Equation 3-19.

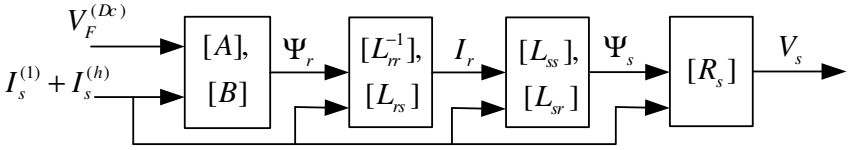

Figure 3.4. Flow of SG variables for the simulation in HD

3.4. Steady-State Operation of a Synchronous Generator under Harmonically Polluted Operating Conditions

The synchronous generator rotor (load) angle is one of the most important parameters for power system studies and is determined by the active power demand. Presence of time and space harmonics can cause variations in fundamental

components of the stator flux and voltage. This will result in an increase or reduction of the generated power, assuming constant fundamental components of the stator current. In order to calculate the synchronous generator active power, the harmonic domain analysis is used. This approach facilitates the understanding of rotor and stator harmonic fluxes and simplifies the procedure for computing the fundamental stator fluxes due to fundamental and harmonic components of the stator and rotor currents.

Based on Equation 3-19, the stator current time harmonic order (h^{time}) in the presence of space harmonic order (h^{space}) can produce rotor and stator harmonic fluxes of order ($h^{time} \pm h^{space}$) and ($h^{time} \pm 2h^{space}$), respectively. The sequences of the produced fluxes depend on the sequence of time harmonic and the order of space harmonic. These results are similar to [41] which introduces the impact of frequency conversion on the harmonic components of the synchronous generator .

Therefore, the generated stator flux (ψ_s) includes fundamental and harmonic components which may not be balanced at three phases (Figure 3.15). The stator zero sequence fluxes and harmonic rotating fields (having different speeds with respect to the rotor) do not produce constant torques and will not be considered in the calculations of the output active power and load angle. Therefore, the fundamental stator flux will be modified by considering the additional terms due to the interaction between time and space harmonics. This will influence the steady state value of the synchronous generator load angle. Figure 3.5 shows the additional time harmonics imposed by the presence of space harmonics in stator windings.

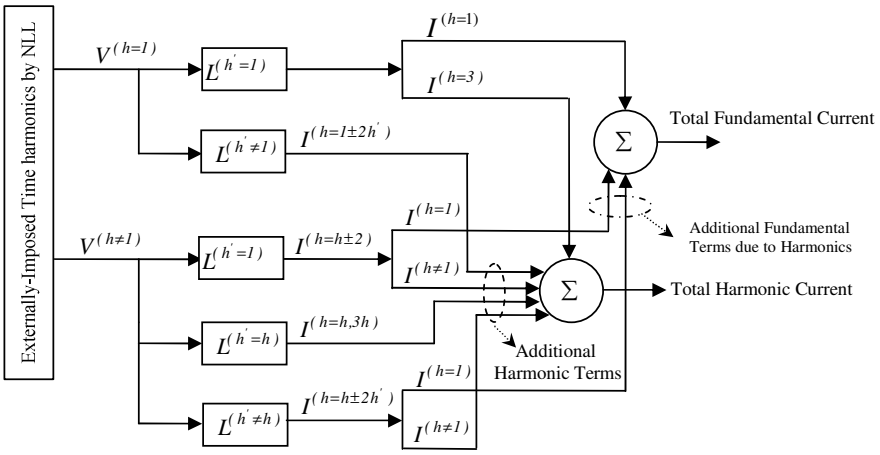

Figure 3.5. Additional stator-winding time harmonics imposed by the presence of space harmonics.

3.4.1. Stator Flux Analysis in the *abc*-Frame of Reference

The orders of time and space harmonics which contribute to producing stator flux components can be calculated from Equation 3-19. As an example, considering the harmonics up to order 10, the stator contains odd harmonics and the rotor contains even harmonics, the following space and time harmonics contribute to the 7th stator flux harmonic:

$$\begin{aligned}\psi_s^{(7)} = {} & L_{ss}^{(2)} i_s^{(9)} + L_{ss}^{(2)} i_s^{(5)} + L_{ss}^{(0)} i_s^{(7)} + L_{ss}^{(4)} i_s^{(3)} + L_{ss}^{(6)} i_s^{(1)} + L_{ss}^{(8)} i_s^{(1)} + L_{ss}^{(10)} i_s^{(3)} + \\ & L_{sr}^{(1)} i_r^{(8)} + L_{sr}^{(1)} i_r^{(6)} + L_{sr}^{(3)} i_r^{(4)} + L_{sr}^{(3)} i_r^{(10)} + L_{sr}^{(5)} i_r^{(2)} + L_{sr}^{(7)} i_r^{(0)} + L_{sr}^{(9)} i_r^{(2)}\end{aligned} \tag{3-20}$$

The above formulation is written in closed form, which means each term includes two components of the Fourier coefficients. For example, the first term generates the following stator fluxes in the time domain:

$$L_{ss}^{(2)} i_s^{(9)} \xrightarrow{Time\ \ Domain} L_{ss}^{(-2)} i_s^{(+9)} e^{+7j\omega t} + L_{ss}^{(+2)} i_s^{(-9)} e^{-7j\omega t} = \psi_s^{(+7)} e^{+7j\omega t} + \psi_s^{(-7)} e^{-7j\omega t} \tag{3-21}$$

Combination of these two components generates a cosine waveform of harmonic order 7 in each phase which results in a stator rotating field with the speed of 7ω, where ω is the synchronous speed. Expressions similar to Equation 3-21 can be written for the other terms of Equation 3-20.

Similar to Equation 3-20, the following expression can be written for the space and time harmonics contributing to the fundamental stator flux:

$$\begin{aligned}\psi_s^{(1)} = {} & L_{ss}^{(10)} i_s^{(9)} + L_{ss}^{(8)} i_s^{(9)} + L_{ss}^{(8)} i_s^{(7)} + L_{ss}^{(6)} i_s^{(7)} + L_{ss}^{(6)} i_s^{(5)} + L_{ss}^{(4)} i_s^{(5)} + L_{ss}^{(4)} i_s^{(3)} \\ & + L_{ss}^{(2)} i_s^{(3)} + L_{ss}^{(2)} i_s^{(1)} + L_{ss}^{(0)} i_s^{(1)} + L_{sr}^{(1)} i_r^{(2)} + L_{sr}^{(1)} i_r^{(0)} + L_{sr}^{(3)} i_r^{(2)} + L_{sr}^{(3)} i_r^{(4)} \\ & + L_{sr}^{(5)} i_r^{(4)} + L_{sr}^{(5)} i_r^{(6)} + L_{sr}^{(7)} i_r^{(6)} + L_{sr}^{(7)} i_r^{(8)} + L_{sr}^{(9)} i_r^{(8)} + L_{sr}^{(9)} i_r^{(10)}\end{aligned} \tag{3-22}$$

The above equation can be simplified as the following form:

$$\psi_s^{(1)} = L_{ss}^{(2)} i_s^{(1)} + L_{ss}^{(0)} i_s^{(1)} + L_{sr}^{(1)} i_r^{(0)} + \psi_s^{due\ to\ harm} \tag{3-23}$$

Under sinusoidal operating conditions, the additional terms due to the interaction of time and space harmonics ($\psi_s^{due\ to\ harm}$) will be zero and the conventional relation will be achieved [2].

Note that each term of Equation 3-22 results in a rotating magnetic field in the stator. Table 3-1 summarizes the impact of stator and rotor time harmonics on the fundamental stator flux in the presence of self-stator and mutual stator-rotor space harmonics. According to this table, different harmonic orders result in the forward rotating, backward rotating and zero sequence fields in the stator. Hence, it can be concluded that the presence of harmonics in the power system can lead to an asymmetrical situation. As these results are based on the mathematical relations between different harmonic orders, they are independent of the load angle or initial values of stator currents. However, the magnitudes of the generated fluxes depend on the operating conditions.

In order to verify the mathematical results shown in Table 3-1, a synchronous generator that includes space harmonics and operates under distorted operating conditions, was simulated. The generator parameters and the operating conditions are similar to Case 3 of Section 3-5.

Figure 3.6 shows the forward rotating, backward rotating and zero sequence components of the fundamental stator field in the time domain. It is observed that the presence of time and space harmonics can produce unbalanced stator fluxes and voltages in the generator terminals.

Table 3-1
Fundamental component of stator flux resulting from time and space harmonics

Produced stator flux	Description
STATOR CURRENT AND SELF-STATOR INDUCTANCE HARMONICS	
$L_{ss}^{(-10)} I_s^{(+9)} e^{(-j\omega t)} + L_{ss}^{(+10)} I_s^{(-9)} e^{(+j\omega t)}$	field magnitude is zero
$L_{ss}^{(+8)} I_s^{(-9)} e^{(-j\omega t)} + L_{ss}^{(-8)} I_s^{(+9)} e^{(+j\omega t)}$	backward rotating field
$L_{ss}^{(-8)} I_s^{(+7)} e^{(-j\omega t)} + L_{ss}^{(+8)} I_s^{(-7)} e^{(+j\omega t)}$	forward rotating field
$L_{ss}^{(+6)} I_s^{(-7)} e^{(-j\omega t)} + L_{ss}^{(-6)} I_s^{(+7)} e^{(+j\omega t)}$	field magnitude is zero
$L_{ss}^{(-6)} I_s^{(+5)} e^{(-j\omega t)} + L_{ss}^{(+6)} I_s^{(-5)} e^{(+j\omega t)}$	field magnitude is zero
$L_{ss}^{(+4)} I_s^{(-5)} e^{(-j\omega t)} + L_{ss}^{(-4)} I_s^{(+5)} e^{(+j\omega t)}$	zero sequence
$L_{ss}^{(-4)} I_s^{(+3)} e^{(-j\omega t)} + L_{ss}^{(+4)} I_s^{(-3)} e^{(+j\omega t)}$	zero sequence
$L_{ss}^{(+2)} I_s^{(-3)} e^{(-j\omega t)} + L_{ss}^{(-2)} I_s^{(+3)} e^{(+j\omega t)}$	backward rotating field
$L_{ss}^{(-2)} I_s^{(+1)} e^{(-j\omega t)} + L_{ss}^{(+2)} I_s^{(-1)} e^{(+j\omega t)}$	forward rotating field
$L_{ss}^{(0)} I_s^{(-1)} e^{(-j\omega t)} + L_{ss}^{(0)} I_s^{(+1)} e^{(+j\omega t)}$	forward rotating field
ROTOR CURRENT AND STATOR-ROTOR INDUCTANCE HARMONICS	
$L_{sr}^{(+1)} I_r^{(-2)} e^{(-j\omega t)} + L_{sr}^{(-1)} I_r^{(+2)} e^{(+j\omega t)}$	backward rotating field
$L_{sr}^{(-1)} I_r^{(0)} e^{(-j\omega t)} + L_{sr}^{(+1)} I_r^{(0)} e^{(+j\omega t)}$	forward rotating field
$L_{sr}^{(-3)} I_r^{(+2)} e^{(-j\omega t)} + L_{sr}^{(+3)} I_r^{(-2)} e^{(+j\omega t)}$	zero sequence
$L_{sr}^{(+3)} I_r^{(-4)} e^{(-j\omega t)} + L_{sr}^{(-3)} I_r^{(+4)} e^{(+j\omega t)}$	zero sequence
$L_s^{(-5)} I_r^{(+4)} e^{(-j\omega t)} + L_{sr}^{(+5)} I_r^{(-4)} e^{(+j\omega t)}$	backward rotating field
$L_{sr}^{(+5)} I_r^{(-6)} e^{(-j\omega t)} + L_{sr}^{(-5)} I_r^{(+6)} e^{(+j\omega t)}$	forward rotating field
$L_{sr}^{(-7)} I_r^{(+6)} e^{(-j\omega t)} + L_{sr}^{(+7)} I_r^{(-6)} e^{(+j\omega t)}$	forward rotating field
$L_{sr}^{(+7)} I_r^{(-8)} e^{(-j\omega t)} + L_{sr}^{(-7)} I_r^{(+8)} e^{(+j\omega t)}$	backward rotating field
$L_{sr}^{(-9)} I_r^{(+8)} e^{(-j\omega t)} + L_{sr}^{(+9)} I_r^{(-8)} e^{(+j\omega t)}$	zero sequence
$L_{sr}^{(+9)} I_r^{(-10)} e^{(-j\omega t)} + L_{sr}^{(-9)} I_r^{(+10)} e^{(+j\omega t)}$	zero sequence

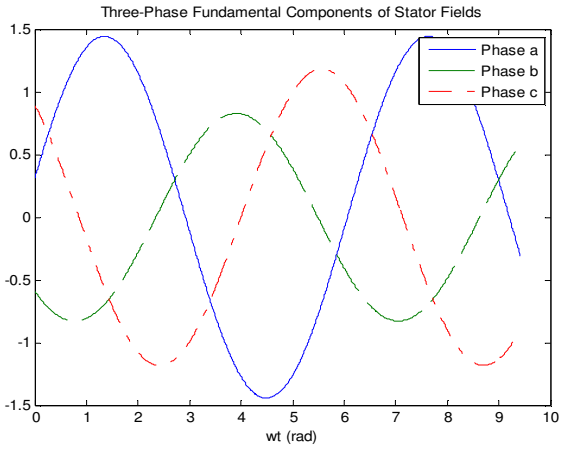

(a)

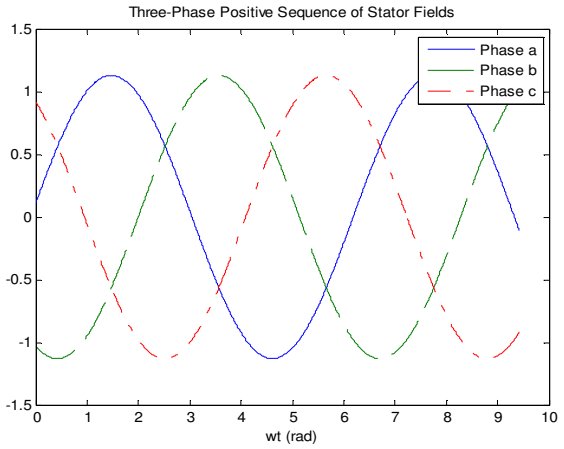

(b)

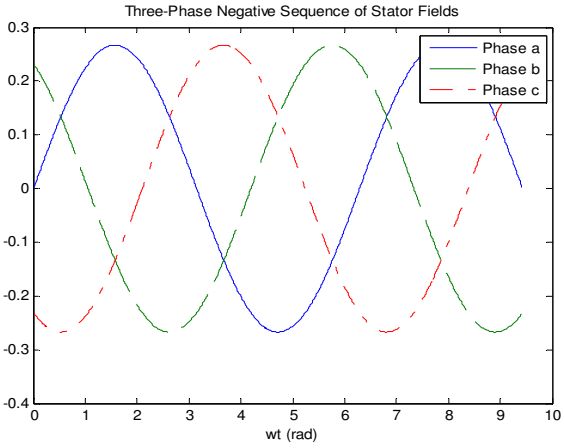

(c)

Figure 3.6. Fundamental components of three-phase stator fields considering time and space harmonics; (a) three-phase fundamental components, (b) fundamental positive sequence, (c) fundamental negative sequence, (d) zero sequence

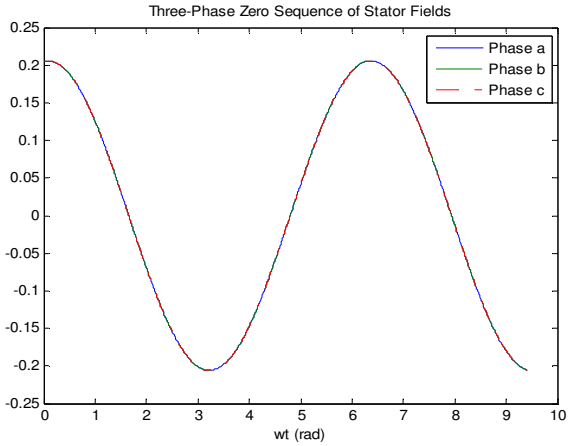

(d)

Figure 3.6. …continued

It is shown in Table 3-1 that the interaction of certain time and space harmonics will produce a stator field with magnitude of zero. Summations of these components are illustrated in Figure 3.7.

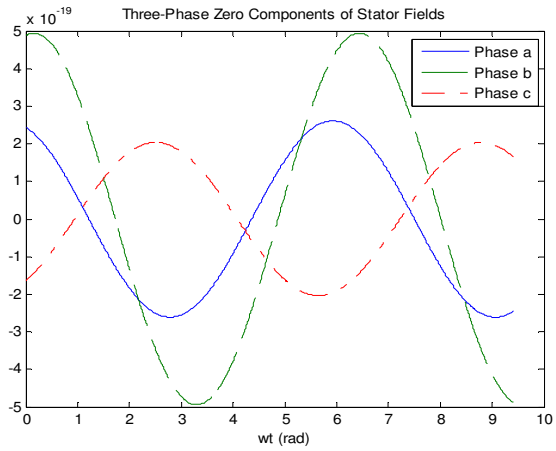

Figure 3.7. Zero components of the stator field produced by the interaction of space and time harmonics

Based on Equation 3-19, stator time harmonics induce current harmonics in the rotor. Therefore, damper windings can be effective in the steady-state operation of synchronous generators in the presence of harmonics. The impact of damper windings is investigated in Section 3.5.

3.4.2. Stator Flux Analysis in the *dq*-Frame of Reference

To incorporate the presence of time and space harmonics on the generator steady-state operation, the frame of reference is changed from the *abc*-coordinates to the *dq*-coordinates using Park Transformation. As the modified fundamental stator flux (including additional terms of $\psi_s^{due\ to\ harm}$) is rotating with the same speed as the rotor, applying the Park transformation will result in constant flux components on the *d* and *q* axes, as demonstrated by the following equation:

$$\begin{aligned}\psi_d^{(\mathrm{modified})} &= -L_d I_d^{(1)} + M_F^{(1)} I_F^{(DC)} + \psi_d^{due\ to\ harm} \\ \psi_q^{(\mathrm{modified})} &= -L_q I_q^{(1)} + \psi_q^{due\ to\ harm}\end{aligned} \tag{3-24}$$

where L_d and L_q are the conventional generator inductances in direct and quadrate axes, respectively. $M_F^{(1)}$ is the fundamental magnitude of the mutual inductance between the stator and rotor. $\psi_d^{due\ to\ harm}$ and $\psi_q^{due\ to\ harm}$ are the stator fluxes resulting from interaction between time and space harmonics and will be zero under sinusoidal operating conditions. The variables of Equation 3-24 are defined as follows:

$$\begin{aligned}L_d &= L_s + M_s + (3/2)L_m \\ L_q &= L_s + M_s - (3/2)L_m\end{aligned}$$

$$\begin{aligned}\psi_d^{due\ to\ harm} &= \sum_{K=F,D} \left(\frac{I_K^{(h)}}{2}\right)\left(M_K^{(h+1)} + M_K^{(h-1)}\right)\cos\left(h\theta_0 - \theta_K^{(h)}\right) - \\ &\sum_{K=G,Q} \left(\frac{I_K^{(h)}}{2}\right)\left(M_K^{(h+1)} + M_K^{(h-1)}\right)\sin\left(h\theta_0 - \theta_K^{(h)}\right) + k\left(\frac{I_S^{(h')}}{2}\right)\left(L_m^{(h'+1)}\right)\cos\left(h'\theta_0 - \theta_{is}^{(h')}\right)\end{aligned}$$

$$\begin{aligned}\psi_q^{due\ to\ harm} &= \sum_{K=F,D} \left(\frac{I_K^{(h)}}{2}\right)\left(M_K^{(h+1)} - M_K^{(h-1)}\right)\sin\left(h\theta_0 - \theta_K^{(h)}\right) + \\ &\sum_{K=G,Q} \left(\frac{I_K^{(h)}}{2}\right)\left(M_K^{(h+1)} - M_K^{(h-1)}\right)\cos\left(h\theta_0 - \theta_K^{(h)}\right) + k\left(\frac{I_S^{(h')}}{2}\right)\left(L_m^{(h'+1)}\right)\sin\left(h'\theta_0 - \theta_{is}^{(h')}\right)\end{aligned}$$

$$\theta_\circ = (\delta_\circ - \pi/2) \tag{3-25}$$

where:

$L_m^{(h)}$ = harmonic order h of the stator self or mutual inductance

$M_K^{(h)}$ = harmonic order h of the stator-rotor (winding K) mutual inductance

$\theta_K^{(h)}$= phase angle of the h^{th} current harmonic in rotor winding K

$\theta_{is}^{(h')}$= phase angle of the h'^{th} current harmonic in stator winding

$I_K^{(h)}$= magnitude of the h^{th} current harmonic in rotor winding K

$I_S^{(h')}$= magnitude of the h'^{th} current harmonic in stator winding.

Note that h and h' are the rotor and stator harmonic orders, which contribute to the fundamental forward rotating field in the stator. Coefficient k is a function of h' and can be computed by applying Park transformations to the result of Equation 3-19. As an example, k = -1 for h'= 7. Equation 3-25 shows that, the additional induced stator fluxes due to harmonics depend on the load angle.

3.4.3. Modification of the Synchronous Generator Steady-State Rotor Angle Due to the Presence of Time and Space Harmonics

Calculating the initial characteristics of the synchronous generator, such as the load angle, is essential in studying the steady-state, transient, dynamic and harmonic behaviour of the power system. Hence, in distorted power systems, it is necessary to compute the initial conditions and the modified rotor angle of the synchronous generator as a function of non-sinusoidal terminal quantities.

The fundamental component of the armature terminal voltage ($\tilde{E}_t^{(1)}$) which rotates at synchronous speed is considered as the reference. The relationships between *dq* components of the fundamental armature terminal voltages and currents in per unit form are defined as [2]:

$$\begin{cases} e_d^{(1)} = -\omega_r \psi_q^{(modified)} - R_a I_d^{(1)} \\ e_q^{(1)} = \omega_r \psi_d^{(modified)} - R_a I_q^{(1)} \end{cases} \tag{3-26}$$

Similar to conventional sinusoidal studies, the positions of the *d* and *q* axes should be identified relative to the fundamental stator voltage phasor (synchronous rotating reference) [2]. Defining the voltage $\tilde{E}_q$ as follows:

$$\tilde{E}_q = \tilde{E}_t^{(1)} + (R_a + j\omega_r L_q)\tilde{I}_t^{(1)} + \omega_r \psi_q^{due\ to\ harm} \tag{3-27}$$

The corresponding phasor diagram (Figure 3.8) demonstrates that $\tilde{E}_q$ lies along the *q*-axis. Thus, the position of the *q*-axis with respect to $\tilde{E}_t^{(1)}$ (rotor angle, δ_0) can be identified by computing $\tilde{E}_q$.

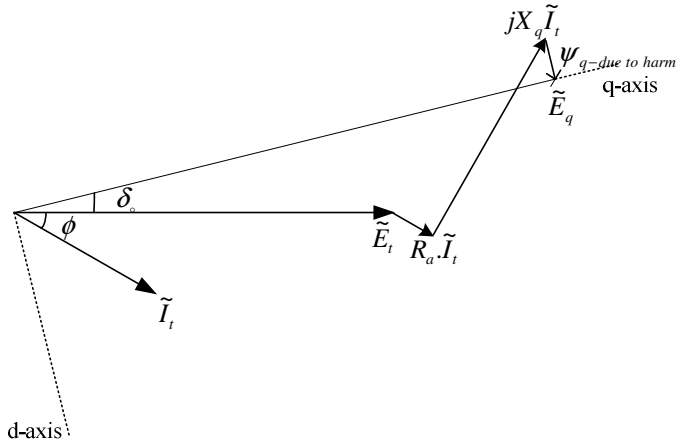

Figure 3.8. Steady-state phasor diagram of the fundamental terminal voltage and current in the presence of time and space harmonics

It is observed from Equation 3-27 that the angle of $\tilde{E}_q$ depends on the value of $\psi_q^{due\ to\ harm}$ which is a function of the harmonics. Therefore, the rotor angle will vary with the magnitudes and phase angles of the injected time harmonics. Using Figure 3.8, the internal rotor angle can be written as:

$$\delta_0 = \tan^{-1}\left(\frac{\omega_r L_q I_t^{(1)}\cos(\phi) - R_a I_t^{(1)}\sin(\phi) - \omega_r \psi_q^{due\ to\ harm}\cos(\delta_0)}{E_t^{(1)} + R_a I_t^{(1)}\cos(\phi) + \omega_r L_q I_t^{(1)}\sin(\phi) + \omega_r \psi_q^{due\ to\ harm}\sin(\delta_0)}\right) \quad (3\text{-}28)$$

where ϕ is the power factor. Equation 3-28 is a general form for calculating δ_0 which will be similar to the conventional (sinusoidal) form [2] when harmonics are eliminated. This equation can be solved using numerical methods.

The following steps outline the proposed iterative algorithm for computing the synchronous generator load angle in the presence of time and space harmonics:

Step 1: Compute the rotor angle for sinusoidal conditions using Equation 3-28, assuming $\psi_q^{due\ to\ harm}$=0. The sinusoidal result is used as the initial value ($\delta_{initial}$) for the non-sinusoidal calculations.

Step 2: Considering the specified or assumed stator time harmonics and inductance space harmonics, calculate the induced harmonic currents in the rotor windings using the harmonic domain model of a synchronous generator (Equation 3-19).

Step 3: Determine the stator and rotor current harmonics contributing to the fundamental forward rotating field using Equation 3-22 and Table 3-1.

Step 4: Compute the additional terms of the fundamental stator flux due to harmonics, in the *dq*-frame using Equation 3-25.

Step 5: Calculate the rotor angle from Equation 3-28, using a numerical method (δ_0).

Step 6: If the convergence criterion ($|\delta_{initial} \quad \delta_0| < \varepsilon$) is satisfied, stop. Otherwise, set $\delta_{initial} = \delta_0$ and go to Step 2.

Figure 3.9 shows a flowchart of the proposed algorithm.

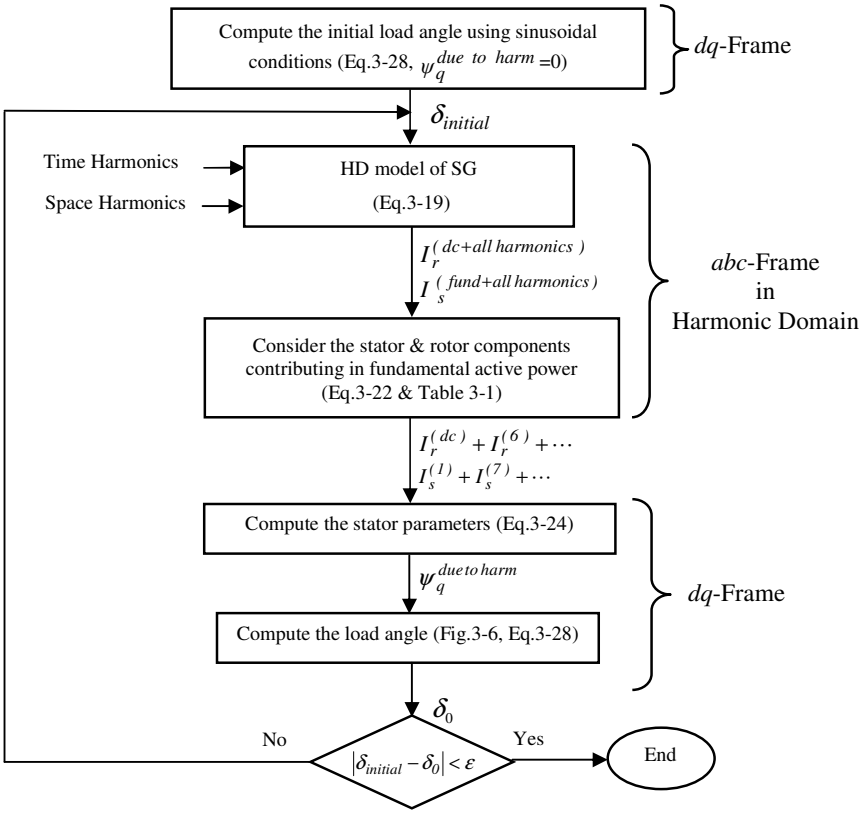

Figure 3.9. The proposed algorithm for computing the synchronous generator load angle in the presence of time and space harmonics

3.5. Simulation of a Synchronous Generator under Different Operating Conditions

To illustrate the impact of time and space harmonics, as well as damper windings on the steady-state operation of a synchronous generator, simulations were conducted under three different operating conditions. The results from the simulations under distorted conditions were compared with the results for operation under sinusoidal conditions.

A 555 MVA, 24 kV, 0.9p.f, 60 Hz, 3600 RPM turbine generator was used in the analysis. The system, stator and rotor parameters (in per unit of machine rating) are given below:

Stator Parameters:

L_s=1.060 L_m=0.0140 M_s=0.4550 R_a =0.003

Rotor Parameters:

R_F =0.0006 L_F = 1.551 L_{FD}=1.386

R_D =0.0284 L_D = 1.5573 L_{GQ}=1.344

R_G =0.00619 L_G = 2.0692 L_{FG}= L_{FQ}= L_{DG}= L_{DQ}=0

R_Q =0.02368 L_Q = 1.469

Stator Rotor Mutual Parameters:

M_F =M_D= 1.386 M_G =M_Q=1.344

Case 1- Sinusoidal Operation:

In this case the effects of space harmonics are ignored and the stator current is assumed to be sinusoidal. The synchronous generator delivers *555 MVA* at *0.9 pf (lag)* at rated terminal voltages. The effects of magnetic saturation are neglected. Four rotor windings are considered which consist of a rotor-field winding and three damper windings (one along the *d*-axis and two along the *q*-axis). Using equations 3-19, 3-24 and 3-18, the generator parameters and rotor angle are calculated as:

L_d= *1.5360,* L_q= *1.4940,* $I_d = 0.9058$, $I_q = 0.4239$, $\delta_0 = 39.0757^\circ$

As expected, damper windings have no effect on the sinusoidal steady-state operating quantities. The above values could be computed from the conventional equations in sinusoidal conditions. Figures 3.10 and 3.11 show the stator fluxes and voltages in the *abc*-frame of reference for sinusoidal operating conditions.

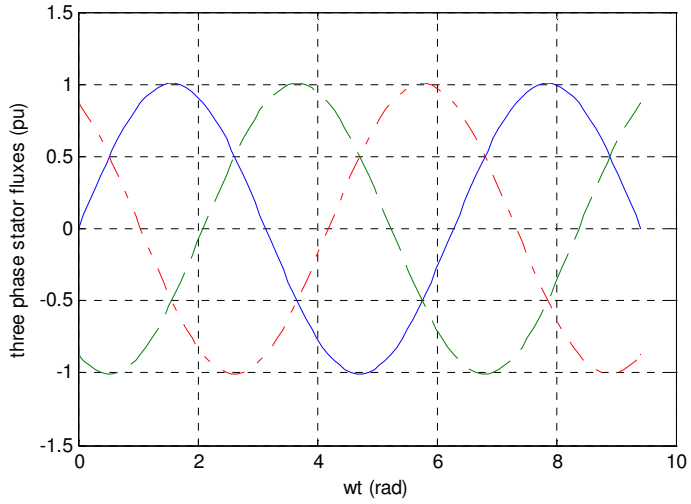

Figure 3.10. Three-phase stator fluxes for sinusoidal operating conditions

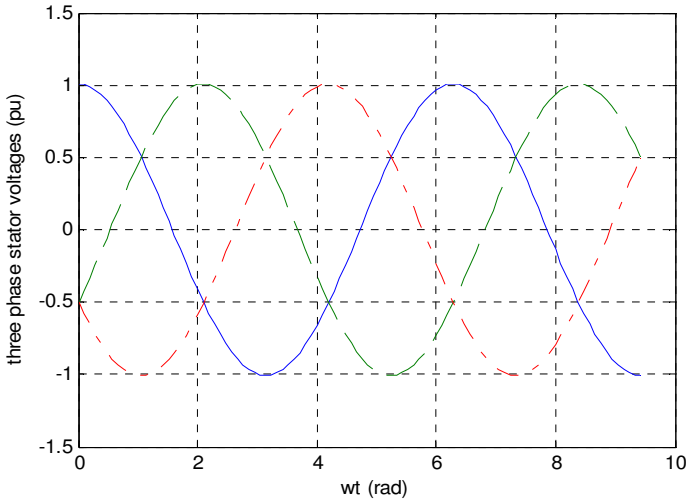

Figure 3.11. Three-phase stator voltages for sinusoidal operating conditions

Case 2- Non-Sinusoidal Operation with Space Harmonics:

In this case self-stator inductances are assumed to have additional even harmonic components (up to the 10^{th} harmonic) and the mutual stator-rotor inductances contain odd components (up to the 9^{th} harmonic). Table 3-2 shows the induced rotor currents and the corresponding load angles for two levels of space harmonics and the same loading condition as Case 1. The selected space harmonics for the base level, $Base_S$, were 0.3, 0.2, 0.1 and 0.01 of the first and second harmonic for stator-rotor and stator, respectively [48].

The impact of damper windings is also presented in Table 3-2. It is observed that the induced harmonic currents on the damper windings are considerable and their impacts on rotor angle should not be ignored.

Table 3-2
Impact of space harmonics on stator parameters, rotor current harmonics and load angle

Space Harmonic Level	Stator Parameters	Load Angle (δ_o) [%Δ**]
Without Damper Windings		
$Base_S$*	$\psi_d = 0.8290$ $\psi_q = -0.6320$ $I_d = 0.9054$ $I_q = 0.4248$	39.01^o [-0.17%]
$2\times Base_S$	$\psi_d = 0.9826$ $\psi_q = -0.6294$ $I_d = 0.9037$ $I_q = 0.4284$	38.78^o [-0.75%]
With Damper Windings		
$Base_S$	$\psi_d = 0.8834$ $\psi_q = -0.6311$ $I_d = 0.9047$ $I_q = 0.4261$	38.93^o [-0.37%]
$2\times Base_S$	$\psi_d = 1.1986$ $\psi_q = -0.6250$ $I_d = 0.9013$ $I_q = 0.4333$	38.47^o [-1.55%]

*) *0.3, 0.2, 0.1* and *0.01* of the second and the first harmonics for self-stator and stator-rotor inductances, respectively.

**) Percentage of deviation from the sinusoidal conditions (39.075^o) without harmonics.

Three-phase stator fluxes and voltages are shown in figures 3.12 and 3.13.

Figure 3.14 shows the harmonic spectrum of the stator terminal voltages.

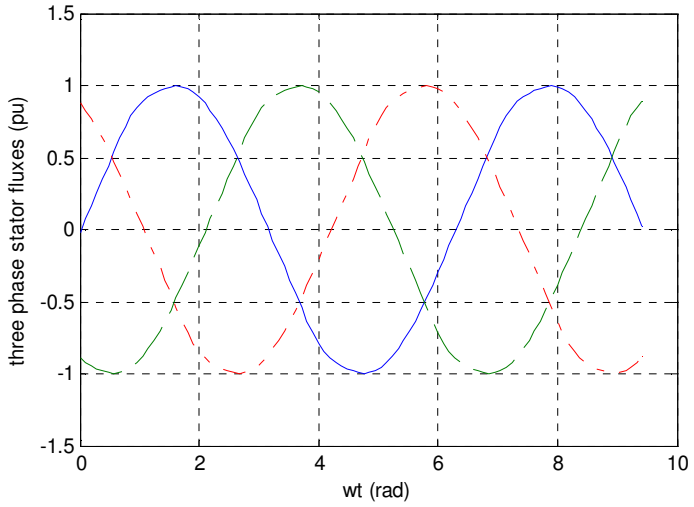

Figure 3.12. Three-phase stator fluxes for distorted operating conditions in the presence of space harmonics (Table 3-2, row 4)

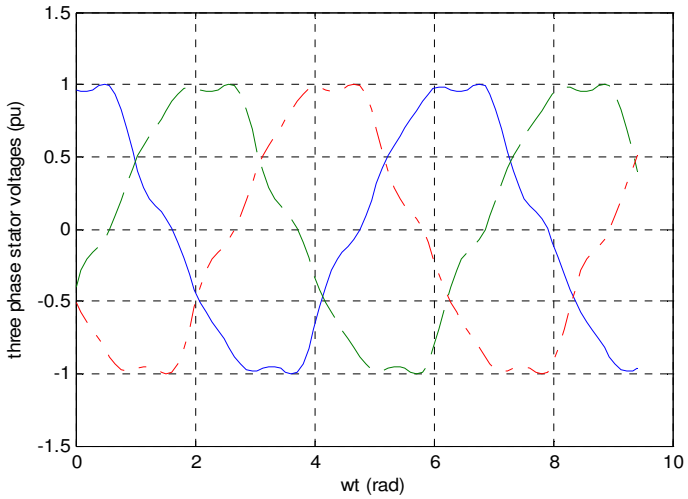

Figure 3.13. Three-phase stator voltages for distorted operating conditions in the presence of space harmonics (Table 3-2, row 4)

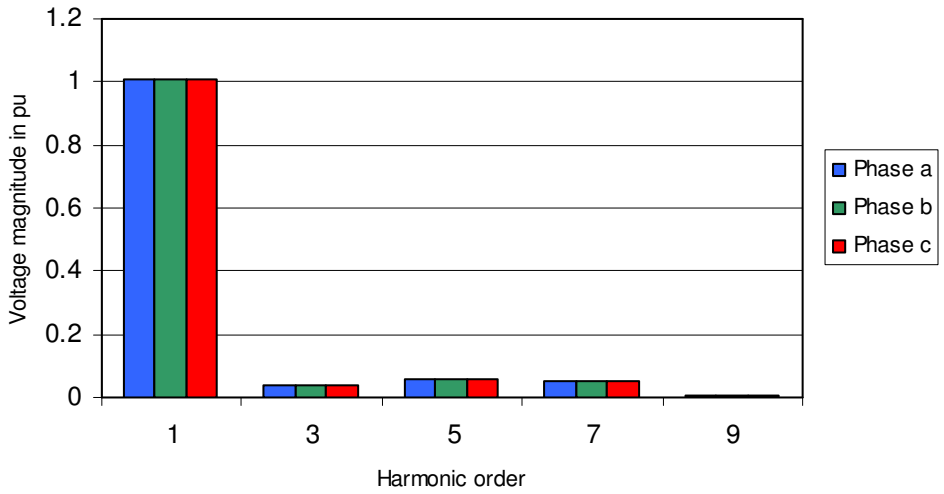

Figure 3.14. Harmonic spectrum of SG terminal voltage (Table 3-2, row 4)

Case 3- Non-Sinusoidal Operation with Time and Space Harmonics:

In this case, the interaction of space and time harmonics and their effects on the rotor harmonic currents and load angle are investigated. Space harmonics are assumed to be at $2\times Base_S$, as defined in Case 2. The selected time harmonics for the base level, $Base_T$, were 0.03pu, 0.02pu, 0.01pu and 0.001pu for the 3rd to 9th harmonics, respectively.

To highlight the impact of current harmonic phase angles two values of phase angle, 0 and $\pi/2$, are considered at each time harmonic level. The results given in Table 3-3 demonstrate that harmonic phase angles have considerable impact on the steady-state performance of the synchronous generator.

Table 3-3 also shows the impact of time and space harmonics on the synchronous generator parameters with and without damper windings.

Figures 3.15 and 3.16 show stator fluxes and voltages in the presence of time and space harmonics, with and without damper windings. In the cases with damper windings three windings were considered, two along the q-axis (L_G, L_Q) and one along the d-axis (L_D).

Table 3-3
Impact of space and time harmonics on stator parameters, induced rotor current harmonics and load angle (space harmonics are at *2×Base level* of Table 3-2)

Time Harm	Stator Parameters	Load Angle (δ_o) [$\%\Delta^{**}$]
Without Damper Windings		
$Base_T^{*}\ (\theta_i^{(h)}=0)$	$\psi_d=0.9082$ $\psi_q=-0.6287$ $I_d=0.9037$ $I_q=0.4284$	*38.78°* *[-0.75%]*
$Base_T\ (\theta_i^{(h)}=\pi/2)$	$\psi_d=0.9677$ $\psi_q=-0.6379$ $I_d=0.9087$ $I_q=0.4175$	*39.47° [+1.01%]*
$2\times Base_T\ (\theta_i^{(h)}=0)$	$\psi_d=0.8340$ $\psi_q=-0.6289$ $I_d=0.9034$ $I_q=0.4288$	*38.76°* *[-0.80%]*
$2\times Base_T\ (\theta_i^{(h)}=\pi/2)$	$\psi_d=0.9422$ $\psi_q=-0.6471$ $I_d=0.9133$ $I_q=0.4075$	*40.10° [+2.62%]*
With Damper Windings		
$Base_T^{*}\ (\theta_i^{(h)}=0)$	$\psi_d=1.1948$ $\psi_q=-0.6249$ $I_d=0.9013$ $I_q=0.4333$	*38.47°* *[-1.55%]*
$Base_T\ (\theta_i^{(h)}=\pi/2)$	$\psi_d=1.1933$ $\psi_q=-0.6124$ $I_d=0.8991$ $I_q=0.4378$	*38.18°* *[-2.29%]*
$2\times Base_T\ (\theta_i^{(h)}=0)$	$\psi_d=1.1909$ $\psi_q=-0.6248$ $I_d=0.9013$ $I_q=0.4333$	*38.47°* *[-1.55%]*
$2\times Base_T\ (\theta_i^{(h)}=\pi/2)$	$\psi_d=1.1976$ $\psi_q=-0.6259$ $I_d=0.9017$ $I_q=0.4324$	38.53° *[-1.39%]*

*) *0.03pu, 0.02pu, 0.01*pu and *0.001*pu for the 3rd to 9th harmonics, respectively.

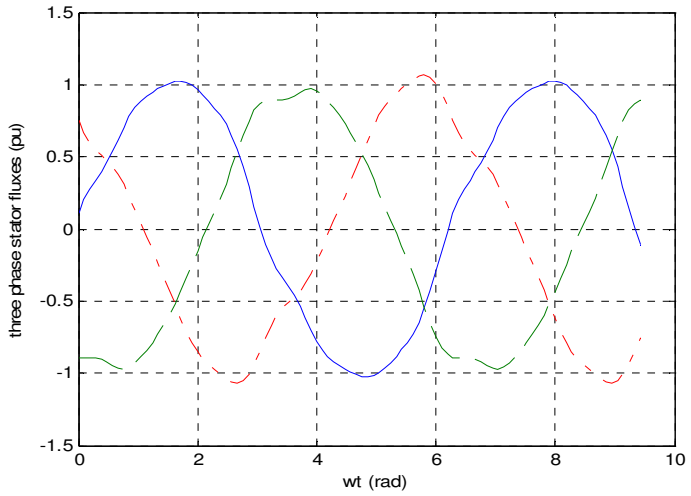

(a)

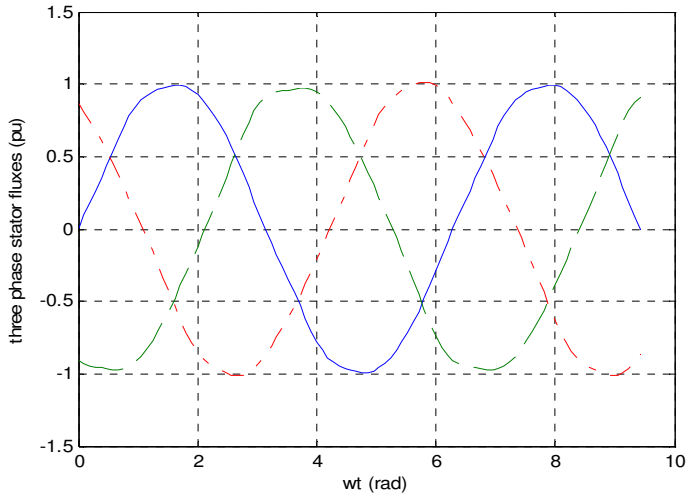

(b)

Figure 3.15. Three-phase stator fluxes in the presence of time and space harmonics; (a) without damper windings (Table 3-3, row 5), (b) with three damper windings (Table 3-3, row 10)

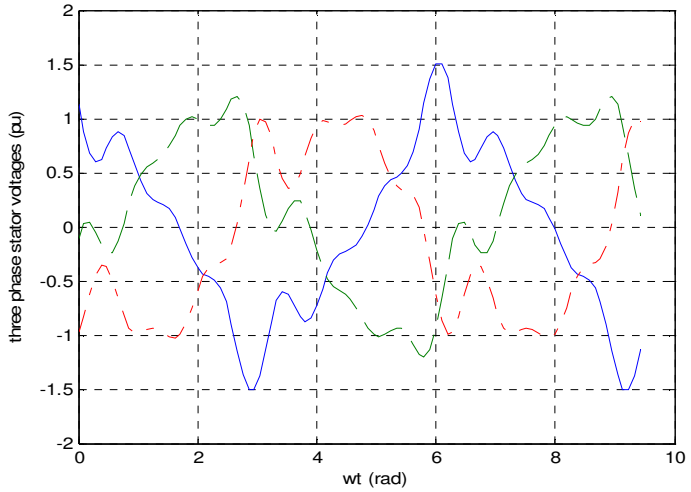

(a)

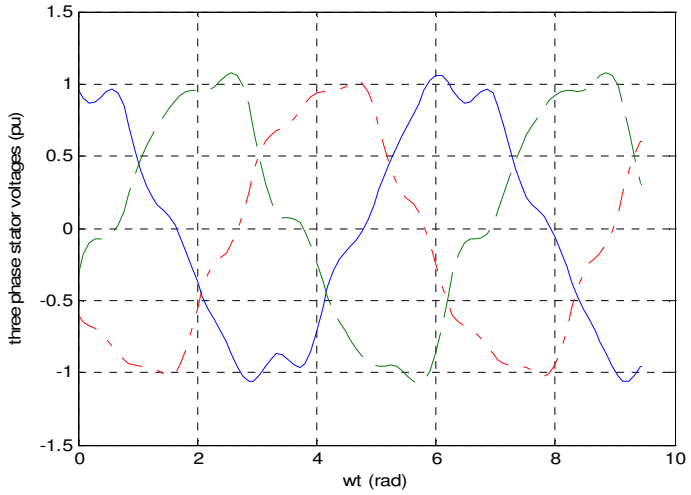

(b)

Figure 3.16. Three-phase stator voltages in the presence of time and space harmonics (a) without damper windings (Table3-3, row5) and (b) with three damper windings (Table3-3, row10)

Harmonic spectra of the synchronous generator stator voltages with and without damper windings are shown in Figure 3.17. It is observed that damper windings can reduce the amount of voltage harmonics and also improve the terminal voltage balance.

Comparing Figure 3.14 with Figure 3.17 shows that the interaction between time and space harmonics introduces unbalanced voltages in stator terminals at the fundamental and harmonic frequencies. However, damper windings are effective in regulating the three-phase voltage and decreasing the harmonic components.

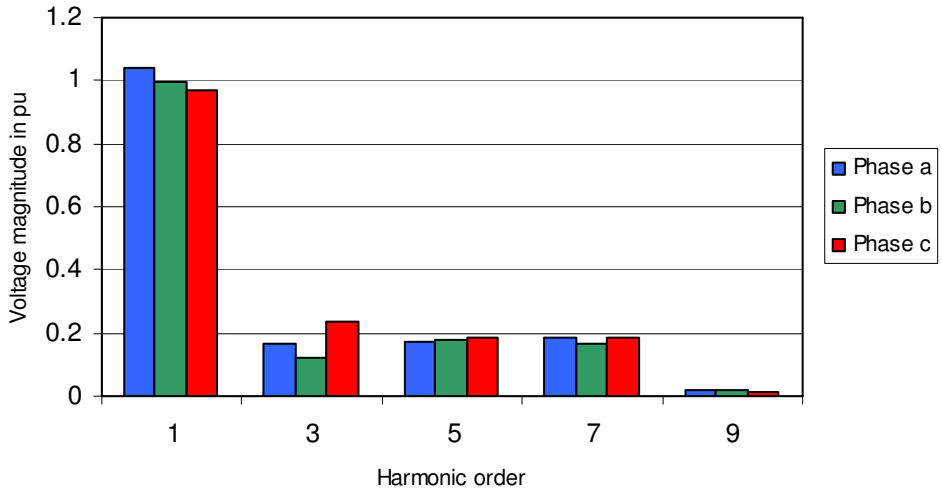

(a)

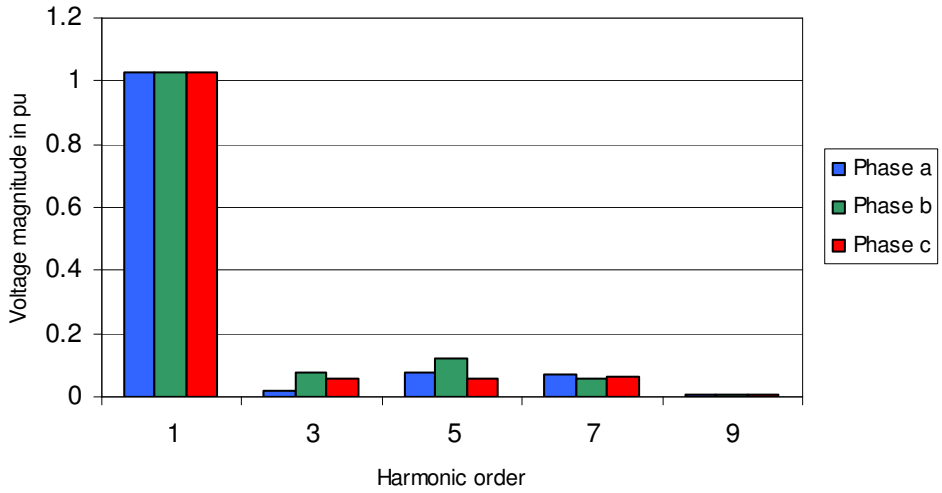

(b)

Figure 3.17. Harmonic spectra of SG terminal voltages; (a) without damper windings (Table 3-3, row 3), (b) with damper windings (Table3-3, row 8)

The rotor current waveforms under sinusoidal and distorted conditions are demonstrated in Figure 3.18. This figure shows that under sinusoidal steady-state

operation, there is no current in the damper windings while DC current flows in the field winding. From the nonlinear model of the generator (Equation 3-19 and Figure 3.4), it is observed that under distorted conditions, even orders of harmonic currents will be induced in the rotor windings.

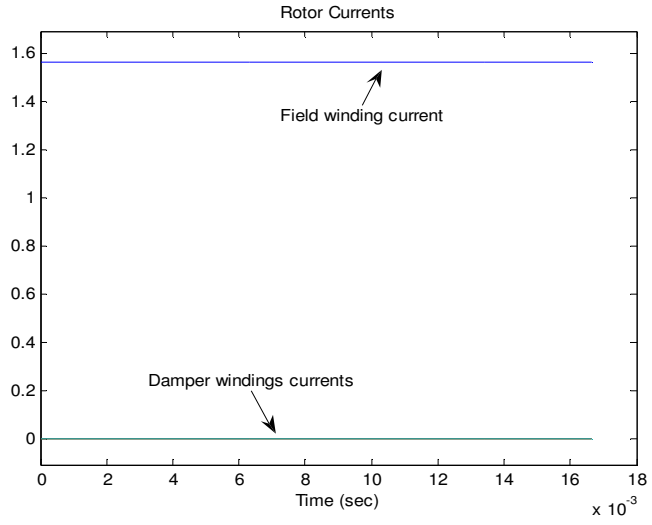

(a)

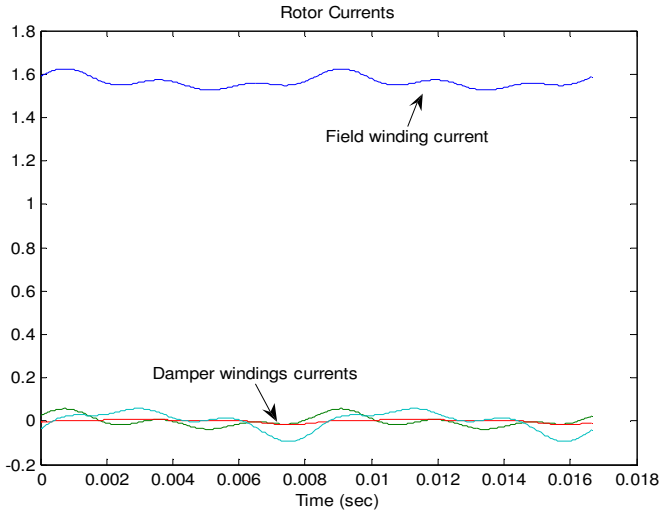

(b)

Figure 3.18. Rotor currents; (a) sinusoidal conditions, (b) in the presence of time and space harmonics

Time Domain Simulation of the Electromagnetic Torque:

As mentioned in Section 3.4, the presence of harmonics can impose pulsating torque on the rotor shaft. In this section the produced electromagnetic torque is calculated and plotted in the time domain. This approach allows the impact of all harmonic components to be considered. The electromagnetic power calculation is based on the instantaneous stator currents and rotational voltages [52].

This simulation is performed using Matlab and Simulink and a nonlinear model of the synchronous generator (Equation 3-19).

The electromagnetic torque is related to the instantaneous power flows across the air gap from stator to rotor via the actual rotor speed (ω_r) by the following equation:

$$T_{em}(t) = P_{em}(t) / \omega_r \tag{3-29}$$

where for polyphase AC machines, the electromagnetic air gap power is defined as the product of the instantaneous rotational voltage component in each armature phase and the instantaneous phase current. Hence, the produced electromagnetic power is calculated using the following equation [52]:

$$P_{em} = \hat{e}_a.i_a + \hat{e}_b.i_b + \hat{e}_c.i_c = \hat{E}_{abc}.I_{abc} \tag{3-30}$$

Where, $\hat{e}_a$, $\hat{e}_b$ and $\hat{e}_c$ are the rotational phase voltage terms and i_a , i_b and i_c are the stator three-phase currents.

The rotational voltage components are defined as:

$$\hat{E}_{abc} = \dot{L}_{abc}.I \tag{3-31}$$

Where,

$$\dot{L}_{abc} = dL_{abc} / dt$$

Taking phase "a" as an example, Equation 3-31 becomes:

$$\begin{aligned}\hat{e}_a = {} & (dL_{aa} / dt)i_a + (dL_{ab} / dt)i_b + (dL_{ac} / dt)i_c + (dL_{aF} / dt)i_F + (dL_{aD} / dt)i_D + \\ & (dL_{aG} / dt)i_G + (dL_{aQ} / dt)i_Q\end{aligned} \tag{3-32}$$

Similar expressions can be written for $\hat{e}_b$ and $\hat{e}_c$.

The overall block diagram of the simulated model in Simulink is shown in Figure 3.19. Figure 3.20 shows the block diagram for the electromagnetic torque calculation.

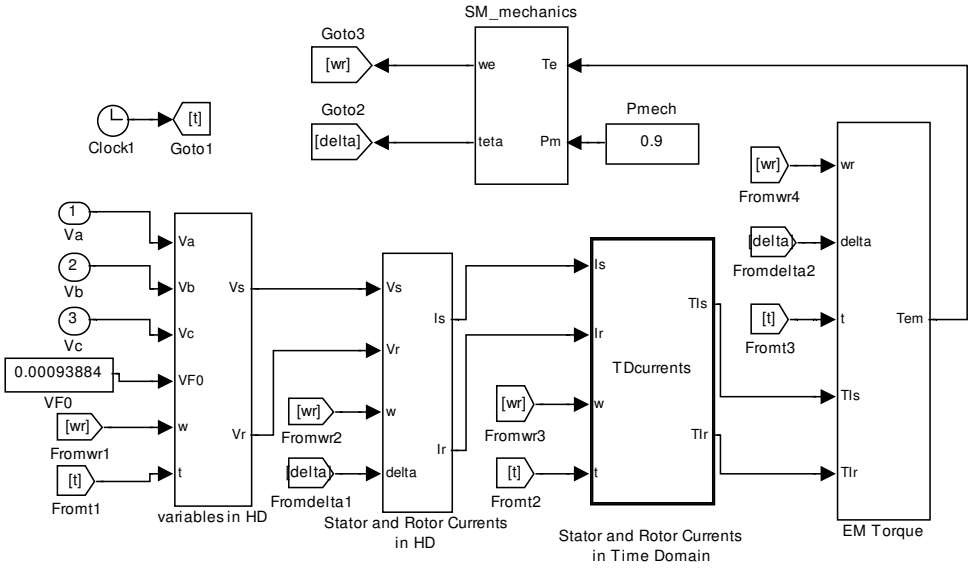

Figure 3.19. Proposed nonlinear model of a SG

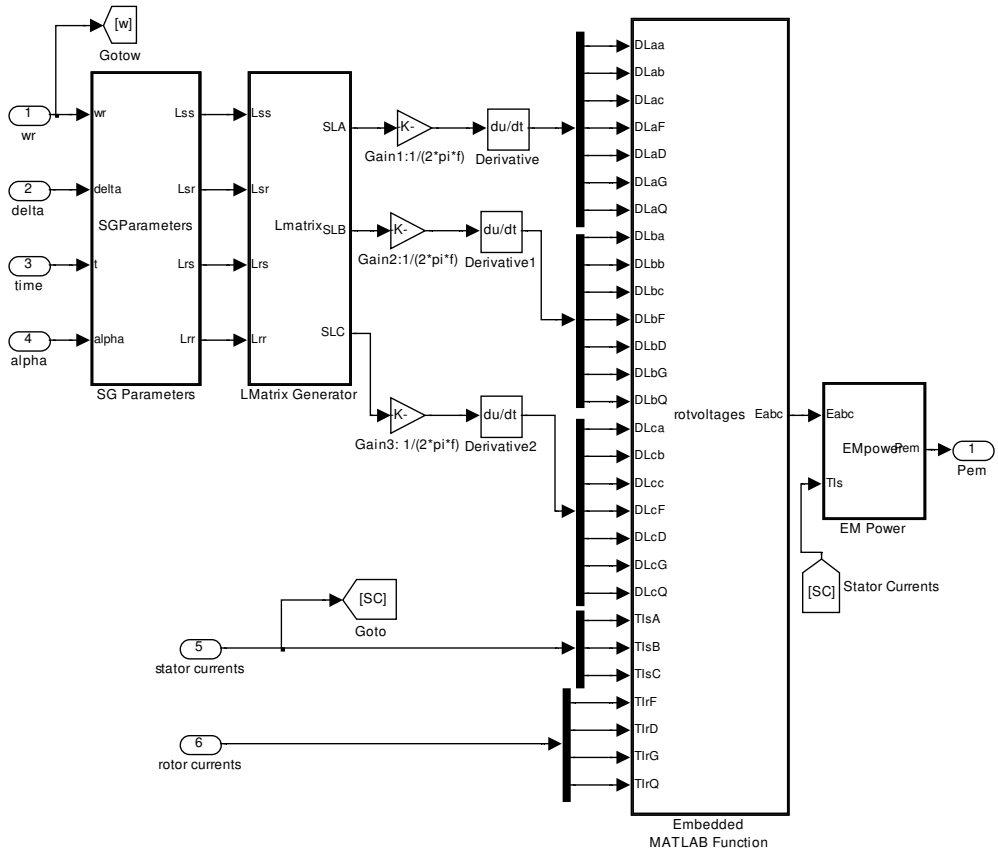

Figure 3.20. Block diagram for time domain calculation of electromagnetic torque

Figure 3.21 demonstrates the instantaneous electromagnetic torques under sinusoidal and harmonic operating conditions (Table 3-3, row 6). In Figure 3-21(a), the produced torque in the sinusoidal system is compared with that produced in the presence of space harmonics. It is observed that space harmonics can cause pulsations in the electromagnetic torque.

Figure 3.21(b) shows that the interaction between time and space harmonics can result in higher electromagnetic torque perturbations.

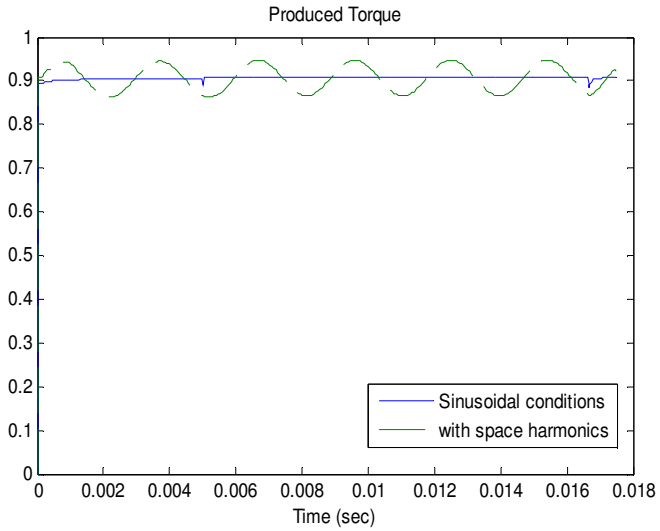

(a)

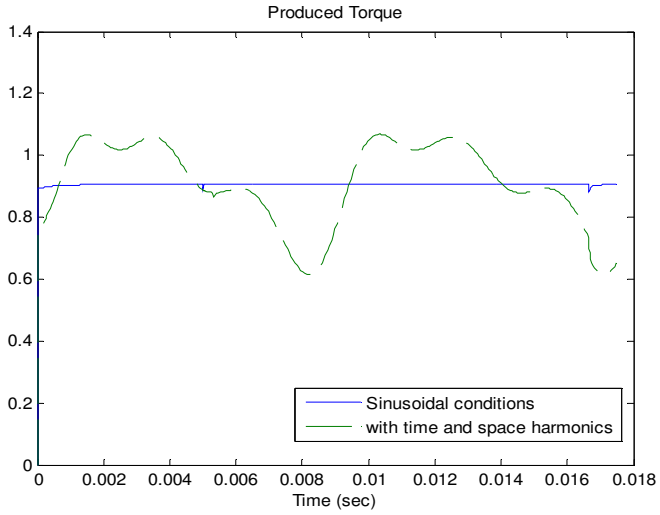

(b)

Figure 3.21. Electromagnetic torques in the presence of (a) space (b) time and space harmonics

Time Domain Simulation of the Rotor Angle:

The rotor angle can also be calculated in the time domain using the electromagnetic torque. This allows further validation of the proposed modified rotor angle calculation method outlined in the previous section.

The variations on rotor angle are related to the electromagnetic torque via the equation of motion (swing equation).

Applying the electromagnetic torque from Figure 3.21(b) to the synchronous generator results in rotor angle variations as shown in Figure 3.22.

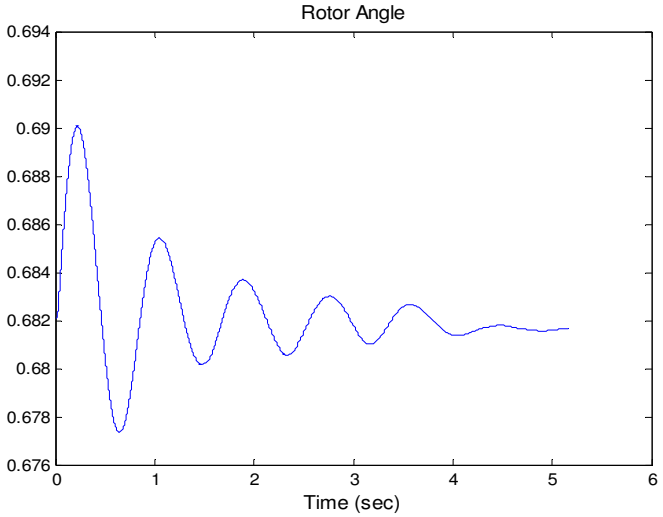

(a)

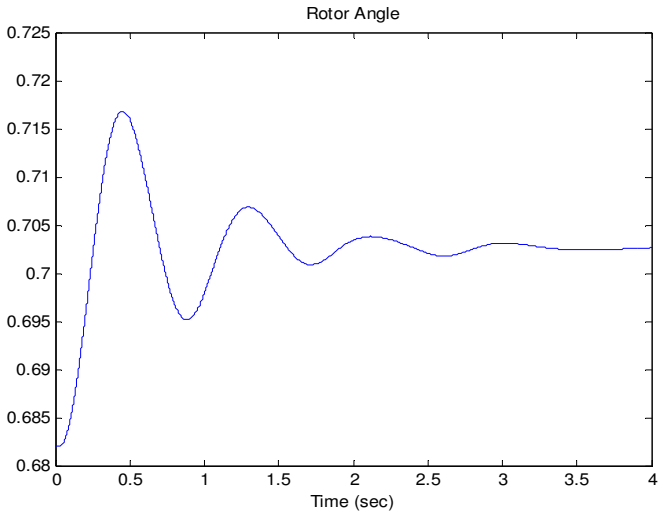

(b)

Figure 3.22. Rotor angle; (a) sinusoidal conditions, (b) in the presence of time and space harmonics

3.6. Conclusions

In this chapter, the operation of a synchronous generator under distorted operating conditions was investigated. A nonlinear model of synchronous generator in the harmonic domain was used to compute the modified stator flux in the presence of time and space harmonics in the *abc*-frame of reference. The effects of damper windings, interaction between time and space harmonics, as well as harmonic phase angles were included and investigated. Park transformation was applied to compute the fundamental component of the modified stator flux and the load angle.

The presence of harmonics in a power system can modify the steady-state operating conditions of synchronous generators. This can cause variations in the induced fundamental component of the stator flux in the synchronous generator, which will result in an increase or reduction in the generated power and hence affect the rotor angle (tables 3-2 and 3-3) and dynamic behaviour of the power system.

Harmonics also impose pulsating torques on the shaft and change the constant component of the electromagnetic torque. They can produce unbalanced three-phase fluxes in stator windings and inject zero sequence voltage into the system.

The main contributions are:

- Time and space harmonics introduce new terms in the main machine equations (Equation 3-19) and may change the steady-state operating point in highly non-sinusoidal environments.
- The fundamental component of the stator flux will contain additional terms due to the interaction between time and space harmonics (Equation 3-24). The modified stator flux is a function of the non-sinusoidal operating conditions.
- Time and space harmonics will change the steady-state operating parameters of a synchronous generator (equations 3-23 to 3-28 and tables 3-2 and 3-3). This may cause variations in system dynamic behaviour as will be demonstrated in the following chapters.
- The induced harmonic currents on damper windings are considerable (tables 3-2 and 3-3) and their impacts on the rotor angle should not be ignored.

- Harmonic phase angles have influence on the steady-state performance of a synchronous generator (Equation 3-25, tables 3-2 and 3-3).

The new operating conditions may trigger some unpredicted problems in the power systems, such as: moving the system eigenvalues, which can cause system instability and modifying the system harmonic resonance points.

Results of this chapter including the modified load angle and fundamental stator fluxes are used for stability studies of distorted power systems in following chapters.

CHAPTER FOUR

SMALL-SIGNAL STABILITY ANALYSIS OF DISTORTED SMIB SYSTEMS

4.1. Introduction

The previous chapter showed that the presence of harmonics can affect the steady state operating conditions of a synchronous generator and apply additional terms to the machine fundamental components. This chapter investigates the influence of these changes on the small-signal stability of a Single Machine Infinite Bus (SMIB) system.

The dynamic behaviour of a power system is determined by fundamental and high frequency oscillations. The high frequency oscillations decay rapidly in the power system and do not have considerable effect on the system small-signal stability. Therefore in this thesis, the impact of harmonics on the system dynamic behaviour is investigated through their impact on the fundamental components of the system parameters. The previous chapter showed that the additional terms into the fundamental components of the stator parameters (fluxes, voltages and currents) are functions of the (non)sinusoidal stator currents, winding structure and the load angle. It means that even considering the constant harmonic values in the period of the dynamic fluctuations, the magnitudes of these additional terms will change by the change of the load angle. This influences the small signal stability of the system and may relocate the system modes. Consequently, harmonic pollution in power system tends to initiate and/or amplify stability problems in distorted power systems. Especially, the increasing application of nonlinear loads and distributed generation due to renewable energy sources in interconnected and isolated power systems causes concerns with respect to the impact of harmonics and poor power quality on the performance and stability of synchronous generators.

In this chapter, the eigenvalues analysis method is used to investigate the influence of harmonics on small-signal behaviour of a distorted power system. Dynamic stability of the power system is evaluated based on the Lyapunov's first method as described in Chapter 2. The system state space equations are calculated by linearizing the differential equations around the operating point using an analytical method. As the system equations will be very complex in the presence of harmonics, a SMIB system is chosen to simplify the calculations. This system helps understanding the behaviour and stability of large Multi Machine Multi Bus power systems. Also, a simple model is considered for the generation bus and the impacts of the excitation system and turbine-governor are not included. The reason for that is to further simplifying the calculations. However, a similar method can be followed to include the dynamics of these components. A complete model of the generation buses in an actual system is studied in Chapter six.

A general configuration of a distorted power system is shown in Figure 4.1. For dynamic analysis, the system is simplified as a single synchronous machine connected to a large system as shown in Figure 4.2. Note that space harmonics are included at the generator bus and time harmonics are considered at the distorted infinite bus.

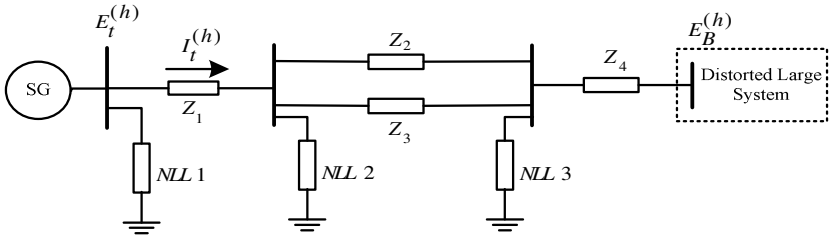

Figure 4.1. A distorted SMIB power system

4.2. State Space Equations of a Distorted SMIB System

The eigenvalue analysis method is used to conduct the small signal stability studies of a distorted SMIB system, shown in Figure 4.2. The influences of nonlinear loads in the system are considered as harmonic voltages at the infinite bus. The voltage

harmonics at the infinite bus and the corresponding current harmonics through the transmission line can be calculated using harmonic power flow methods.

In this section, the effects of damper windings on small-signal stability are ignored. These will be included in the next section.

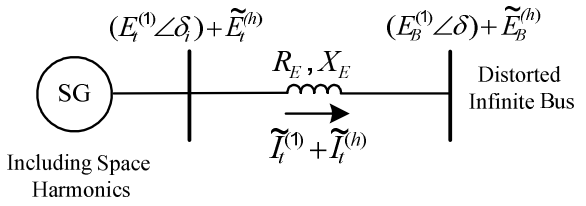

Figure 4.2. A distorted SMIB system equivalent circuit

The system state space equations are arranged in the following general form [2]:

$$\begin{bmatrix}\Delta\dot{\omega}_r\\ \Delta\dot{\delta}\\ \Delta\dot{\psi}_{fd}\end{bmatrix}=[A]\begin{bmatrix}\Delta\omega_r\\ \Delta\delta\\ \Delta\psi_{fd}\end{bmatrix}+[B]\begin{bmatrix}\Delta T_m\\ \Delta E_{fd}\end{bmatrix} \tag{4-1}$$

where matrices *[A]* and *[B]* are calculated using the linearized swing equation and the rotor circuit dynamic equation as follows:

$$\begin{aligned}\frac{d\Delta\omega_r}{dt}&=\frac{1}{2H}(\Delta T_m-\Delta T_e^{(1)}-K_D\,\Delta\omega_r)\\ \frac{d\Delta\delta}{dt}&=\omega_0\,\Delta\omega_r\\ \frac{d\Delta\psi_{Fd}}{dt}&=\omega_0(\Delta e_{Fd}-R_{Fd}\,\Delta I_F)\end{aligned} \tag{4-2}$$

In the above equations, K_D is the damping factor ("pu torque" divided by "pu angular velocity") and H is the unit inertia constant. The electromagnetic torque at synchronous speed due to the fundamental and harmonic currents and voltages, $T_e^{(1)}$, is computed using the following equation [2]:

$$T_e^{(1)}=\psi_d^{(modified)}\,i_q^{(1)}-\psi_q^{(modified)}\,i_d^{(1)} \tag{4-3}$$

$\psi_d^{(modified)}$ and $\psi_q^{(modified)}$ are the modified fluxes and contain additional terms due to the presence of time and space harmonics. These can be computed using Equation 3-24, which is repeated as follows:

$$\begin{aligned}\psi_d^{(1)} &= \psi_d^{(modified)} = -L_d i_d^{(1)} + M_F^{(1)} I_F^{(DC)} + \psi_d^{due\ to\ harm} \\ \psi_q^{(1)} &= \psi_q^{(modified)} = -L_q i_q^{(1)} + \psi_q^{due\ to\ harm}\end{aligned} \tag{4-4}$$

To computed currents $i_d^{(1)}$ and $i_q^{(1)}$, the system and machine equations are written and solved. It should be mentioned that the method employed is similar to the conventional one, however including the harmonics make the calculation more complex.

System Equations:

The system equation is written in the *abc*-frame [2]:

$$\tilde{E}_t^{(1)} = (R_E + jX_E)\tilde{I}_t^{(1)} + \tilde{E}_B^{(1)} \tag{4-5}$$

The above equation is transferred into the *dq*-frame of reference:

$$\begin{cases} e_d^{(1)} = R_E\, i_d^{(1)} - X_E\, i_q^{(1)} + E_{Bd}^{(1)} \\ e_q^{(1)} = R_E\, i_q^{(1)} + X_E\, i_d^{(1)} + E_{Bq}^{(1)} \end{cases} \tag{4-6}$$

where:

$$\begin{cases} e_d^{(1)} = E_t^{(1)} \sin(\delta_i) \\ e_q^{(1)} = E_t^{(1)} \cos(\delta_i) \end{cases}, \quad \begin{cases} E_{Bd}^{(1)} = E_B^{(1)} \sin(\delta) \\ E_{Bq}^{(1)} = E_B^{(1)} \cos(\delta) \end{cases} \tag{4-7}$$

From equations 4-6 and 4-7, the rotor angle (δ_i) can be calculated as a function of the system parameters:

$$\delta_i = \arctan\left(\frac{E_B^{(1)} \sin(\delta) + R_E i_d^{(1)} - X_E i_q^{(1)}}{E_B^{(1)} \cos(\delta) + R_E i_q^{(1)} + X_E i_d^{(1)}}\right) \tag{4-8}$$

Machine Equations:

The fundamental stator voltages in the *dq*-frame of reference have the following conventional form [2]:

$$\begin{cases} e_d^{(1)} = -R_a\, i_d^{(1)} - \psi_q^{(1)} \\ e_q^{(1)} = -R_a\, i_q^{(1)} + \psi_d^{(1)} \end{cases} \tag{4-9}$$

And the field winding current can be calculated as:

$$I_F = \frac{\psi_{Fd} + M_F^{(1)} i_d^{(1)}}{L_F} \tag{4-10}$$

Using equations 4-6, 4-7 and 4-9, the fundamental stator currents are obtained:

$$i_d^{(1)} = \frac{X_{Tq}[\psi_{Fd}(\frac{M_F^{(1)}}{L_F}) - E_B^{(1)} cos(\delta) + \psi_d^{due\ to\ harm}] - (\psi_q^{due\ to\ harm} + E_B^{(1)} sin(\delta))R_T}{D}$$

$$i_q^{(1)} = \frac{R_T[\psi_{Fd}(\frac{M_F^{(1)}}{L_F}) - E_B^{(1)} cos(\delta) + \psi_d^{due\ to\ harm}] + (\psi_q^{due\ to\ harm} + E_B^{(1)} sin(\delta))X_{Td}}{D}$$

$$\begin{aligned} X_{Tq} &= X_E + L_q \\ X_{Td} &= X_E + L_d - \frac{(M_F^{(1)})^2}{L_F} \\ R_T &= R_E + R_a \\ D &= X_{Tq}\ X_{Td} + R_T^2 \end{aligned} \tag{4-11}$$

In order to identify the system eigenvalues, the electromagnetic torque is linearized around the operating point:

$$\Delta T_e^{(1)} = \Delta\psi_d^{(1)} i_{q0}^{(1)} + \psi_{d0}^{(1)} \Delta i_q^{(1)} - \Delta\psi_q^{(1)} i_{d0}^{(1)} - \psi_{q0}^{(1)} \Delta i_d^{(1)} \tag{4-12}$$

The initial values of the stator currents and fluxes can be calculated using equations 3-28, 4-4 and 4-11. Deviations of the stator fluxes and currents should be calculated as a function of state variables in the general form of:

$$\begin{cases} \Delta f = e_{1f}\Delta\psi_{Fd} + e_{2f}\Delta\delta \\ f = i_d, i_q, \psi_d, \psi_q \end{cases} \tag{4-13}$$

Linearizing Equation 4-11 around the operating point, deviations of the stator currents are computed as:

$$\begin{aligned} \Delta i_d^{(1)} &= m_1\Delta\psi_{Fd} + m_2\Delta\delta + m_3\Delta\psi_d^{due\ to\ harm} + m_4\Delta\psi_q^{due\ to\ harm} \\ \Delta i_q^{(1)} &= n_1\Delta\psi_{Fd} + n_2\Delta\delta + n_3\Delta\psi_d^{due\ to\ harm} + n_4\Delta\psi_q^{due\ to\ harm} \end{aligned} \tag{4-14}$$

$$m_1 = \frac{X_{Tq} M_F^{(1)}}{L_F D},\ m_2 = \frac{X_{Tq} E_B^{(1)} \sin(\delta_0) - R_T E_B^{(1)} \cos(\delta_0)}{D},\ m_3 = \frac{X_{Tq}}{D},\quad m_4 = -\frac{R_T}{D}$$

$$n_1 = \frac{R_T M_F^{(1)}}{L_F D},\ n_2 = \frac{R_T E_B^{(1)} \sin(\delta_0) + X_{Td} E_B^{(1)} \cos(\delta_0)}{D},\ n_3 = \frac{R_T}{D},\quad n_4 = \frac{X_{Td}}{D}$$

The deviations of the additional stator flux components ($\Delta\psi_d^{due\ to\ harm}$ and $\Delta\psi_q^{due\ to\ harm}$) are also calculated as a function of state variables.

Considering constant harmonic currents in the field winding during perturbation, and using Equation 3-25, $\Delta\psi_d^{due\ to\ harm}$ and $\Delta\psi_q^{due\ to\ harm}$ can be determined as a function of $\Delta\theta_i$, where $\theta_i = (\delta_i - \pi/2)$. θ_i is equal to $\theta_\circ$ for the steady-state operation.

$$\begin{aligned}\Delta\psi_d^{due\ to\ harm} &= N\,\Delta\theta_i \\ \Delta\psi_q^{due\ to\ harm} &= M\,\Delta\theta_i\end{aligned} \tag{4-15}$$

where

$$N = (-h)\left(\frac{I_F^{(h)}}{2}\right)\left(M_F^{(h+1)} + M_F^{(h-1)}\right)\sin\left(h\theta_0 - \theta_F^{(h)}\right) - (h)k\left(\frac{I_S^{(h')}}{2}\right)\left(L_m^{(h'+1)}\right)\sin\left(h'\theta_0 - \theta_{is}^{(h')}\right)$$

$$M = (h)\left(\frac{I_F^{(h)}}{2}\right)\left(M_F^{(h+1)} - M_F^{(h-1)}\right)\cos\left(h\theta_0 - \theta_F^{(h)}\right) + (h)k\left(\frac{I_S^{(h')}}{2}\right)\left(L_m^{(h'+1)}\right)\cos\left(h'\theta_0 - \theta_{is}^{(h')}\right)$$

From Equation 4-7:

$$\begin{aligned}&\delta_i = \arctan(P), \quad P = \frac{R_E\, i_d^{(1)} - X_E\, i_q^{(1)} + E_B^{(1)}\sin(\delta)}{R_E\, i_q^{(1)} + X_E\, i_d^{(1)} + E_B^{(1)}\cos(\delta)} \\ &\Delta\delta_i = \frac{1}{P_0^2 + 1}\left[A\,\Delta\delta + B\,\Delta i_d^{(1)} + C\,\Delta i_q^{(1)}\right] \\ &P_0 = P\big|_{\delta=\delta_0, i_d=i_{d0}, i_q=i_{q0}} \\ &A = \left.\frac{dP}{d\delta}\right|_{\delta=\delta_0, i_d=i_{d0}, i_q=i_{q0}}, B = \left.\frac{dP}{di_d^{(1)}}\right|_{\delta=\delta_0, i_d=i_{d0}, i_q=i_{q0}}, C = \left.\frac{dP}{di_q^{(1)}}\right|_{\delta=\delta_0, i_d=i_{d0}, i_q=i_{q0}}\end{aligned} \tag{4-16}$$

and $\Delta\theta_i = \Delta\delta_i$.

Substituting $\Delta\theta_i$ into Equation 4-15:

$$\begin{aligned}\Delta\psi_d^{due\ to\ harm} &= \frac{N}{\mathrm{P}_0^2+1}[A\,\Delta\delta + B\,\Delta i_d^{(1)} + C\,\Delta i_q^{(1)}] \\ \Delta\psi_q^{due\ to\ harm} &= \frac{M}{\mathrm{P}_0^2+1}[A\,\Delta\delta + B\,\Delta i_d^{(1)} + C\,\Delta i_q^{(1)}]\end{aligned} \tag{4-17}$$

Solving equations 4-4, 4-14 and 4-17, deviations of the stator currents and fluxes can be computed in the desired form:

$$\begin{cases}\Delta i_d^{(1)} = g_{d1}\,\Delta\psi_{Fd} + g_{d2}\Delta\delta \\ \Delta i_q^{(1)} = g_{q1}\Delta\psi_{Fd} + g_{q2}\Delta\delta\end{cases}, \quad \begin{cases}\Delta\psi_d^{(1)} = f_{d1}\,\Delta\psi_{Fd} + f_{d2}\Delta\delta \\ \Delta\psi_q^{(1)} = f_{q1}\Delta\psi_{Fd} + f_{q2}\Delta\delta\end{cases} \tag{4-18}$$

where f and g are functions of the initial values of the stator currents (fundamental and time harmonics), stator fluxes, steady-state load angle, rotor currents (dc and harmonic components) and space harmonics (Details are given in Appendix B).

Substituting the expressions for the stator currents and fluxes from Equation 4-18 into Equation 4-12, the deviation of electromagnetic torque is calculated as:

$$\begin{aligned}\Delta T_e &= K_1^{(harm)}\Delta\delta + K_2^{(harm)}\Delta\psi_{Fd} \\ K_1^{(harm)} &= i_{q0}^{(1)} f_{d2} + \psi_{d0}^{(1)} g_{q2} - i_{d0}^{(1)} f_{q2} - \psi_{q0}^{(1)} g_{d2} \\ K_2^{(harm)} &= i_{q0}^{(1)} f_{d1} + \psi_{d0}^{(1)} g_{q1} - i_{d0}^{(1)} f_{q1} - \psi_{q0}^{(1)} g_{d1}\end{aligned} \tag{4-19}$$

Linearizing the field circuit dynamic equation around the operating point gives:

$$\Delta\dot{\psi}_{Fd} = \omega_0(\,\Delta e_{Fd} - R_{Fd}\,\Delta I_F\,) \tag{4-20}$$

From equations 4-10 and 4-18:

$$\Delta I_F = (\frac{1}{L_F} + \frac{g_{d1}M_F^{(1)}}{L_F})\Delta\psi_{Fd} + (\frac{g_{d2}M_F^{(1)}}{L_F})\Delta\delta \tag{4-21}$$

Using equations 4-2, 4-19 and 4-20, the state space equations for the distorted SMIB system are obtained in the desired form:

$$\begin{bmatrix}\Delta\dot{\omega}_r \\ \Delta\dot{\delta} \\ \Delta\dot{\psi}_{fd}\end{bmatrix} = \begin{bmatrix}a_{11} & a_{12}^{(harm)} & a_{13}^{(harm)} \\ a_{21} & 0 & 0 \\ 0 & a_{32}^{(harm)} & a_{33}^{(harm)}\end{bmatrix}\begin{bmatrix}\Delta\omega_r \\ \Delta\delta \\ \Delta\psi_{fd}\end{bmatrix} + \begin{bmatrix}b_{11} & 0 \\ 0 & 0 \\ 0 & b_{32}\end{bmatrix}\begin{bmatrix}\Delta T_m \\ \Delta e_{fd}\end{bmatrix} \tag{4-22}$$

where

$$a_{11} = \frac{-K_D}{2H},\ a_{12}^{(harm)} = \frac{-K_1^{(harm)}}{2H},\ a_{13}^{(harm)} = \frac{-K_2^{(harm)}}{2H}$$

$$a_{21} = \omega_0$$

$$a_{32}^{(harm)} = \frac{-R_{Fd}\omega_0 g_{d2} M_F^{(1)}}{L_F},\ a_{33}^{(harm)} = \frac{-R_{Fd}\omega_0 (1 + g_{d1} M_F^{(1)})}{L_F}$$

$$b_{11} = \frac{1}{2H}$$

$$b_{32} = \omega_0$$

Two points are important to note in the above analysis:

Firstly, the spectra of the injected stator harmonic currents due to the presence of nonlinear loads are assumed to be constant and can be measured at the synchronous generator bus or calculated by performing harmonic power flow calculations. However, the approach is valid for any given stator harmonic configuration.

Secondly, the induced rotor harmonic currents are computed using the proposed synchronous generator nonlinear model of Chapter three for distorted steady state operating point and is assumed constant during the perturbation.

Figure 4.3 shows a block diagram representation for evaluating the dynamic behaviour of the distorted SMIB system shown in Figure 4.2. Constants $K_1^{(harm)}$, $K_2^{(harm)}$, $K_3^{(harm)}$, $K_4^{(harm)}$ and $T_3^{(harm)}$ account for dynamic characteristics of the system and are functions of the synchronous generator parameters, system initial conditions and the harmonic distortion levels. These constants also include additional terms due to the interaction between time and space harmonics.

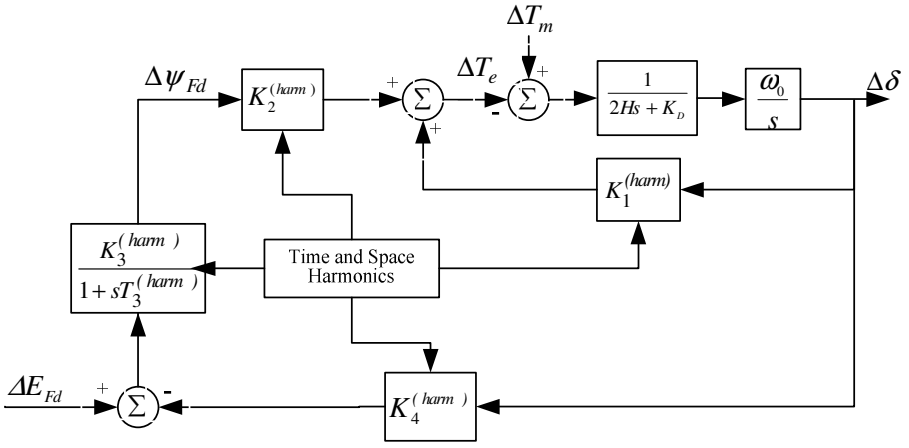

Figure 4.3. Modified Heffron- Phillips model of the distorted SMIB system for dynamic studies

Ignoring the presence of harmonics, the block diagram of Figure 4.3 and the expressions for the constants will be identical to the conventional forms of sinusoidal analysis [2]. However, when considering harmonics the values of the constants are modified as follows:

$K_1^{(harm)}$ and $K_2^{(harm)}$, as defined in Equation 4-19,

$$\begin{cases} K_1^{(harm)} = i_{q0}^{(1)} f_{d2} + \psi_{d0}^{(1)} g_{q2} - i_{d0}^{(1)} f_{q2} - \psi_{q0}^{(1)} g_{d2} \\ K_2^{(harm)} = i_{q0}^{(1)} f_{d1} + \psi_{d0}^{(1)} g_{q1} - i_{d0}^{(1)} f_{q1} - \psi_{q0}^{(1)} g_{d1} \end{cases}$$

$$K_3^{(harm)} = -\frac{b_{32}}{a_{33}^{(harm)}}, \quad K_4^{(harm)} = -\frac{a_{32}^{(harm)}}{b_{32}} \tag{4-23}$$

$$T_3^{(harm)} = -\frac{1}{a_{33}^{(harm)}}$$

where $a_{32}^{(harm)}$, $a_{33}^{(harm)}$ and b_{32} are defined in Equation 4-22.

4.2.1. Impact of Damper Windings on the Dynamic Behaviour of a Distorted SMIB System

Under sinusoidal conditions, damper windings can improve dynamic behaviour of the power systems [2]. Chapter three shows that for harmonically polluted conditions, damper windings affect the steady-state operating parameters of a synchronous generator, such as the load angle.

To investigate the impact of damper windings on the dynamic behaviour of the distorted SMIB system, three damper windings, one on the *d*-axis (L_D) and two on the *q*-axis (L_G, L_Q) are included in the generator model. Additional rotor circuit equations are as follows:

$$\begin{aligned} \frac{d\psi_D}{dt} &= -\omega_0 R_D I_D \\ \frac{d\psi_G}{dt} &= -\omega_0 R_G I_G \\ \frac{d\psi_Q}{dt} &= -\omega_0 R_Q I_Q \end{aligned} \tag{4-24}$$

The damper windings' fluxes are considered as the additional state variables in the system state equations.

To calculate the system state matrix, a similar approach as outlined in Section 4-2 is followed with some modifications of the machine equations to include the damper windings:

Stator fluxes:

$$\begin{cases} \psi_d^{(1)} = \psi_d^{(modified)} = -L_d i_d^{(1)} + M_F^{(1)} I_F + M_D^{(1)} I_D + \psi_d^{due\ to\ harm} \\ \psi_q^{(1)} = \psi_q^{(modified)} = -L_q i_q^{(1)} + M_G^{(1)} I_G + M_Q^{(1)} I_Q + \psi_q^{due\ to\ harm} \end{cases} \tag{4-25}$$

Rotor fluxes:

$$\begin{cases} \psi_F = -M_F i_d^{(1)} + L_F I_F + L_{FD} I_D \\ \psi_D = -M_D i_d^{(1)} + L_D I_D + L_{FD} I_F \\ \psi_G = -M_G i_q^{(1)} + L_G I_G + L_{GQ} I_Q \\ \psi_Q = -M_Q i_q^{(1)} + L_Q I_Q + L_{GQ} I_G \end{cases} \tag{4-26}$$

Expressions for the deviations of the additional fundamental stator fluxes due to harmonics in *dq* axes (Equation 4-15) are modified as:

$$\begin{aligned} \Delta\psi_d^{due\ to\ harm} &= N\,\Delta\theta_i \\ \Delta\psi_q^{due\ to\ harm} &= M\,\Delta\theta_i \end{aligned} \tag{4-27}$$

where

$$N = \sum_{K=F,D} (-h)\left(\frac{I_K^{(h)}}{2}\right)\left(M_K^{(h+1)} + M_K^{(h-1)}\right) sin\left(h\theta_0 - \theta_K^{(h)}\right) -$$

$$\sum_{K=G,Q} (h)\left(\frac{I_K^{(h)}}{2}\right)\left(M_K^{(h+1)} + M_K^{(h-1)}\right) cos\left(h\theta_0 - \theta_K^{(h)}\right) - (h)k\left(\frac{I_S^{(h')}}{2}\right)\left(L_m^{(h'+1)}\right) sin\left(h'\theta_0 - \theta_{is}^{(h')}\right)$$

$$M = \sum_{K=F,D} (h)\left(\frac{I_K^{(h)}}{2}\right)\left(M_K^{(h+1)} - M_K^{(h-1)}\right) cos\left(h\theta_0 - \theta_K^{(h)}\right) +$$

$$\sum_{K=G,Q} (-h)\left(\frac{I_K^{(h)}}{2}\right)\left(M_K^{(h+1)} - M_K^{(h-1)}\right) sin\left(h\theta_0 - \theta_K^{(h)}\right) + (h)k\left(\frac{I_S^{(h')}}{2}\right)\left(L_m^{(h'+1)}\right) cos\left(h'\theta_0 - \theta_{is}^{(h')}\right)$$

Using equations 4-6, 4-7 and 4-9 along with equations 4-25 and 4-26, the deviations of stator and rotor currents can be calculated as:

Stator Currents:

$$\begin{cases} \Delta i_d^{(1)} = m_1\Delta\delta + m_2\Delta\psi_F + m_3\Delta\psi_D + m_4\Delta\psi_G + m_5\Delta\psi_Q \\ \Delta i_q^{(1)} = n_1\Delta\delta + n_2\Delta\psi_F + n_3\Delta\psi_D + n_4\Delta\psi_G + n_5\Delta\psi_Q \end{cases} \tag{4-28}$$

Rotor Currents:

$$\begin{cases} \Delta I_F = F_1\Delta\delta + F_2\Delta\psi_F + F_3\Delta\psi_D + F_4\Delta\psi_G + F_5\Delta\psi_Q \\ \Delta I_D = D_1\Delta\delta + D_2\Delta\psi_F + D_3\Delta\psi_D + D_4\Delta\psi_G + D_5\Delta\psi_Q \\ \Delta I_G = G_1\Delta\delta + G_2\Delta\psi_F + G_3\Delta\psi_D + G_4\Delta\psi_G + G_5\Delta\psi_Q \\ \Delta I_Q = Q_1\Delta\delta + Q_2\Delta\psi_F + Q_3\Delta\psi_D + Q_4\Delta\psi_G + Q_5\Delta\psi_Q \end{cases} \tag{4-29}$$

where the expressions for the coefficients *m, n, F, D, G* and *Q* are presented in Appendix B, equations B-11 and B-12.

Next, the stator fluxes (Equation 4-25) are linearized around the operating point using Equation 4-27 and the expressions for the stator and rotor currents are substituted from equations 4-28 and 4-29 to get:

$$\begin{cases} \Delta\psi_d^{(1)} = s_1\Delta\delta + s_2\Delta\psi_F + s_3\Delta\psi_D + s_4\Delta\psi_G + s_5\Delta\psi_Q \\ \Delta\psi_q^{(1)} = t_1\Delta\delta + t_2\Delta\psi_F + t_3\Delta\psi_D + t_4\Delta\psi_G + t_5\Delta\psi_Q \end{cases} \tag{4-30}$$

where coefficients ' s_1 to s_5' and ' t_1 to t_5' are defined in Appendix B, Equation B-13.

Using the above equations, the electromagnetic torque (Equation 4-19) is modified to include the fluxes of damper windings; as follows:

$$\begin{aligned} \Delta T_e &= K_1^{(harm)}\Delta\delta + K_2^{(harm)}\Delta\psi_F + K_3^{(harm)}\Delta\psi_D + K_4^{(harm)}\Delta\psi_G + K_5^{(harm)}\Delta\psi_Q \\ K_1^{(harm)} &= i_{q0}^{(1)}s_1 + \psi_{d0}^{(1)}n_1 - i_{d0}^{(1)}t_1 - \psi_{q0}^{(1)}m_1 \\ K_2^{(harm)} &= i_{q0}^{(1)}s_2 + \psi_{d0}^{(1)}n_2 - i_{d0}^{(1)}t_2 - \psi_{q0}^{(1)}m_2 \\ K_3^{(harm)} &= i_{q0}^{(1)}s_3 + \psi_{d0}^{(1)}n_3 - i_{d0}^{(1)}t_3 - \psi_{q0}^{(1)}m_3 \\ K_4^{(harm)} &= i_{q0}^{(1)}s_4 + \psi_{d0}^{(1)}n_4 - i_{d0}^{(1)}t_4 - \psi_{q0}^{(1)}m_4 \\ K_5^{(harm)} &= i_{q0}^{(1)}s_5 + \psi_{d0}^{(1)}n_5 - i_{d0}^{(1)}t_5 - \psi_{q0}^{(1)}m_5 \end{aligned} \tag{4-31}$$

Linearizing the rotor circuit dynamic equations (Equation 4-23) and substituting the electromagnetic torque deviation (Equation 4-30) into the swing equation, the following state space equations are obtained for the distorted SMIB system:

$$\begin{bmatrix} \Delta\dot{\omega}_r \\ \Delta\dot{\delta} \\ \Delta\dot{\psi}_F \\ \Delta\dot{\psi}_D \\ \Delta\dot{\psi}_G \\ \Delta\dot{\psi}_Q \end{bmatrix} = \begin{bmatrix} a_{11} & a_{12}^{(harm)} & a_{13}^{(harm)} & a_{14}^{(harm)} & a_{15}^{(harm)} & a_{16}^{(harm)} \\ a_{21} & 0 & 0 & 0 & 0 & 0 \\ 0 & a_{32}^{(harm)} & a_{33}^{(harm)} & a_{34}^{(harm)} & a_{35}^{(harm)} & a_{36}^{(harm)} \\ 0 & a_{42}^{(harm)} & a_{43}^{(harm)} & a_{44}^{(harm)} & a_{45}^{(harm)} & a_{46}^{(harm)} \\ 0 & a_{52}^{(harm)} & a_{53}^{(harm)} & a_{54}^{(harm)} & a_{55}^{(harm)} & a_{56}^{(harm)} \\ 0 & a_{62}^{(harm)} & a_{63}^{(harm)} & a_{64}^{(harm)} & a_{65}^{(harm)} & a_{66}^{(harm)} \end{bmatrix} \begin{bmatrix} \Delta\omega_r \\ \Delta\delta \\ \Delta\psi_F \\ \Delta\psi_D \\ \Delta\psi_G \\ \Delta\psi_Q \end{bmatrix} + \begin{bmatrix} b_{11} & 0 \\ 0 & 0 \\ 0 & b_{32} \\ 0 & 0 \\ 0 & 0 \\ 0 & 0 \end{bmatrix} \begin{bmatrix} \Delta T_m \\ \Delta e_{fd} \end{bmatrix} \quad (4\text{-}32)$$

where

$$a_{11} = \frac{K_D}{2H},\ a_{12}^{(harm)} = \frac{K_1^{(harm)}}{2H},\ a_{13}^{(harm)} = \frac{K_2^{(harm)}}{2H},\ a_{14}^{(harm)} = \frac{K_3^{(harm)}}{2H},$$

$$a_{15}^{(harm)} = \frac{K_4^{(harm)}}{2H},\ a_{16}^{(harm)} = \frac{K_5^{(harm)}}{2H}$$

$$a_{21} = \omega_0$$

$$a_{32}^{(harm)} = R_F\omega_0 F_1,\ a_{33}^{(harm)} = R_F\omega_0 F_2,\ a_{34}^{(harm)} = R_F\omega_0 F_3,$$

$$a_{35}^{(harm)} = R_F\omega_0 F_4,\ a_{36}^{(harm)} = R_F\omega_0 F_5$$

$$a_{42}^{(harm)} = R_D\omega_0 D_1,\ a_{43}^{(harm)} = R_D\omega_0 D_2,\ a_{44}^{(harm)} = R_D\omega_0 D_3,$$

$$a_{45}^{(harm)} = R_D\omega_0 D_4,\ a_{46}^{(harm)} = R_D\omega_0 D_5$$

$$a_{52}^{(harm)} = R_G\omega_0 G_1,\ a_{53}^{(harm)} = R_G\omega_0 G_2,\ a_{54}^{(harm)} = R_G\omega_0 G_3,$$

$$a_{55}^{(harm)} = R_G\omega_0 G_4,\ a_{56}^{(harm)} = R_G\omega_0 G_5$$

$$a_{62}^{(harm)} = R_G\omega_0 Q_1,\ a_{63}^{(harm)} = R_G\omega_0 Q_2,\ a_{64}^{(harm)} = R_G\omega_0 Q_3,$$

$$a_{65}^{(harm)} = R_G\omega_0 Q_4,\ a_{66}^{(harm)} = R_G\omega_0 Q_5$$

$$b_{11} = \frac{1}{2H},\ b_{32} = \omega_0$$

4.3. Dynamic Simulation of a Distorted SMIB System

The small-signal stability of a distorted SMIB system, shown in Figure 4.2, is investigated using eigenvalue analysis. The synchronous generator characteristics used are the same as those presented in Section 3.5. This generator is connected to the infinite bus through a transmission line with the total reactance of 0.65pu. Results for different harmonic levels are compared to results for sinusoidal operation and the impact of damper windings is investigated.

Case 1- Sinusoidal Operation:

The system is assumed to be sinusoidal and the synchronous generator is delivering 555 MVA at 0.9p.f. (lag) at rated terminal voltages. The effect of magnetic saturation is neglected.

The system initial conditions and eigenvalues are calculated for the synchronous generator model with and without damper windings.

(a) Without Damper Windings

The system initial conditions are the same as those in Section 3.5:

$L_d = 1.5360,\ L_q = 1.4940$

$\delta_0 = 39.0757,\ I_{d0} = 0.9058,\ I_{q0} = 0.4239$

Using Equation 4-22, the system eigenvalues and the corresponding damped frequency and damping ratio are calculated as:

$$\begin{cases} \lambda_{1,2} = -0.1232 \pm 6.0218j, (\ \omega_d = 0.95Hz,\ \zeta = 0.02\ ) \\ \lambda_3 = -0.0901 \end{cases}$$

Examining the participation matrix, the oscillatory mode is found to be associated primarily with the rotor speed and rotor angle:

$$P = \begin{matrix} \\ \\ \\ \end{matrix} \begin{matrix} \lambda_1 \\ \lambda_2 \\ \lambda_3 \end{matrix} \begin{bmatrix} 0.5003 - 0.0102i & 0.5003 + 0.0102i & -0.0006 \\ 0.5003 - 0.0102i & 0.5003 + 0.0102i & -0.0006 \\ -0.0006 + 0.0205i & -0.0006 - 0.0205i & 1.0012 - 0.0000i \end{bmatrix} \begin{matrix} \Delta\omega_r \\ \Delta\delta \\ \Delta\psi_{fd} \end{matrix}$$

Figure 4.4 shows the time response of the synchronous generator speed and electromagnetic torque variations when the generator subject to a mechanical input power change of 0.1pu, at t=5sec.

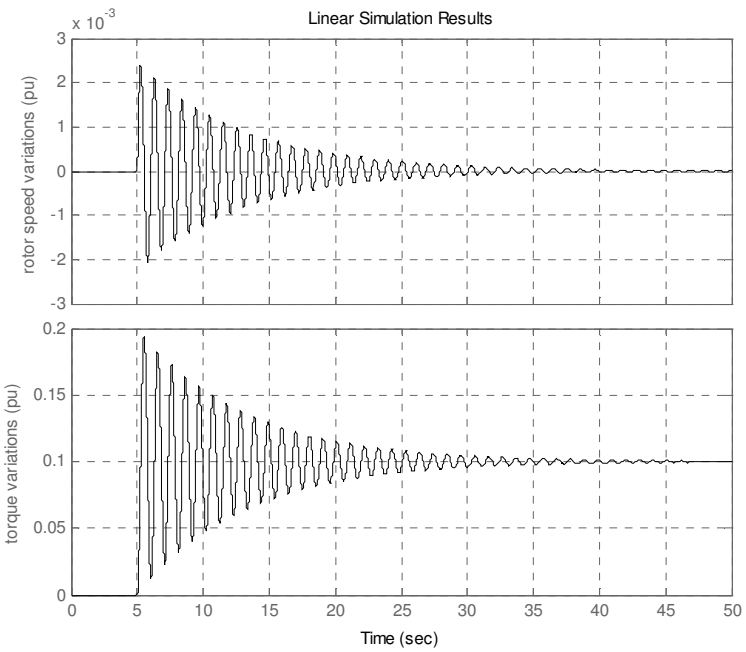

Figure 4.4. Time response of rotor speed and electromagnetic torque variations with input power perturbation under sinusoidal conditions and without damper windings

(b) With Damper Windings

Three damper windings are considered on the rotor, two on the *q*-axis and one on the *d*-axis. The system initial conditions and eigenvalues are calculated as follows:

$$\delta_0 = 39.0757,\ I_{d0} = 0.9058,\ I_{q0} = 0.4239$$

Using Equation 4-32 with no time and space harmonics, the system eigenvalues are calculated as:

$$\begin{cases} \lambda_1 = -36.54 \\ \lambda_2 = -22.67 \\ \lambda_{3,4} = -0.2035 \pm 6.0841j,\ (\omega_d = 0.97Hz,\ \zeta = 0.033) \\ \lambda_5 = -0.085 \\ \lambda_6 = -1.81 \end{cases}$$

The participation matrix indicates that oscillating modes are associated with the rotor speed and rotor angle.

$$
\mathrm{P}=\begin{bmatrix}
-0.0024 & -0.0014 & 0.5029-0.0067i & 0.5029+0.0067i & -0.0006 & -0.0014 \\
-0.0024 & -0.0014 & 0.5029-0.0067i & 0.5029+0.0067i & -0.0006 & -0.0014 \\
0.0123 & 0 & 0.0027+0.0191i & 0.0027-0.0191i & 0.9791 & 0.0032 \\
0.9926 & 0 & -0.0054-0.0063i & -0.0054+0.0063i & 0.0183 & 0 \\
0 & 0.0471 & -0.0003+0.0027i & -0.0003-0.0027i & 0.003 & 0.9505 \\
0 & 0.9556 & -0.0028-0.002i & -0.0028+0.002i & 0.0008 & 0.0491
\end{bmatrix}
\begin{matrix}
\Delta\omega_r \\ \Delta\delta \\ \Delta\psi_{fd} \\ \Delta\psi_D \\ \Delta\psi_G \\ \Delta\psi_Q
\end{matrix}
$$

$$
\begin{matrix}
\lambda_1 & \lambda_2 & \lambda_3 & \lambda_4 & \lambda_5 & \lambda_6
\end{matrix}
$$

Comparing the results to the case with no damper windings shows the frequency of the oscillating mode has increased very slightly from 0.95Hz to 0.97Hz and the damping ratio is improved from (0.02) to (0.033). However, dampers have also slightly shifted the field circuit mode toward the right hand side of the *s*-plane (from -0.09 to -0.085).

The results match in principle with the results of Example 12.5 from [2], which shows the impact of damper windings on the system dynamic stability for sinusoidal conditions.

Figure 4.5 shows the synchronous generator speed and electromagnetic torque variations when the system is subject to an input power change of 0.1pu. Comparing this figure to Figure 4.4 shows that damper windings have improved the torque damping coefficient.

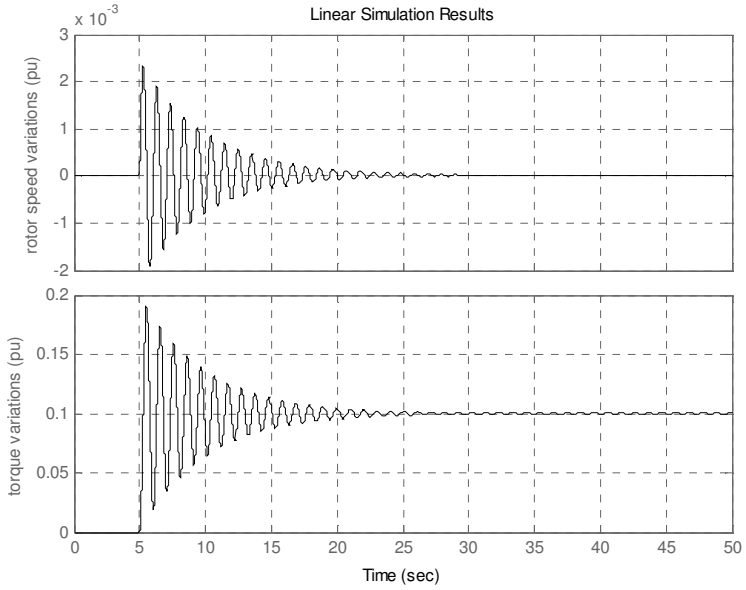

Figure 4.5. Time response of rotor speed and electromagnetic torque variations with input power perturbation under sinusoidal conditions and with damper windings

Case 2- Non-Sinusoidal Operation:

The same configuration and levels of time and space harmonics as outlined in Section 3-5, Case 3 are considered and the generator is delivering its rated power to the system. The steady-state parameters including the load angle, stator currents and stator fluxes are the same as those listed in Table 3-3.

a- Without Damper Windings

Table 4-1 shows the impact of time and space harmonics on the eigenvalues of the distorted SMIB system (using Equation 4-23) when ignoring the impact of damper windings.

Table 4-1
Impact of space and time harmonics on the eigenvalues of distorted SMIB system (without dampers)

Time Harmonic Level	**System Eigenvalues**	**Damped Freq. (ω_d) and Damping Ratio (ξ)**
No harmonics	$\lambda_{1,2} = -0.1232 \pm 6.0218i$ $\lambda_3 = -0.0901$	ω_d =0.9584 ξ =0.0204
1: $Base_T$ * ($\theta_i^{(h)} = 0$)	$\lambda_{1,2} = -0.1103 \pm 6.3021i$ $\lambda_3 = -0.0966$	ω_d =1.003 ξ =0.0175
2: $Base_T$ ($\theta_i^{(h)} = \pi/2$)	$\lambda_{1,2} = -0.1595 \pm 5.4738i$ $\lambda_3 = -0.0517$	ω_d =0.8711 ξ =0.0291
3 : $2\times Base_T$ ($\theta_i^{(h)} = 0$)	$\lambda_{1,2} = -0.108 \pm 6.303i$ $\lambda_3 = -0.0994$	ω_d =1.003 ξ =0.017
4: $2\times Base_T$ * ($\theta_i^{(h)} = \pi/2$)	$\lambda_{1,2}$ = -0.2338 ± 4.4171i $\lambda_3 = 0.0348$	ω_d =0.703 ξ =0.049

*) *0.03pu, 0.05pu, 0.02*pu and *0.01*pu for the 3rd to 9th harmonics, respectively.

The results demonstrate that when the level of the harmonic distortion is increased, considerable variations in the system eigenvalues are observed. The influence of phase angle can not be neglected as it may cause instability on the system by shifting the eigenvalues to the right hand side of the imaginary axis in the *s*-plane (row 6 of Table 4-1).

At harmonic level 4 (row 6 of Table 4-1), the system becomes unstable through the non-oscillatory mode. From the participation matrix, it is observed that the unstable mode is associated with the field circuit.

$$P = \begin{bmatrix} 0.4996 - 0.0264i & 0.4996 + 0.0264i & 0.0008 \\ 0.4996 - 0.0264i & 0.4996 + 0.0264i & 0.0008 \\ 0.0008 + 0.0528i & 0.0008 + 0.0528i & 0.9984 \end{bmatrix} \begin{matrix} \Delta\omega_r \\ \Delta\delta \\ \Delta\psi_{fd} \end{matrix}$$
$$\begin{matrix} \lambda_1 & \lambda_2 & \lambda_3 \end{matrix}$$

Figure 4.6 shows the system time response to a mechanical input power change of 0.1pu for harmonic level 4. It can be seen that although oscillatory modes have positive damping, the system will be unstable through the non-oscillating mode.

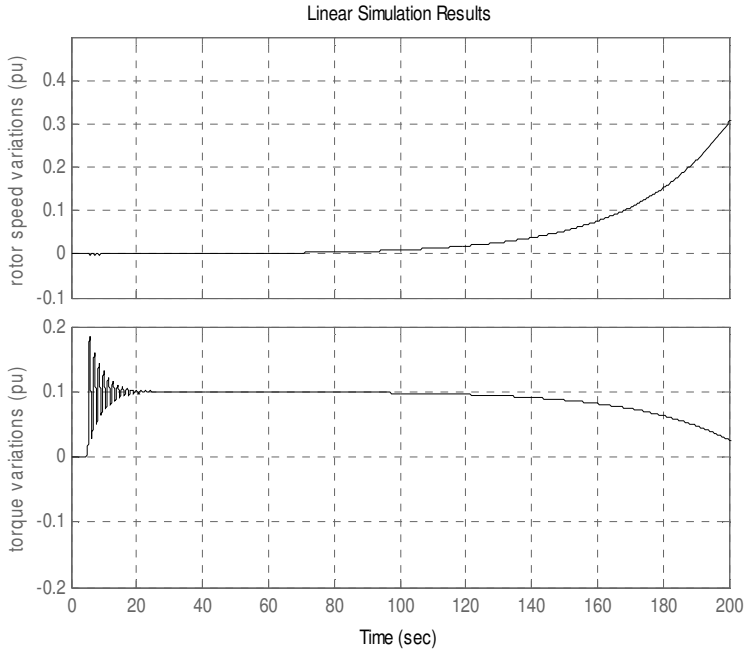

Figure 4.6. Time response of rotor speed and electromagnetic torque variations subject to an input power perturbation in the presence of time and space harmonics (without damper windings) for the SMIB of Figure 4.2.

The torque synchronizing coefficients and damping coefficients for steady and oscillating modes are presented in Table 4-2. It is observed that harmonics can significantly change these coefficients. At harmonic level 4, the system becomes unstable through negative steady synchronizing torque. This can be of great concern

in weak or marginally stable systems (for example isolated or distributed generation system).

Table 4-2
Impact of space and time harmonics on damping and synchronizing coefficients of the SMIB system

Time Harmonic Level	Steady torque Synchronizing and Damping Coefficients	Oscillating torque Synchronizing and Damping Coefficients	Status
No harmonics	Ks= 0.1803 KD=0	Ks= 0.6725 KD= 1.7218	Stable
1: $Base_T^*$ $(\theta_i^{(h)}=0)$	Ks= 0.2132 KD=0	Ks= 0.7235 KD= 1.5837	Stable
2: $Base_T^*$ $(\theta_i^{(h)}=\pi/2)$	Ks= 0.0974 KD=0	Ks= 0.5844 KD= 2.1058	Stable
3 : $2\times Base_T^*$ $(\theta_i^{(h)}=0)$	Ks= 0.1316 KD=0	Ks= 0.6116 KD= 1.9507	Stable
4: $2\times Base_T^*$ $(\theta_i^{(h)}=\pi/2)$	Ks= -0.0292 KD=0	Ks= 0.3593 KD= 3.2493	Unstable

*) *0.03pu, 0.05pu, 0.02*pu and *0.01*pu for the 3rd to 9th harmonics, respectively.

(b) With Damper Windings

Considering three damper windings on the rotor circuit, characteristics are the same as Section 3.5, the system eigenvalues are calculated from Equation 3-32 and are shown in Table 4-3 for four harmonic levels.

Table 4-3
Impact of space and time harmonics on the eigenvalues of distorted SMIB system (with dampers)

Time Harmonic Level	**System Eigenvalues**	**Damped Freq. (ω_d) and Damping Ratio (ξ)**
No harmonics	$\lambda_1 = -36.54$ $\lambda_2 = -22.67$ $\lambda_{3,4} = -0.2035 \pm 6.0841j$ $\lambda_5 = -0.085$ $\lambda_6 = -1.81$	ω_d =0.968 ξ =0.033
1: $Base_T$* ($\theta_i^{(h)} = 0$)	$\lambda_1 = -35.31$ $\lambda_2 = -23.14$ $\lambda_{3,4} = -0.0504 \pm 7.057j$ $\lambda_5 = -0.148$ $\lambda_6 = -1.91$	ω_d =1.123 ξ =0.0071
2: $Base_T$ ($\theta_i^{(h)} = \pi/2$)	$\lambda_1 = -35.68$ $\lambda_2 = -23.25$ $\lambda_{3,4} = -0.11 \pm 6.92j$ $\lambda_5 = -0.118$ $\lambda_6 = -1.90$	ω_d =1.102 ξ =0.0164
3 : 2× $Base_T$ ($\theta_i^{(h)} = 0$)	$\lambda_1 = -35.27$ $\lambda_2 = -22.80$ $\lambda_{3,4} = -0.025 \pm 7.2j$ $\lambda_5 = -0.151$ $\lambda_6 = -1.89$	ω_d =1.145 ξ =0.0035
4: 2× $Base_T$ ($\theta_i^{(h)} = \pi/2$)	$\lambda_1 = -36.06$ $\lambda_2 = -22.83$ $\lambda_{3,4} = -0.16 \pm 6.88j$ $\lambda_5 = -0.103$ $\lambda_6 = -1.85$	ω_d =1.095 ξ =0.0231

*) *0.03pu, 0.05pu, 0.02*pu and *0.01*pu for the 3rd to 9th harmonics, respectively.

Comparison of Table 4-1 and Table 4-3 indicates that damper windings have slightly improved the relative stability of the mode corresponding to the rotor field winding (λ_5). However, their impact on the oscillatory mode depends on both the level and phase angle of the harmonic spectrum. Under the influence of harmonics, damper

windings are less effective on improving the relative stability and damping ratio of the oscillatory modes. The effectiveness is a nonlinear function of the magnitude and angle of the system time and generator space harmonics. Therefore, the impact of harmonics on the system stability needs to be studied individually for different system harmonic levels.

The participation matrix for harmonic level 4 (7th row of Table 4-3) shows that the oscillatory modes (λ_3, λ_4) are associated with the rotor speed and angle. And the eigenvalue with the lowest relative stability (λ_5) corresponds to the rotor field circuit.

$$
\mathrm{P} = \begin{bmatrix}
-0.001 & 0.0013 & 0.4993-0.0014i & 0.4993+0.0014i & -0.0002 & 0.0013 & \Delta\omega_r \\
-0.001 & 0.0013 & 0.4993-0.0014i & 0.4993+0.0014i & -0.0002 & 0.0013 & \Delta\delta \\
0.0145 & 0 & 0.0008+0.0054i & 0.0008-0.0054i & 0.9828 & 0.0012 & \Delta\psi_{fd} \\
0.988 & -0.0001 & -0.0022-0.0024i & -0.0022+0.0024i & 0.0165 & 0 & \Delta\psi_D \\
0 & 0.0461 & 0.0003-0.0021i & 0.0003+0.0021i & 0.001 & 0.9524 & \Delta\psi_G \\
-0.0004 & 0.9515 & 0.0025+0.0019i & 0.0025-0.0019i & 0.0002 & 0.0437 & \Delta\psi_Q \\
\lambda_1 & \lambda_2 & \lambda_3 & \lambda_4 & \lambda_5 & \lambda_6 &
\end{bmatrix}
$$

Figure 4.7 shows the system time response to a mechanical input power change of 0.1pu for harmonic level 4. Comparing this figure to Figure 4.6 shows the increase of the relative stability of the field winding.

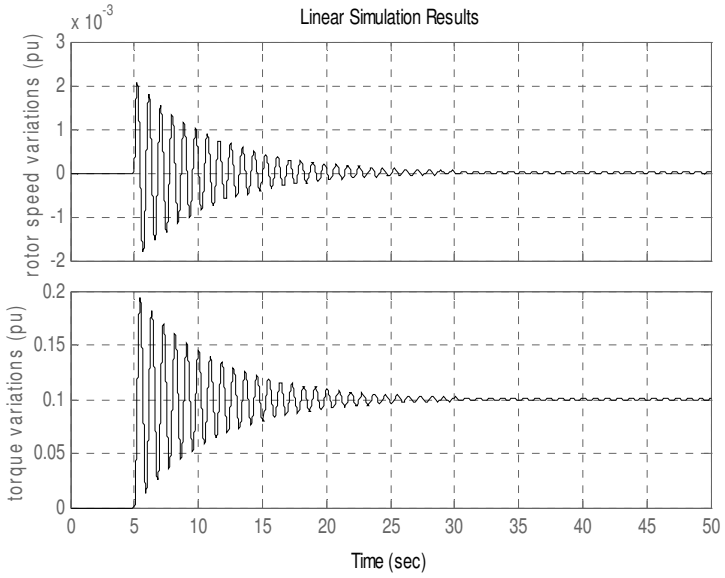

Figure 4.7. Time response of the rotor speed and electromagnetic torque variations subject to an input power perturbation in the presence of time and space harmonics (with damper windings) for the SMIB of Figure 4.2.

4.4. Conclusions

In this chapter the small-signal stability of a distorted Single Machine Infinite Bus system under the influences of time and space harmonics was investigated. The modified model of a synchronous generator considering the impact of time and space harmonics in the *dq*-frame and the eigenvalue analysis method were used. An analytical method was used to calculate the system state space equations from the differential equations. However, the additional terms due to harmonics made the calculation more sophisticated. The impacts of current harmonic phase angles and damper windings were also investigated.

The system simulation was performed for two different levels of time and space harmonics. It was demonstrated that by increasing the level of harmonic distortion, considerable variations in the system eigenvalues are observed. The influence of phase angle cannot be neglected as it may cause instability in the system by shifting the eigenvalues to the right hand side of the imaginary axis in the *s*-plane.

Simulation results for sinusoidal and distorted conditions were presented and the following outcomes were achieved:

- Time and space harmonics change the elements of the system state matrix, introducing new terms in stator current and fluxes (equations 4-22, 4-32).
- Time and space harmonics will change the system eigenvalues and hence affect the system dynamic behaviour (Figure 4.6 and Table 4-1).
- Harmonic phase angles have considerable impact on the steady state and dynamic behaviour of the system; they can move the locations of eigenvalues and cause power system instability (Figure 4.6 and Table 4-1).
- Damper windings are effective in increasing the damping ratio of the oscillating modes under sinusoidal conditions. However, they are less effective when harmonics are present in the system (Figure 4.7 and Table 4-3).

CHAPTER FIVE

OPTIMAL SELECTION OF SSSC BASED DAMPING CONTROLLER PARAMETERS IN THE PRESENCE OF HARMONICS

5.1. Introduction

The concept of FACTS as a total network control philosophy was first introduced by Hingorani [62] from the Electric Power Research Institute (EPRI) in the USA in 1988, although the power electronic controlled devices had been used in the transmission network for many years before that. The application of FACTS in electric power system is intended for the control of power flow, improvement of stability, voltage profile management, power factor correction, and loss minimisation.

Many FACTS devices connected in shunt, series, and series-shunt configurations with or without magnetic or superconductive storage element have been proposed and implemented [21, 63-66]. Supplementary control signals can be applied to some FACTS devices to damp electromechanical oscillations in power system and increase the system damping capability. These signals are produced by power oscillation damping (POD) controllers.

Static synchronous series compensators (SSSC) are solid-state controllable voltage source inverters that are connected in series with the power transmission lines. With the injected voltage in quadrature with the line current and the capability of dynamically changing their reactance characteristics from capacitive to inductive, SSSCs are very effective for power flow control [67]. In addition, an auxiliary stabilizing signal can be superimposed on their power flow control functions to improve power system oscillations damping [23].

In this chapter, the dynamic behaviour of a distorted SMIB system installed with an SSSC is investigated using eigenvalue analysis. An auxiliary POD controller is

applied to the SSSC to improve the system dynamic behaviour. This PID controller adds three state variables to the system state equations. An observability matrix is used to determine the proper feedback signal from the system. The main goal of the designed POD controller is to improve the damping of the critical modes while minimizing any deterioration in the damping of the other modes, within the permissible region of the controller gains. Hence, the design of the POD controller can be considered as a constrained optimization problem and different optimization methods such as nonlinear programming, simulated annealing and Tabu search can be used. Most traditional optimization approaches move from one point in the decision hyperspace to another point using some deterministic rule. They are fast, but they suffer from the inability to escape the local optimal solutions.

In this work, optimal POD parameters for improving the power oscillation damping are determined using a hybrid genetic-fuzzy algorithm. To ensure a dynamically stable system in a wide spectrum of harmonic distortions, system eigenvalues are computed for different levels of space and time harmonics and incorporated in the proposed optimization method.

It should be mentioned that, there are many different types of SSSC main controller available. They are also called power flow controller, as their main goal is to affect the transferred power. However, using new methods they can also be effective on the power system stability. In this work, it is assumed that the main controller affects the power system steady state operation and has minimal impact on the system dynamics. For this reason it is not necessary to include a model of the SSSC main controller in the system dynamic analysis.

Simulation results for sinusoidal and distorted operating conditions are presented and compared to show the ability of the proposed SSSC based POD controller in remaining effective in distorted conditions.

5.2. Dynamic Behaviour of a Distorted SMIB Systems Installed with SSSC

Installing an SSSC in a power system with a proper controller can affect the entire system dynamic behaviour and relocate the system eigenvalues. In this section, the eigenvalue analysis method is used to investigate the impact of harmonics on the small signal stability of the distorted SMIB system installed with an SSSC, shown in Figure 5.1.

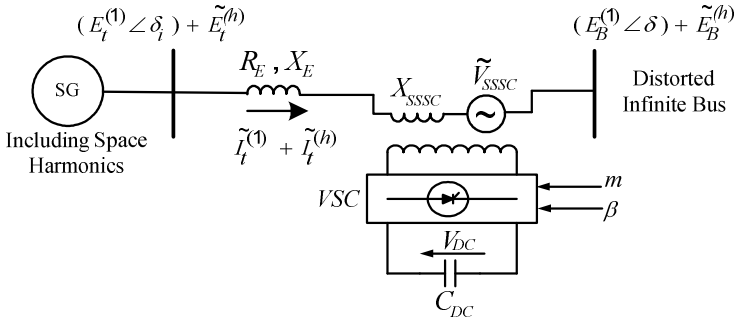

Figure 5.1. The simulated distorted SMIB system installed with SSSC

The depicted SSSC consists of a boosting transformer with a leakage reactance of X_{sssc} , a three-phase GTO based voltage source converter (V_{SSSC}) and a DC capacitor (C_{DC}). The influence of system nonlinear loads is considered as harmonic voltages at the infinite bus. These voltages can be calculated using harmonic power flow algorithms. SSSCs can inject voltage harmonics into the power system and increase the level of harmonic pollution. However, the impact of SSSC in deteriorating the system power quality is not studied in this thesis.

To derive the state space equations of the distorted SMIB system, the SSSC differential equations are written and linearized around the operating point. Also the system equations, equations 4-5 and 4-6, will be modified considering the reactance of the boosting transformer and the injected voltage by the SSSC. Hence, the system state space equations contain one additional state variable due to the introduction of SSSC dynamics and can be calculated as Equation 5-1.

$$\begin{bmatrix} \Delta\dot{\omega}_r \\ \Delta\dot{\delta} \\ \Delta\dot{\psi}_{fd} \\ \Delta\dot{V}_{DC} \end{bmatrix} = A \begin{bmatrix} \Delta\omega_r \\ \Delta\delta \\ \Delta\psi_{fd} \\ \Delta V_{DC} \end{bmatrix} + B \begin{bmatrix} \Delta T_m \\ \Delta E_{fd} \\ \Delta m \end{bmatrix} \tag{5-1}$$

The SSSC and system equations are as follows [23]:

SSSC Equations:

$$\begin{aligned} &\overline{V}_{SSSC} = mkV_{DC}\angle\beta \\ &\frac{dV_{DC}}{dt} = \frac{mk}{C_{DC}}(i_d^{(1)}\cos\beta + i_q^{(1)}\sin\beta) \\ &\beta = \phi \pm 90^\circ \end{aligned} \tag{5-2}$$

where, k is the ratio between AC and DC voltages and depends on the inverter structure and φ is the current angle. Signal m is the modulation ratio of the Pulse Width Modulation (PWM) based Voltage Source Converter (VSC), which is the input control signal of SSSC and determines the magnitude of the inserted voltage. The main controller determines the steady state value of this signal. Signal β is the phase of the injected voltage and is kept in quadrature with the line current while inverter losses are ignored. Therefore, the compensation level of the SSSC can be controlled dynamically by changing the magnitude of the injected voltage. This SSSC model, however, may not be valid for transient phenomena and/or asymmetrical operating conditions [23].

System Equations:

$$\tilde{E}_t^{(1)} = V_{SSSC} + \tilde{E}_B^{(1)} + (R_E + j(X_E + X_{sssc}))\tilde{I}_t^{(1)}$$

$$\begin{cases} e_d^{(1)} = E_{Bd}^{(1)} + V_{SSSCd} + R_E i_d^{(1)} - (X_E + X_{sssc}) i_q^{(1)} \\ e_q^{(1)} = E_{Bq}^{(1)} + V_{SSSCq} + R_E i_q^{(1)} + (X_E + X_{sssc}) i_d^{(1)} \end{cases} \tag{5-3}$$

The machine equations can be written similar to equations 4-9 and 4-10.

Using the system and machine equations, the fundamental stator currents are obtained as:

$$i_d^{(1)} = \frac{X_{Tq}[\psi_{Fd}(\frac{M_F^{(1)}}{L_{Fd}}) - E_{Bq} + \psi_d^{due\ to\ harm} - mkV_{DC}\sin\beta]}{X_{Tq}\ X_{Td} + R_T^2} - \frac{(\psi_q^{due\ to\ harm} + E_{Bd} + mkV_{DC}\cos\beta)R_T}{X_{Tq}\ X_{Td} + R_T^2}$$

$$i_q^{(1)} = \frac{R_T[\psi_{Fd}(\frac{M_F^{(1)}}{L_{Fd}}) - E_{Bq} + \psi_d^{due\ to\ harm} - mkV_{DC}\sin\beta]}{X_{Tq}\ X_{Td} + R_T^2} + \frac{(\psi_q^{due\ to\ harm} + E_{Bd} + mkV_{DC}\cos\beta)X_{Td}}{X_{Tq}\ X_{Td} + R_T^2}$$

$$X_{Tq}=X_E+X_{sssc}+L_q$$

$$X_{Td}=X_E+X_{sssc}+L_d\ \frac{M_F^{(1)}}{L_{Fd}} \qquad (5\text{-}4)$$

$$R_T=R_E+R_a$$

An expression similar to Equation 4-12 is used to linearize the electromagnetic torque around the operating point and the deviations of stator current and fluxes on the *dq* axis are modified considering the impact of SSSC. These variables are calculated in the following general form using equations 4-4 and 5-4:

$$\begin{cases} \Delta f = a_{1f}\Delta\psi_{Fd} + a_{2f}\Delta\delta + a_{3f}\Delta\psi_d^{due\ to\ harm} + a_{4f}\Delta\psi_q^{due\ to\ harm} + a_{5f}\Delta V_{DC} + a_{6f}\Delta m \\ f = i_d, i_q, \psi_d, \psi_q \end{cases} \qquad (5\text{-}5)$$

Coefficients $a_{1f} - a_{6f}$ are functions of the initial conditions and the system parameters. $\Delta\psi_d^{due\ to\ harm}$ and $\Delta\psi_q^{due\ to\ harm}$ are determined as a function of $\Delta\theta_i$ in Equation 4-15, where $\theta_i = \pi/2 - \delta_i$ and $\Delta\theta_i = \Delta\delta_i$.

From Equation 5-3:

$$\delta_i = \arctan[\frac{E_{Bd}^{(1)} + V_{SSSCd} + R_E\, i_d^{(1)} - (X_E + X_{sssc})\, i_q^{(1)}}{E_{Bq}^{(1)} + V_{SSSCq} + R_E\, i_q^{(1)} + (X_E + X_{sssc})\, i_d^{(1)}}] \qquad (5\text{-}6)$$

Therefore, deviations of the stator flux additional terms, $\Delta\psi_d^{due\ to\ harm}$ and $\Delta\psi_q^{due\ to\ harm}$, are calculated as a function of the state space variables:

$$\begin{aligned} \Delta\psi_d^{due\ to\ harm} &= b_{1d}\,\Delta\delta + b_{2d}\,\Delta\psi_{fd} + b_{3d}\,\Delta V_{DC} + b_{4d}\,\Delta m \\ \Delta\psi_q^{due\ to\ harm} &= b_{1q}\,\Delta\delta + b_{2q}\,\Delta\psi_{fd} + b_{3q}\,\Delta V_{DC} + b_{4q}\,\Delta m \end{aligned} \qquad (5\text{-}7)$$

Using the above formulation, the electromechanical torque deviation can be obtained in the following form:

$$\Delta T_e^{(1)} = K_1^{(harm)}\Delta\delta + K_2^{(harm)}\Delta\psi_{Fd} + K_{pDC}^{(harm)}\Delta V_{DC} + K_{pm}^{(harm)}\Delta m \qquad (5\text{-}8)$$

where $K_1^{(harm)}, K_2^{(harm)}, K_{pDC}^{(harm)}$ *and* $K_{pm}^{(harm)}$ are functions of the initial stator currents, initial stator fluxes, steady state load angle, rotor currents, DC capacitor voltage, modulation ratio of the PWM based VSC and harmonics. More details are presented in Appendix C.

Using Equation 5-2 and substituting the values for currents from Equation 5-4, the derivatives of DC capacitor voltage and field flux are calculated as,

$$\begin{aligned}\Delta\dot{\psi}_{fd} &= K_{f\delta}^{(harm)}\Delta\delta + K_{f\psi}^{(harm)}\Delta\psi_{Fd} + K_{fDC}^{(harm)}\Delta V_{DC} + K_{fE}\,\Delta E_{fd} + K_{fm}^{(harm)}\,\Delta m \\ \Delta\dot{V}_{DC} &= K_{d\delta}^{(harm)}\Delta\delta + K_{d\psi}^{(harm)}\Delta\psi_{Fd} + K_{dDC}^{(harm)}\Delta V_{DC} + K_{dm}^{(harm)}\Delta m\end{aligned} \tag{5-9}$$

The coefficients in the above equation are also functions of the initial operating conditions. These coefficients are expressed in Appendix C, Equation C-8.

From the swing equation and equations 5-8 and 5-9, the elements of the system state equation are obtained as follows:

$$\begin{bmatrix}\Delta\dot{\omega}_r \\ \Delta\dot{\delta} \\ \Delta\dot{\psi}_{fd} \\ \Delta\dot{V}_{DC}\end{bmatrix} = \begin{bmatrix}a_{11} & a_{12}^{(h)} & a_{13}^{(h)} & a_{14}^{(h)} \\ a_{21} & 0 & 0 & 0 \\ 0 & a_{32}^{(h)} & a_{33}^{(h)} & a_{34}^{(h)} \\ 0 & a_{42}^{(h)} & a_{43}^{(h)} & a_{44}^{(h)}\end{bmatrix}\begin{bmatrix}\Delta\omega_r \\ \Delta\delta \\ \Delta\psi_{fd} \\ \Delta V_{DC}\end{bmatrix} + \begin{bmatrix}b_{11} & 0 & b_{13}^{(h)} \\ 0 & 0 & 0 \\ 0 & b_{32} & b_{33}^{(h)} \\ 0 & 0 & b_{43}^{(h)}\end{bmatrix}\begin{bmatrix}\Delta T_m \\ \Delta E_{fd} \\ \Delta m\end{bmatrix} \tag{5-10}$$

$$a_{11} = \frac{-K_D}{2H},\ a_{12}^{(h)} = \frac{-K_1^{(harm)}}{2H},\ a_{13}^{(h)} = \frac{-K_2^{(harm)}}{2H},\ a_{14}^{(h)} = \frac{-K_{pDC}^{(harm)}}{2H}$$

$$a_{21} = \omega_0$$

$$a_{32}^{(h)} = K_{f\delta}^{(harm)},\ a_{33}^{(h)} = K_{f\psi}^{(harm)},\ a_{34}^{(h)} = K_{fDC}^{(harm)}$$

$$a_{42}^{(h)} = K_{d\delta}^{(harm)},\ a_{43}^{(h)} = K_{d\psi}^{(harm)},\ a_{44}^{(h)} = K_{dDC}^{(harm)}$$

$$b_{11} = \frac{1}{2H},\ b_{13}^{(h)} = \frac{-K_{pm}^{(harm)}}{2H}$$

$$b_{32} = K_{fE} = \frac{\omega_0 R_{fd}}{M_F^{(1)}},\ b_{33}^{(h)} = K_{fm}^{(harm)}$$

$$b_{43}^{(h)} = K_{dm}^{(harm)}$$

Figure 5.2 illustrates the block diagram of the distorted SMIB system installed with an SSSC where $K_1^{(harm)}$, $K_2^{(harm)}$, $K_{pDC}^{(harm)}$ and $K_{pm}^{(harm)}$ are defined in Equation 5-7, and

$$K_3^{(harm)} = -\frac{b_{32}}{a_{33}^{(h)}},\ K_4^{(harm)} = -\frac{a_{32}^{(h)}}{b_{32}},\ T_3^{(harm)} = -\frac{1}{a_{33}^{(h)}}$$

$$K_5^{(harm)} = a_{42}^{(h)},\quad K_6^{(harm)} = a_{43}^{(h)},\quad K_7^{(harm)} = -\frac{b_{33}^{(h)}}{b_{32}},\quad K_8^{(harm)} = -\frac{a_{34}^{(h)}}{b_{32}}.$$

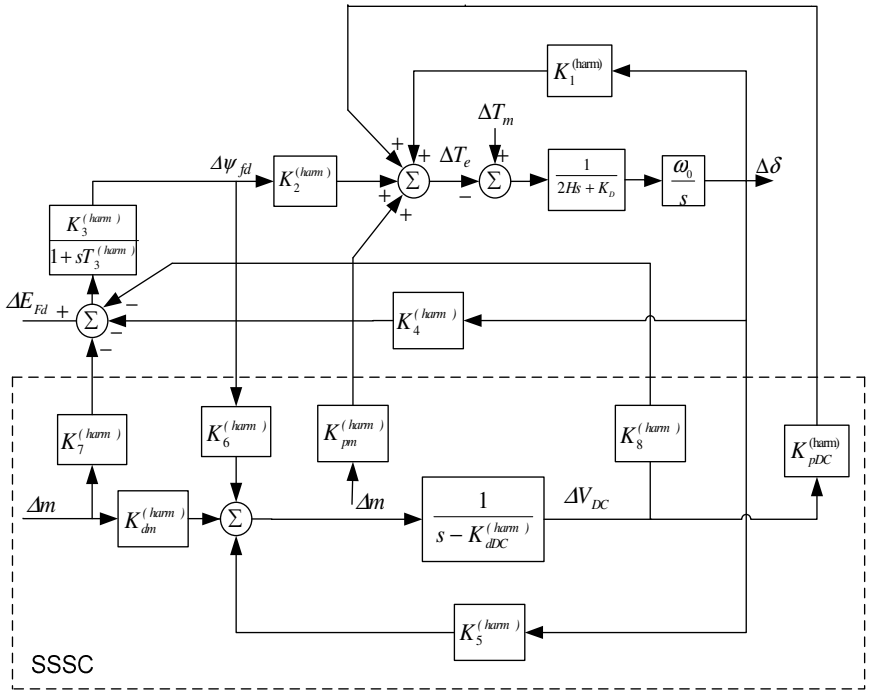

Figure 5.2. Heffron-Phillips model of a distorted SMIB system installed with SSSC

5.3. The SSSC Based Power Oscillations Damping Controller

The power oscillations damping controller (POD) is applied to the SSSC in order to improve system dynamics under the influence of time and space harmonics. The applied POD has the conventional PID structure [23] and consists of the gain, signal wash-out and phase compensator blocks as shown in Figure 5.3. The "signal wash-out" block is a high-pass filter that modifies the SSSC input signal and prevents steady changes in active power. Therefore, T_ω should have a large value to allow the passage of signals associated with active power oscillations with no modifications. The value of T_ω is not critical and may be in the range of 1 to 20 seconds.

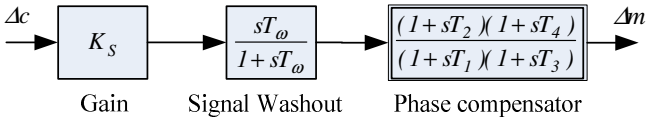

Figure 5.3. The SSSC based damping controller (parameters to be selected considering time and space harmonics)

The main purpose of the proposed POD is to push the critical modes, lightly damped or un-damped modes, toward a pre-specified region on the left hand side of the *s*-plane with an acceptable damping ratio and relative stability. It was shown in the previous section that the presence of time and space harmonics in the distorted power systems can relocate system eigenvalues. Hence, it is important to ensure that the controller satisfies the system stability criteria under the influence of harmonics, while keeping the controller parameters within the specified limits. Therefore, tuning the POD controller is formulated as a constrained optimization problem. In this section, a hybrid genetic-fuzzy algorithm is proposed for the optimal computation of the phase compensator block parameters and the gain value.

The observability matrix is used to select the proper input signal to the POD controller (Δc). The selected signal should have good observability of the system electromechanical modes under consideration. Local signals, such as tie-line current magnitude, tie-line active power and bus voltage magnitude, can be utilized as the controller input signals. It is possible to use remote signals such as the speed deviation of remote generators, phase angle deviation of remote buses and active power of the nearby buses. As the SSSC device is usually located in transmission systems, local input signals are always preferred. The controller output signal (Δm), will be added to the main SSSC controller signal (m) to change the inverter firing angle.

The following section gives the controller state equations and the system closed-loop state matrix by adding the auxiliary POD controller.

5.3.1. State Equations of the POD Controller

The POD state variables are shown in the block diagram of Figure 5.4. From this diagram, the POD state space equations are found as:

$$\begin{bmatrix} \Delta\dot{x}_1 \\ \Delta\dot{x}_2 \\ \Delta\dot{x}_3 \end{bmatrix} = \begin{bmatrix} -\frac{1}{T_w} & 0 & 0 \\ 0 & 0 & 1 \\ -\frac{K_S}{T_1 T_3} & -\frac{1}{T_1 T_3} & -\frac{(T_1+T_3)}{T_1 T_3} \end{bmatrix} \begin{bmatrix} \Delta x_1 \\ \Delta x_2 \\ \Delta x_3 \end{bmatrix} + \begin{bmatrix} \frac{1}{T_w} \\ 0 \\ \frac{K_S}{T_1 T_3} \end{bmatrix} [\Delta c]$$

$$[\Delta m]=\left[-K_S\left(\frac{T_2T_4}{T_1T_3}\right)\quad 1-\frac{T_2T_4}{T_1T_3}\quad \frac{-(T_1+T_3)T_2T_4}{T_1T_3}+(T_2+T_4)\right]\begin{bmatrix}\Delta x_1\\ \Delta x_2\\ \Delta x_3\end{bmatrix}+\left[\frac{T_2T_4K_S}{T_1T_3}\right][\Delta c] \tag{5-11}$$

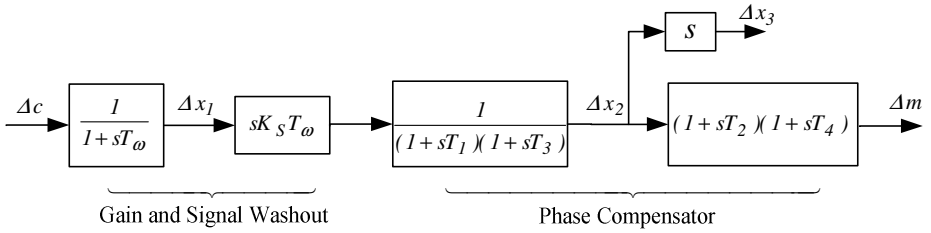

Figure 5.4. POD state variables representation

5.3.2. Closed-Loop State Space Equations of Distorted SMIB System

Applying the dynamic controller, Equation 5-11, will add three additional state variables to the conventional system state equations, Equation 5-10, and the total number of the state variables will increase from 4 to 7. To obtain the closed-loop system eigenvalues, the controller input signal needs to be determined as a function of the system state variables. The active power and magnitude of the current flowing through the tie-line are two locally available control signals which are commonly used. In this section, these two control signals are defined and used to calculate the closed loop system state equations.

Selecting Line Active Power as the POD Input Signal:

The active power through the transmission line is related to the electromagnetic torque (in pu) by the following relation:

$$p_{ele}=T_e-R_a(I_t)^2 \quad\longrightarrow\quad \Delta p_{ele}=\Delta T_e-R_a(\Delta I_t)^2$$

For small disturbances, $(\Delta I_t)^2$ will be small and this value times R_a can be ignored for simplification without causing any considerable error. Hence, $[\Delta p_{ele}]=[\Delta T_e]$.

Now using Equation 5-8, Δp_{ele} is given by:

$$\Delta p_{ele}=K_1^{(harm)}\Delta\delta+K_2^{(harm)}\Delta\psi_{Fd}+K_{pDC}^{(harm)}\Delta V_{DC}+K_{pm}^{(harm)}\Delta m \tag{5-12}$$

Using this input signal, the closed-loop system block diagram is shown in Figure 5.5.

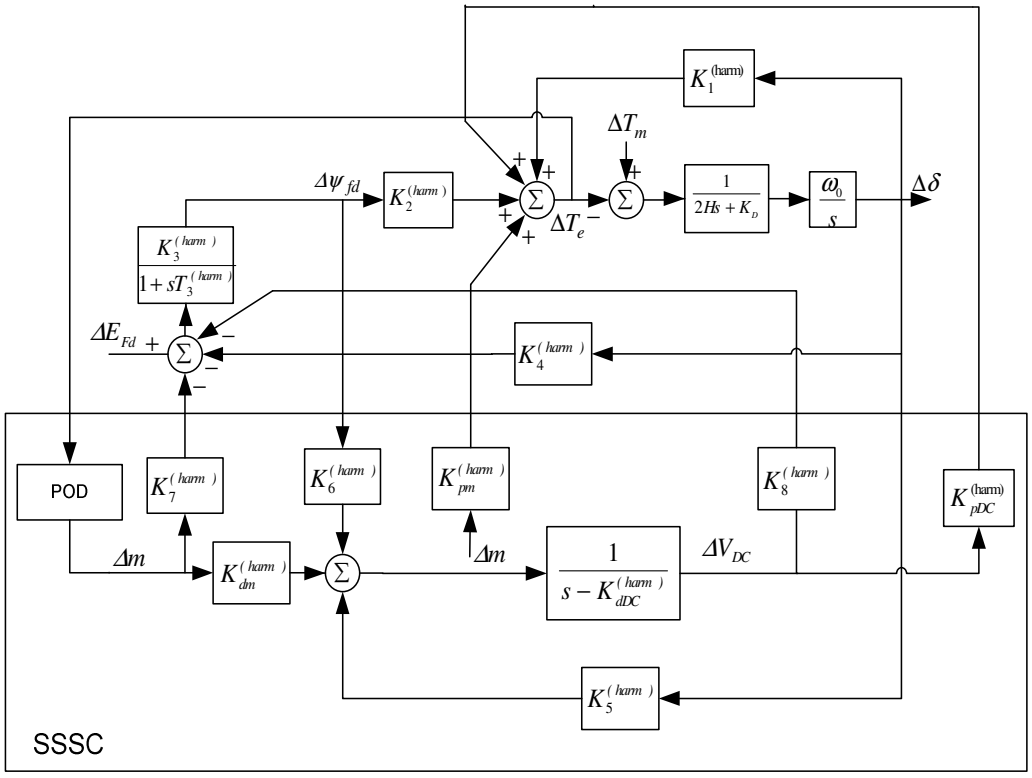

Figure 5.5 Heffron-Phillips model of closed-loop distorted SMIB system installed with SSSC considering line active power as the POD input signal

Selecting Line Current Magnitude as the POD Input signal:

The line current magnitude may be expressed in terms of the *dq* components:

$$I_t = \sqrt{(i_d{}^2 + i_q{}^2)} \quad \Rightarrow \quad \Delta I_t = \frac{i_{d0}\,\Delta i_d + i_{q0}\,\Delta i_q}{I_{t0}} \tag{5-13}$$

where I_{t0} is the current magnitude under steady-state operation. Substituting Δi_d and Δi_q, calculated in Appendix C Equation C-3, into Equation 5-13, the input signal is derived as:

$$\Delta I_t = I_\delta^{(harm)}\,\Delta\delta + I_\psi^{(harm)}\,\Delta\psi_{Fd} + I_{DC}^{(harm)}\,\Delta V_{DC} + I_m^{(harm)}\,\Delta m \tag{5-14}$$

Figure 5.6 shows the closed-loop system using the current magnitude as the controller input signal to the POD block.

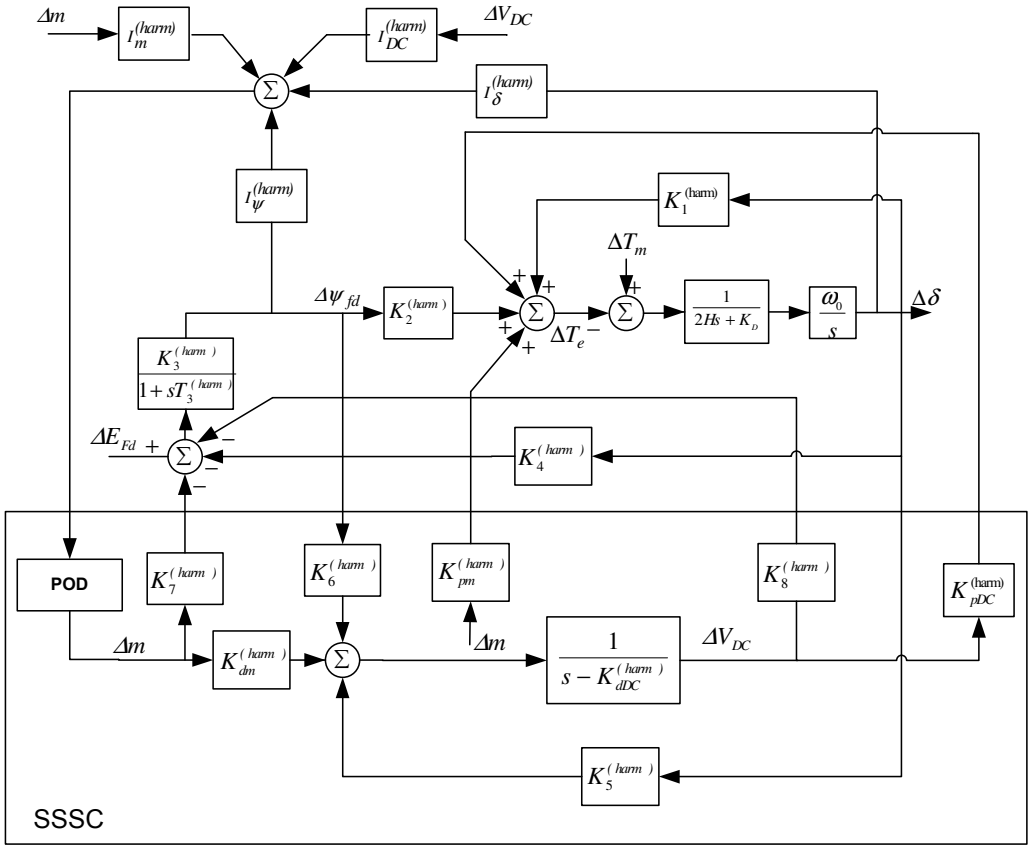

Figure 5.6 Heffron-Phillips model of closed-loop distorted SMIB system installed with SSSC considering line current magnitude as the POD input signal

Closed-Loop System State Equations:

Applying the POD controller to the SSSC, the closed loop system state equations will be obtained with three additional state variables. According to equations 5-12 and 5-14, the input controller signal can be written in the general form as:

$$\Delta c = c_\delta \Delta\delta + c_\psi \Delta\psi_{fd} + c_{DC} \Delta V_{DC} + c_m \Delta m \tag{5-15a}$$

where, for a POD controller with the line active power as the input signal

$$c_\delta = K_1^{(harm)},\ c_\psi = K_2^{(harm)},\ c_{DC} = K_{pDC}^{(harm)},\ c_m = K_{pm}^{(harm)} \tag{5-15b}$$

and for a POD controller with the line current magnitude as the input signal

$$c_\delta = I_\delta^{(harm)},\ c_\psi = I_\psi^{(harm)},\ c_{DC} = I_{DC}^{(harm)},\ c_m = I_m^{(harm)}. \tag{5-15c}$$

Substituting Δc into Equation 5-11, the controller equations can be written in the following form:

$$\Delta m = m_\delta \Delta\delta + m_\psi \Delta\psi_{fd} + m_{DC}\Delta V_{DC} + m_{x1}\Delta x_1 + m_{x2}\Delta x_2 + m_{x3}\Delta x_3 \tag{5-16}$$

In the system state equations, Equation 5-10, applying the input signal (Δm) through the POD controller, using Equation 5-16, the closed-loop system is determined as:

$$\begin{bmatrix} \Delta\dot{\omega}_r \\ \Delta\dot{\delta} \\ \Delta\dot{\psi}_{fd} \\ \Delta\dot{V}_{DC} \\ \Delta\dot{x}_1 \\ \Delta\dot{x}_2 \\ \Delta\dot{x}_3 \end{bmatrix} = A_{(7\times7)} \begin{bmatrix} \Delta\omega_r \\ \Delta\delta \\ \Delta\psi_{fd} \\ \Delta V_{DC} \\ \Delta x_1 \\ \Delta x_2 \\ \Delta x_3 \end{bmatrix} + B_{(7\times2)} \begin{bmatrix} \Delta T_m \\ \Delta E_{fd} \end{bmatrix} \tag{5-17}$$

Where,

A=

$$\begin{bmatrix} a_{11} & a_{12}^{(h)} + b_{13}^{(h)} m_\delta & a_{13}^{(h)} + b_{13}^{(h)} m_\psi & a_{14}^{(h)} + b_{13}^{(h)} m_{DC} & b_{13}^{(h)} m_{x1} & b_{13}^{(h)} m_{x2} & b_{13}^{(h)} m_{x3} \\ a_{21} & 0 & 0 & 0 & 0 & 0 & 0 \\ 0 & a_{32}^{(h)} + b_{33}^{(h)} m_\delta & a_{33}^{(h)} + b_{33}^{(h)} m_\psi & a_{34}^{(h)} + b_{33}^{(h)} m_{DC} & b_{33}^{(h)} m_{x1} & b_{33}^{(h)} m_{x2} & b_{33}^{(h)} m_{x3} \\ 0 & a_{42}^{(h)} + b_{43}^{(h)} m_\delta & a_{43}^{(h)} + b_{43}^{(h)} m_\psi & a_{44}^{(h)} + b_{43}^{(h)} m_{DC} & b_{43}^{(h)} m_{x1} & b_{43}^{(h)} m_{x2} & b_{43}^{(h)} m_{x3} \\ 0 & \dfrac{(c_\delta + c_m m_\delta)}{T_w} & \dfrac{(c_\psi + c_m m_\psi)}{T_w} & \dfrac{(c_{DC} + c_m m_{DC})}{T_w} & \dfrac{c_m m_{x1} - 1}{T_w} & \dfrac{c_m m_{x2}}{T_w} & \dfrac{c_m m_{x3}}{T_w} \\ 0 & 0 & 0 & 0 & 0 & 0 & 1 \\ 0 & \dfrac{K_S(c_\delta + c_m m_\delta)}{T_1 T_3} & \dfrac{K_S(c_\psi + c_m m_\psi)}{T_1 T_3} & \dfrac{K_S(c_\delta + c_m m_\delta)}{T_1 T_3} & \dfrac{K_S(c_m m_{x1} - 1)}{T_1 T_3} & \dfrac{K_S(c_m m_{x2}) - 1}{T_1 T_3} & \dfrac{K_S(c_m m_{x3}) - (T_1 + T_3)}{T_1 T_3} \end{bmatrix}$$

and

$$\text{B=} \begin{bmatrix} b_{11} & 0 \\ 0 & 0 \\ 0 & b_{32} \\ 0 & 0 \\ 0 & 0 \\ 0 & 0 \\ 0 & 0 \end{bmatrix}$$

5.4. Optimal Tuning of SSSC based POD Controller in the Presence of Harmonics using a Proposed Hybrid Genetic-Fuzzy Algorithm

When designing a control system, the main goal is not merely to stabilize a given system, but to shape the dynamic response by placing the closed loop eigenvalues in some pre-specified region in the left hand side of the *s*-plane. The following two important time-domain requirements are included in the performance specifications:

- The response must be sufficiently fast and smooth.
- The response must not exhibit excessive overshoot or oscillation.

For optimal determination of the damping controller parameters, a multi-objective genetic algorithm (GA) in conjunction with Fuzzy approximate reasoning is proposed and used. To assure the robustness of the POD controller against changes in power system nonlinear loads, the dominant system harmonic levels should be considered. The penalties of the real parts and damping ratios of the eigenvalues for the harmonic levels under consideration are defined and fuzzy approximate reasoning is used to compute the fitness function in order to simultaneously satisfy the mode relative stability and damping ratio.

As an example, the following harmonic levels are considered in this section:

Harmonic Level 1: $I^{(h)} = 0$ *and Space Harmonics=* $Base_s$

Harmonic Level 2: $I^{(h)} = Base_t \ (\theta_i^{(h)} = \pi/2)$ *and Space Harmonics=* $Base_s$

Harmonic Level 3: $I^{(h)} = 2 \times Base_t \ (\theta_i^{(h)} = 0)$ *and Space Harmonics=* $Base_s$

Harmonic Level 4: $I^{(h)} = 2 \times Base_t \ (\theta_i^{(h)} = \pi/2)$ *and Space Harmonics=* $Base_s$

(5-18)

where:

- $Base_t$: Time Harmonics= 0.03pu, 0.025pu, 0.02pu and 0.01pu for 3rd, 5th, 7th and 9th harmonics, respectively.
- $Base_s$: Space Harmonics= 0.3, 0.2, 0.1 and 0.01 of the 2nd and 1st harmonics for stator and stator-rotor, respectively.

5.4.1. Genetic Algorithms

Genetic Algorithms (GAs) use the principle of natural evolution and population genetics to search and arrive at a high quality near global solution. The required design variables are encoded into a binary string as a set of genes corresponding to chromosomes in biological systems. Unlike traditional optimization techniques that require one starting point, GAs use a set of points as the initial condition. Each point is called a chromosome, while a group of chromosomes are called a population. The number of chromosomes in a population is usually selected between 30 and 300, with 250 being used in this work. Each chromosome is a string of binary codes (genes) and contains substrings. The merit of a chromosome is judged by the fitness function, which is derived from the objective function and is used in successive genetic operations. During each iterative procedure (referred to as generation), a new set of strings with improved performance is generated using three GA operators, namely reproduction, crossover and mutation.

5.4.2. Structure of the Chromosome

In the proposed method, each chromosome consists of 5 substrings of binary numbers to match the number of parameters in the SSSC based dynamic controller, excluding T_ω which set to 10 seconds. The binary numbers indicate the value of each parameter and the length of each substring limits the maximum value of the parameter to avoid prolonged saturation in the SSSC actuators. In this thesis, the length of each substring is assumed to be 8 bits and the decimal number is normalized between zero and the maximum acceptable value, which depends on the controller structure. Longer substrings correspond to smaller step changes and higher accuracy of results; however, more iterations will be required. Figure 5.7 illustrates the proposed structure of each chromosome.

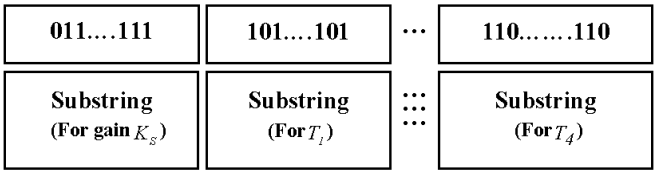

Figure 5.7. Chromosome structure for the proposed hybrid genetic-fuzzy algorithm

5.4.3. The Proposed Fuzzy Fitness Function

The object of the control system is to increase the damping of lightly damped or un-damped modes without deteriorating the other modes under consideration. Placing the real parts of the closed-loop eigenvalues in a sector of the *s*-plane specified by $\sigma^i \le \sigma^d$ guarantees the relative stability, which is determined by the value of σ^d. The eigenvalues should be placed in a wedge-shape zone of the s-plane in order to have an acceptable damping ratio, as showed in Figure 5-19. The value of ζ^{min} determines this zone. To ensure system stability under the influence of harmonics, the fitness function should include the eigenvalues under consideration for all harmonic levels as given in Equation 5-18. In the proposed method, penalties of the real parts and the damping ratios of eigenvalues for each chromosome are combined based on fuzzy approximate reasoning and used as the GA's fitness function. A fuzzy expert system (FES) calculates the fitness value for each chromosome using the membership functions of the total real part and damping ratio penalties of eigenvalues related to all harmonic levels under consideration (Equation 5-18). A concern in the development of fuzzy expert systems is the assignment of appropriate membership functions that could be performed based on intuition, rank ordering or probabilistic methods. However, the choice of membership degree in the interval [0,1] does not matter, as it is the order of magnitude that is important.

The main contribution of this method is an improved fitness function for GAs, capable of improving the damping ratio while directing the real part of eigenvalues toward the stable region of the *s*-plane. This method leads to computing the (near) global solution with lower probability of converging to a local optimum while avoiding numerical complications at harmonic frequencies. In the proposed method, penalties for real parts and damping ratios of eigenvalues for each chromosome are

combined based on fuzzy approximate reasoning and used as the GA's fitness function.

Fuzzification of Total Penalties for the Real Parts of *Eigenvalues*

The summation of the eigenvalues' real part penalties (TP^{σ}) is one of the fuzzy input signals to the fuzzy decision making matrix and is expressed as follows:

$$TP^{\sigma} = \sum_{k=1}^{L} (\sum_{i=1}^{J} P^{\sigma i_k}) \tag{5-19}$$

where L denotes the number of harmonic levels (Equation 5-18) and J is the number of eigenvalues considered at each harmonic level. $P^{\sigma i_k}$ is the penalty related to the real part of the i^{th} eigenvalue of the kth harmonic level and is defined as:

$$P^{\sigma i_k} \begin{cases} 0 , & if \quad \sigma^{i_k} \le \sigma^{d} \\ \sigma^{i_k} - \sigma^{d} & otherwise \end{cases} \tag{5-20}$$

where σ^{d} is the desired value for the real part of the closed-loop eigenvalues and σ^{i_k} is the actual value of the real part related to the i^{th} eigenvalue of the k^{th} harmonic level. Figure 5.8 shows the proposed membership functions for (TP^{σ}) where n is the total number of eigenvalues under consideration in all harmonic levels, and $n = J \times L$. Using the proposed membership function, the eigenvalues with real parts smaller than the desired value are highly related to the low section of the penalty function, whereas critical or unstable modes are assigned a high value in the high section of the penalty membership function.

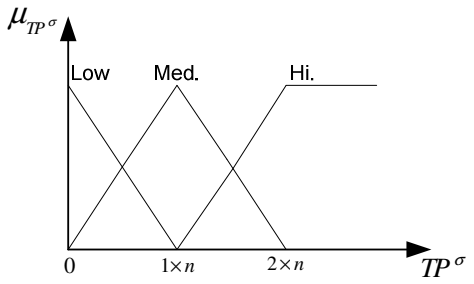

Figure 5.8. Membership functions for total penalties of the real parts of eigenvalues (n is the total number of eigenvalues under consideration)

Fuzzification of Total Penalties for Damping Ratios of Eigenvalues

Another input signal to the fuzzy expert system is the total penalty of the eigenvalues' damping ratios, TP^{ζ}. The expression for TP^{ζ} is given by Equation 5-21 and the corresponding membership functions are shown in Figure 5.9.

$$TP^{\zeta} = \sum_{k=1}^{L} \sum_{i} P^{\zeta i_k} \tag{5-21}$$

where $P^{\zeta i_k}$ is the penalty related to the damping ratio of the i^{th} eigenvalue of the k^{th} harmonic level (Equation 5-18) and is defined as:

$$P^{\zeta i_k} \begin{cases} 0, & \text{if } \zeta^{i} \geq \zeta^{\min} \\ \zeta^{\min} - \zeta^{i_k} & \text{otherwise} \end{cases} \tag{5-22}$$

$\zeta^{\min}$ is the desired value for the damping ratio of the closed-loop eigenvalues and ζ^{i_k} is the actual value of the damping ratio related to the i^{th} eigenvalue of the k^{th} harmonic level.

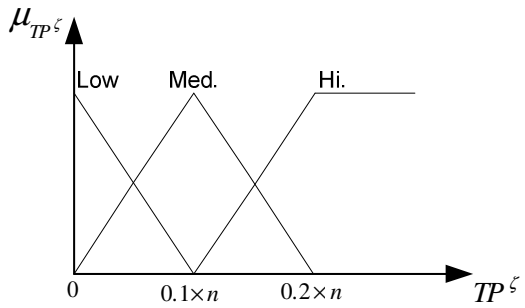

Figure 5.9. Membership functions for total penalties of the damping ratios of eigenvalues (n is the total number of eigenvalues under consideration)

According to Figure 5.9, the highly damped modes belong to the low section of the penalty membership function while the lightly damped (or un-damped) modes are given values in Medium or High sections of the penalty membership function.

Fuzzy Inferencing

Combination of the fuzzy input functions (TP^{σ} and TP^{ζ}) shows the suitability of the solution. For example, a solution that generates eigenvalues with small real parts and large damping ratios is highly desired and should have large fitness value. This

solution has high values in the low sections of the membership functions, as shown in Figure 5.8 and Figure 5.9. With similar interpretation for other combinations of the inputs, the fuzzy decision matrix is generated as shown in Table 5-1.

Table 5-1
Decision matrix for determining the fitness of the solution (chromosome)

AND		*Total penalties of the real parts (TP^{σ})*		
		Low	**Med.**	**Hi.**
Total penalties of damping ratios (TP^{ζ})	***Low***	high	med-high	low
	Med.	med-high	med	low
	Hi.	med	low-med	low

Defuzzification

The Mamdani-max-prod implication method of Equation 5-23 and the proposed fitness membership functions of Figure 5.10 are used to determine the fitness value of each chromosome, as follows:

$$Fitness = \sum \bar{y} \mu_{TP^{\sigma}} \mu_{TP^{\zeta}} \Big/ \sum \mu_{TP^{\sigma}} \mu_{TP^{\zeta}} \tag{5-23}$$

where $\bar{y}$ is the output of the maximum membership value related to the desired section.

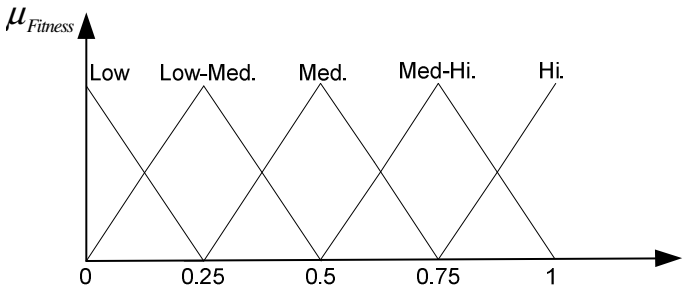

Figure 5.10. Membership functions for the GAs fitness value

Fuzzy approximate reasoning was used to calculate the chromosome's fitness value considering the uncertainty of the fuzzy system inputs as demonstrated in Figure

5.11. Using the proposed fitness function, damping of all critical modes are improved without deteriorating the damping of non-critical modes.

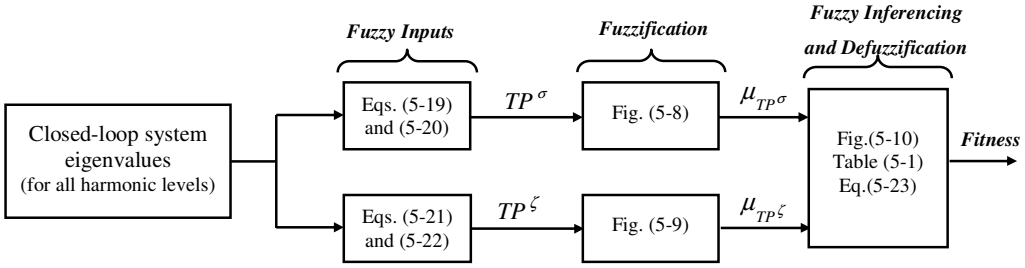

Figure 5.11. The proposed fuzzy fitness function

Genetic Operators

Genetic operators are the stochastic transition rules applied to each chromosome during each generation procedure to generate a new improved population from an old one. A genetic algorithm usually consists of reproduction, crossover and mutation operators.

- Reproduction- is a probabilistic process for selecting two parent strings from the population of strings on the basis of "roulette-wheel" mechanism, using their fitness values. This ensures that the expected number of times a string is selected is proportional to its fitness relative to the rest of the population. Therefore, strings with higher fitness values have a higher probability of contributing offspring.

- Crossover- is the process of selecting a random position in the string and swapping the characters either left or right of this point with another similarly partitioned string. This random position is called the crossover point. In this work the characters to the right of a crossover point are swapped. The probability of parent-chromosomes crossover was set to be between 0.6 and 1.0.

- Mutation- is the process of random modification of a string position by changing "0" to "1" or vice versa, with a small probability. It prevents complete loss of genetic material through reproduction and crossover by ensuring that the probability of searching any region in the problem space is never zero. In this work the probability of mutation was set to be between 0.01 and 0.1.

Convergence Criterion

Regenerations of the genetic algorithm are continued until all generated chromosomes become similar or the maximum number of 100 iterations is achieved.

Solution Methodology

Optimal selection of SSSC based damping controller parameters in the presence of harmonics is formulated as a nonlinear optimization problem and is solved using the proposed genetic-fuzzy algorithm (Figure 5.12) as follows:

Step 1: Input the system parameters, the initial population with N_{chrom}=250 and set $N_{it}=1$.

Step 2 (fitness function using fuzzy approximate reasoning, Figure 5.11*):*

Step 2A: for each chromosome**,** calculated the closed-loop system eigenvalues under consideration for all harmonic levels from Equation 5-18, based on the parameters specified by chromosome substrings (Figure 5.7).

Step 2B: Compute the summation of the eigenvalues' real part penalties (Equation 5-19) and the corresponding membership value (Figure 5.8) for each chromosome.

Step 2C: For each chromosome, compute the summation of the eigenvalues' damping ratio penalties (Equation 5-21) and the corresponding membership value (Figure 5.9).

Step 2D: Compute the fitness function for each chromosome using Table 5-1, Equation 5-23 and Figure 5.10.

Step 3 (Reproduction Process):

Step 3A: Define total fitness as the summation of all fitness values for all chromosomes.

Step 3B: Select a proportion of "roulette wheel" for each chromosome which is equal to the ratio of its fitness number to the total fitness number.

Step 3C: Improve generation by rolling the "roulette wheel" N_{chrom} times. Select a new combination of chromosomes.

Step 4 (Crossover Process):

Step 4A: Select a random number (RND_1) for mating two parent chromosomes.

Step 4B: If RND_1 is between 0.6 and 1.0 then combine the two parents, generate two offspring and go to Step 4D.

Step 4C: Else, transfer chromosome with no crossover.

Step 4D: Repeat Steps 4A to 4C for all chromosomes.

Step 5 (Mutation Process):

Step 5A: Select a random number (RND_2) for mutation of one chromosome.

Step 5B: If RND_2 is between 0.01 and 0.1 then apply the mutation process at a random position and go to Step 5D.

Step 5C: Else, transfer the chromosome with no mutation.

Step 5D: Repeat Steps 5A to 6C for all chromosomes.

Step 6 (Updating Populations): Check all the chromosomes and save the once with the maximum fitness value. Set $N_{it} = N_{it} + 1$ and replace the old population with the improved population generated by Steps 2 to 5.

Step 7 (Convergence): If all chromosomes are similar or the maximum number of iterations ($N_{it} = N^{\max}$) is achieved, print the solution and stop, else go to Step 2.

Figure 5.12 shows the flowchart of the proposed GA method for optimal selection of the POD controller in the presence of space and time harmonics.

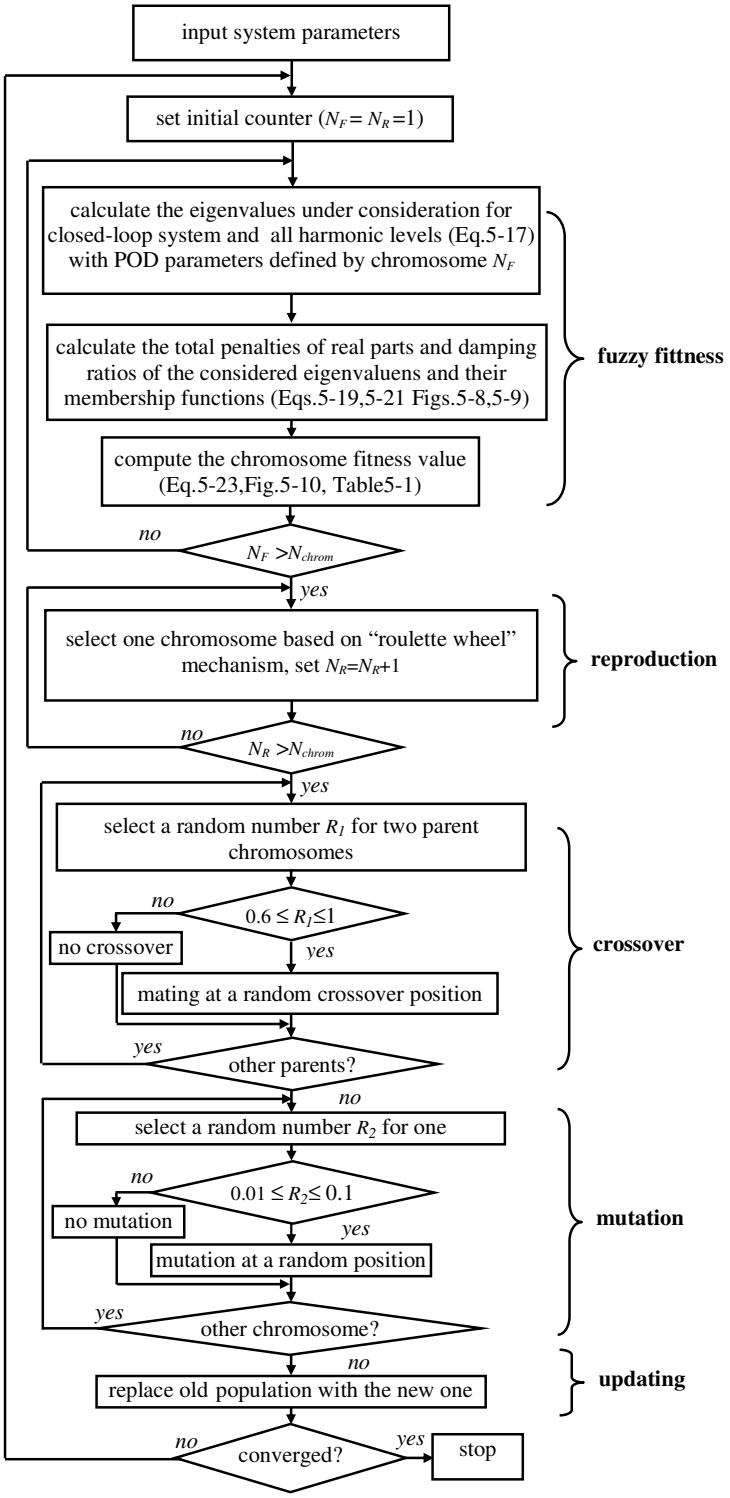

Figure 5.12 Proposed iterative genetic algorithm for optimal selection of SSSC based dynamic controller parameters in the presence of space and time harmonics.

5.5. System Performance and Simulation Results

To study the impact of an SSSC and its controller on the dynamic behaviour of the distorted SMIB system, an SSSC is included in the system investigated in Chapter four, Section 4.3. The system under study is a distorted power system which includes a synchronous generator, a distorted infinite bus (injecting time harmonics) and an SSSC unit that provides series compensation voltages at the fundamental frequency to the transmission line as shown in Figure 5.1. In Section 5.5.1, the open-loop system dynamic performance is investigated and variations of the eigenvalues compared to sinusoidal operation, are used to show the impact of harmonics on the dynamic operation of the system.

To improve the dynamic behaviour of the system in Section 5.5.2, an auxiliary robust POD controller is designed and applied to the SSSC. The proposed hybrid genetic-fuzzy algorithm Figure 5.12 is used for optimal selection of the POD parameters in the presence of time and space harmonics.

The synchronous generator and power system parameters are identical to those used in Chapter four, Section 4.3 and the SSSC specifications are:

$X_{SSSC} = 0.05$, $C_{DC} = 1$, $V_{DC0} = 1$, k=1, and m=0.1.

5.5.1. Dynamic Behaviour of Distorted SMIB System Installed with SSSC

In this section, eigenvalues of the SMIB system installed with an SSSC (Figure 5.1) are calculated using the state matrix of Equation 5-10 under sinusoidal and distorted operating conditions. In order to explore the impact of SSSC installation, similar operating conditions as Section 4.3 are considered and the synchronous generator delivers 555 MVA at 0.9 p.f. (lag) at rated terminal voltages.

Case 1- Sinusoidal Operation:

The system is assumed to be operating under sinusoidal conditions and the effects of magnetic saturation and damper windings are ignored. Using Equation 5-10, system the eigenvalues are calculated as follows:

$$\begin{cases} \lambda_{1,2} = -0.1101 \pm 5.7142i, \ (\omega_d = 0.909Hz, \ \zeta = 0.019) \\ \lambda_3 = -0.0884 \\ \lambda_4 = -0.0162 \end{cases}$$

The system response to an active power change of 0.1pu is illustrated in Figure 5.13.

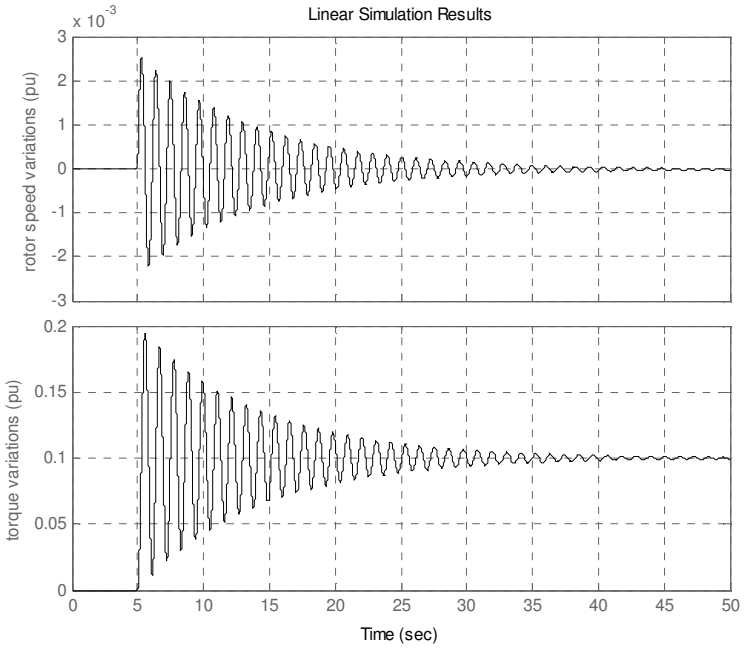

Figure 5.13. Time response of the rotor angle and speed subject to an input power perturbation for the sinusoidal operation of SMIB system installed with SSSC

The participation matrix is calculated as follows:

$$P = \begin{bmatrix} 0.5004 - 0.0096i & 0.5004 + 0.0096i & -0.0008 & 0 \\ 0.5004 - 0.0096i & 0.5004 + 0.0096i & -0.0008 & 0 \\ -0.0007 + 0.0204i & -0.0007 - 0.0204i & 1.0744 & -0.0730 \\ 0.00 - 0.0011i & 0.00 + 0.0011i & -0.0728 & 1.0729 \end{bmatrix} \begin{matrix} \Delta\omega_r \\ \Delta\delta \\ \Delta\psi_{fd} \\ \Delta V_{DC} \end{matrix}$$
$$\begin{matrix} \lambda_1 & \lambda_2 & \lambda_3 & \lambda_4 \end{matrix}$$

From the participation factors, it is observed that SSSC dynamics has no effect on the electromechanical modes. However installing the SSSC on the power system can relocate the electromechanical modes by improving the system parameters.

Case 2- Non-Sinusoidal Operation:

In this section, four different levels of time and space harmonics are considered (similar to Section 4.3). Table 5-2 shows the system eigenvalues, the damped frequencies of the electromechanical modes and their damping ratios.

Table 5-2
Impact of space and time harmonics on eigenvalues of SMIB system installed with SSSC (Figure 5.1)

Time Harmonic Level	**System Eigenvalues**	**Damped Freq. (ω_d) and Damping Ratio (ξ) of Electromechanical modes**
No harmonics	$\lambda_{1,2} = -0.1101 \pm 5.7142i$ $\lambda_3 = -0.0884$ $\lambda_4 = -0.0162$	$\omega_d = 0.909Hz,\ \zeta = 0.019$
1: $Base_T^*$ $(\theta_i^{(h)} = 0)$	$\lambda_{1,2} = -0.0961 \pm 5.9930i$ $\lambda_3 = -0.0962$ $\lambda_4 = -0.0162$	$\omega_d = 0.953Hz,\ \zeta = 0.016$
2: $Base_T^*$ $(\theta_i^{(h)} = \pi/2)$	$\lambda_{1,2} = -0.137 \pm 5.31i$ $\lambda_3 = -0.038 \pm 0.01i$	$\omega_d = 0.845Hz,\ \zeta = 0.025$
$2\times$ $Base_T^*$ $(\theta_i^{(h)} = 0)$	$\lambda_{1,2} = -0.088 \pm 6.11i$ $\lambda_3 = -0.104$ $\lambda_4 = -0.014$	$\omega_d = 0.972Hz,\ \zeta = 0.014$
$2\times$ $Base_T^*$ $(\theta_i^{(h)} = \pi/2)$	$\lambda_{1,2} = -0.218 \pm 4.20i$ $\lambda_{3,4} = 0.005 \pm 0.038i$	$\omega_d = 0.668Hz,\ \zeta = 0.051$

*) *0.03pu, 0.05pu, 0.02*pu and *0.01*pu for the 3rd to 9th harmonics, respectively.

Participation matrices for the four harmonic levels under consideration are:

Participation matrix for harmonic level 1:

$$\begin{array}{c} \\ \Delta\omega_r \\ \Delta\delta \\ \Delta\psi_{fd} \\ \Delta V_{DC} \end{array} \begin{bmatrix} 0.5003 - 0.0082i & 0.5003 + 0.0082i & -0.0007 & 0.000 \\ 0.5003 - 0.0082i & 0.5003 + 0.0082i & -0.0007 & 0.000 \\ -0.0006 + 0.0177i & -0.0006 - 0.0177i & 1.0698 & -0.0686 \\ -0.0000 - 0.0012i & -0.0000 + 0.0012i & -0.0684 & 1.0685 \end{bmatrix} \begin{array}{c} \\ \\ \\ \\ \end{array}$$
$$\lambda_1 \qquad \lambda_2 \qquad \lambda_3 \qquad \lambda_4$$

Participation matrix for harmonic level 2:

$$\begin{array}{c} \begin{bmatrix} 0.5004-0.0129i & 0.5004+0.0129i & -0.0004-0.0007i & -0.0004+0.0007i \\ 0.5004-0.0129i & 0.5004+0.0129i & -0.0004-0.0007i & -0.0004+0.0007i \\ -0.0007+0.0270i & -0.0007-0.0270i & 0.5007+1.1799i & 0.5007-1.1799i \\ -0.0001-0.0012i & -0.0001+0.0012i & 0.5001-1.1786i & 0.5001+1.1786i \end{bmatrix} \begin{matrix} \Delta\omega_r \\ \Delta\delta \\ \Delta\psi_{fd} \\ \Delta V_{DC} \end{matrix} \\ \begin{matrix} \lambda_1 & \lambda_2 & \lambda_3 & \lambda_4 \end{matrix} \end{array}$$

Participation matrix for harmonic level 3:

$$\begin{array}{c} \begin{bmatrix} 0.5003-0.0082i & 0.5003+0.0082i & -0.0007 & 0.000 \\ 0.5003-0.0082i & 0.5003+0.0082i & -0.0007 & 0.000 \\ -0.0006+0.0176i & -0.0006-0.0176i & 1.0538 & -0.0525 \\ -0.0000-0.0012i & -0.0000+0.0012i & -0.0524 & 1.0525 \end{bmatrix} \begin{matrix} \Delta\omega_r \\ \Delta\delta \\ \Delta\psi_{fd} \\ \Delta V_{DC} \end{matrix} \\ \begin{matrix} \lambda_1 & \lambda_2 & \lambda_3 & \lambda_4 \end{matrix} \end{array}$$

Participation matrix for harmonic level 4:

$$\begin{array}{c} \begin{bmatrix} 0.4999-0.0259i & 0.4999+0.0259i & 0.0001+0.0005i & 0.0001-0.0005i \\ 0.4999-0.0259i & 0.4999+0.0259i & 0.0001+0.0005i & 0.0001-0.0005i \\ 0.0004+0.0528i & 0.0004-0.0528i & 0.4996-0.2158i & 0.4996+0.2158i \\ -0.0002-0.0009i & -0.0002+0.0009i & 0.5002+0.2149i & 0.5002-0.2149i \end{bmatrix} \begin{matrix} \Delta\omega_r \\ \Delta\delta \\ \Delta\psi_{fd} \\ \Delta V_{DC} \end{matrix} \\ \begin{matrix} \lambda_1 & \lambda_2 & \lambda_3 & \lambda_4 \end{matrix} \end{array}$$

The participation matrix for the fourth harmonic level shows that the unstable low frequency oscillatory modes are the electrical modes related to dynamics of SSSC and the synchronous generator field winding.

Figure 5.14 shows the system response to the input mechanical power perturbation of 0.1 pu for the last harmonic level. In this figure the system oscillations through electromechanical modes are demonstrated. The effects of undamped oscillating modes related to the electrical circuits are more obvious in Figure 5.15. This figure illustrates how the system becomes unstable through low frequency oscillations related to the SSSC circuit.

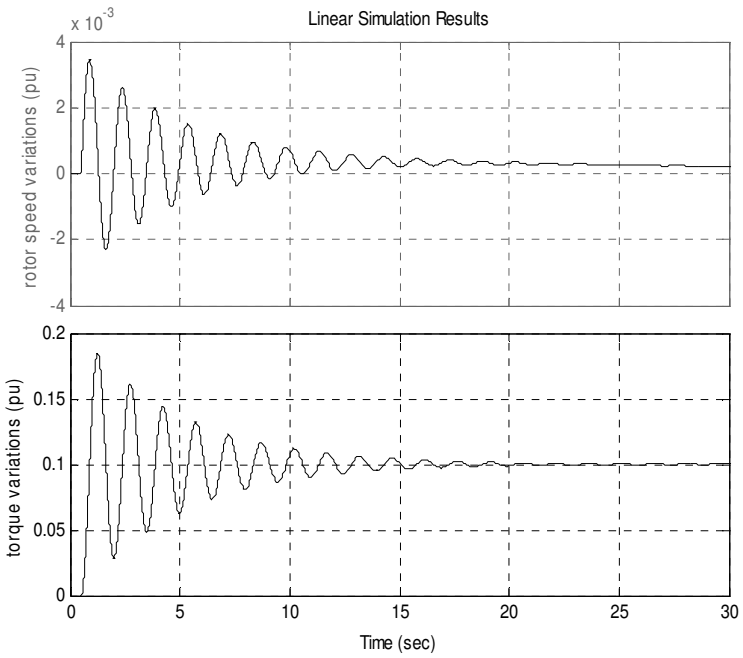

Figure 5.14 Time response of the rotor speed and electromechanical torque subject to an input power perturbation in the presence of time and space harmonics in SMIB system installed with SSSC

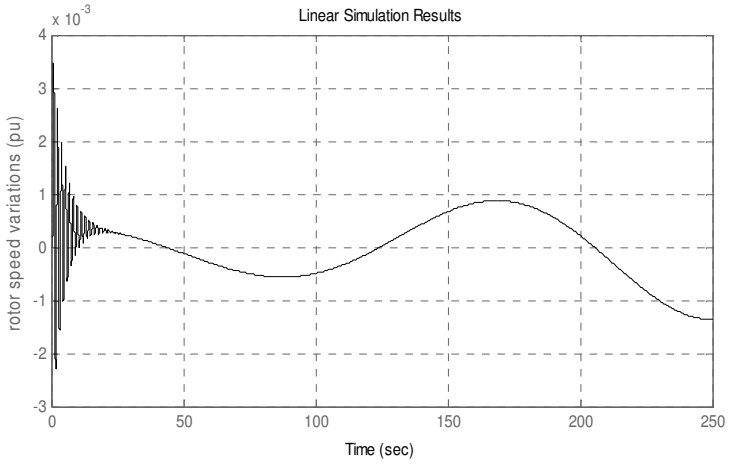

Figure 5.15 System instability through low frequency oscillations

5.5.2. Design of the Robust POD Controller

An auxiliary POD controller is designed and applied to the SSSC installed in the distorted SMIB system (Figure 5.1). The proposed hybrid genetic-fuzzy algorithm (Figure 5.12) is used for optimal selection of the POD parameters in the presence of time and space harmonics. To ensure the robustness of POD controller against changes in nonlinear loads and system conditions, four different harmonic levels (Equation 5-18) are considered. No harmonic distortion is considered at the first harmonic level to assure that the controller is kept effective under sinusoidal operating conditions. Controller parameters are also calculated assuming sinusoidal conditions and the controller performance is investigated under the influence of harmonics.

A. Selection of the POD Input Signal Based on Observability Matrices

To find the proper input signal to the controller, the observability matrices for all harmonic levels (Equation 5-18) are calculated for a number of candidate signals (including speed deviation of synchronous generator, phase angle deviation of the bus, deviation of the tie-line active power and deviation of the line current). With loading condition of P=0.9pu, the observability matrices are calculated as:

- Observability matrix for harmonic level 1:

$$\begin{bmatrix} -0.0003+0.0158i & -0.0003-0.0158i & 0.0002 & 0.000 \\ 0.9993 & 0.9993 & -0.7610 & -0.4556 \\ 0.6630+0.0218i & 0.6630-0.0218i & 0.0001 & 0.000 \\ 0.8271+0.0221i & 1.8271-0.0221i & -0.1469 & -0.1324 \end{bmatrix} \begin{matrix} \Delta\omega_r \\ \Delta\delta \\ \Delta P_e \\ \Delta I \end{matrix}$$
$$\lambda_1 \qquad \lambda_2 \qquad \lambda_3 \qquad \lambda_4$$

- Observability matrix for harmonic level 2:

$$\begin{bmatrix} -0.0004+0.0138i & -0.0004-0.0138i & 0.0001 & 0.0001 \\ 0.9994 & 0.9994 & -0.8013 & -0.8013 \\ 0.5033+0.0279i & 0.5033-0.0279i & 0.000 & 0.000 \\ 0.6760+0.0282i & 0.6760-0.0282i & -0.1695-0.0169i & -0.1695+0.0169i \end{bmatrix} \begin{matrix} \Delta\omega_r \\ \Delta\delta \\ \Delta P_e \\ \Delta I \end{matrix}$$
$$\lambda_1 \qquad \lambda_2 \qquad \lambda_3 \qquad \lambda_4$$

- Observability matrix for harmonic level 3:

$$\begin{bmatrix} -0.0002+0.0162i & -0.0002-0.0162i & 0.0002 & 0.000 \\ 0.9993 & 0.9993 & -0.7207 & -0.3850 \\ 0.6928+0.0201i & 0.6928-0.0201i & 0.0001 & 0.000 \\ 0.8695+0.0202i & 0.8695-0.0202i & -0.1461 & -0.1218 \\ \lambda_1 & \lambda_2 & \lambda_3 & \lambda_4 \end{bmatrix} \begin{matrix} \Delta\omega_r \\ \Delta\delta \\ \Delta P_e \\ \Delta I \end{matrix}$$

- Observability matrix for harmonic level 4:

$$\begin{bmatrix} -0.0006+0.0112i & -0.0006-0.0112i & 0.0001 & 0.0001 \\ 0.9995 & 0.9995 & -0.8778 & -0.877 \\ 0.3275+0.0341i & 0.3275-0.0341i & 0.000 & 0.000 \\ 0.5061+0.0343i & 0.5061-0.0343i & -0.1522-0.025i & -0.1522+0.025i \\ \lambda_1 & \lambda_2 & \lambda_3 & \lambda_4 \end{bmatrix} \begin{matrix} \Delta\omega_r \\ \Delta\delta \\ \Delta P_e \\ \Delta I \end{matrix}$$

The participation matrices (Section 5.5.1, Case 2) show that the first two columns of the observability matrices are related to the electromechanical modes. Hence, the control signals $\Delta\delta, \Delta P_e$ and ΔI have good observability of the electromechanical modes. However, ΔI is a local signal with proper observability of all system modes and is selected as the POD input signal.

To evaluate the observability of the selected input signal under different operating conditions, the rotor mode observability is plotted against the change in line active power for sinusoidal (Figure 5.16) and non-sinusoidal (Figure 5.17) operating conditions considering the four levels of harmonic distortion (Equation 5-18). It is observed that although the presence of harmonics can change the observability characteristic, the line current has proper observability of the rotor mode at different operating points and harmonic levels. Note that for the sinusoidal operating condition, increasing the active power transferred results in higher mode observability.

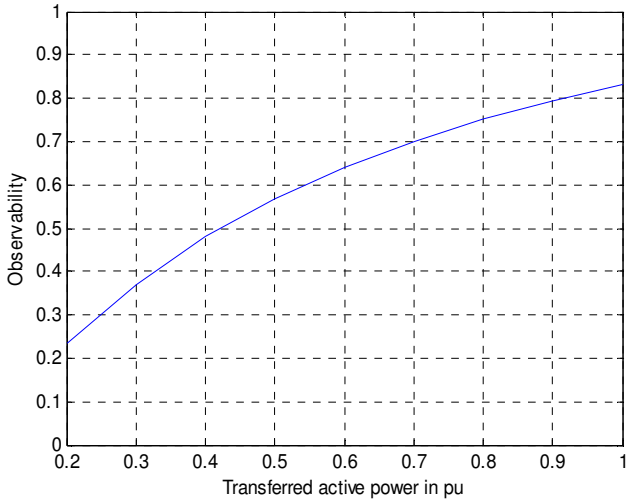

Figure 5.16 Plot of the rotor mode observability against the transferred active power for line control signal (SMIB system with sinusoidal operating conditions)

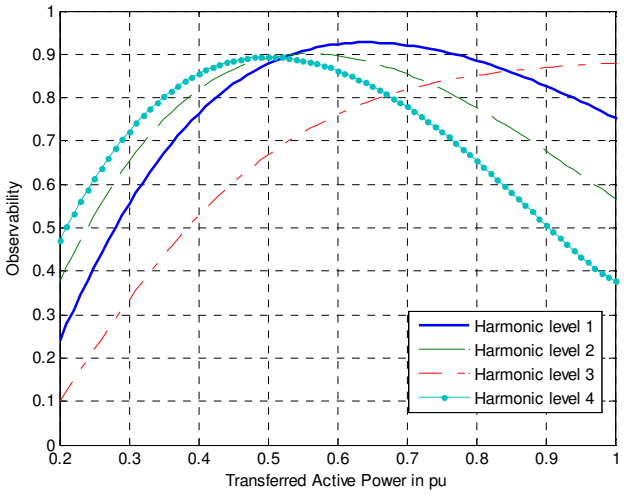

Figure 5.17 Plot of the rotor mode observability against the transferred active power for line control signal (distorted SMIB system with four harmonic levels (Eq. 5-18)).

B. Optimal Values of POD Controller Parameters

The proposed genetic-fuzzy algorithm in Figure 5.12 is used to determine optimum values of POD controller parameters within the desired permissible limits (K_{smax}=*4*, T_{max}=*2*) for the following conditions:

- Sinusoidal Operation- ignoring the presence of time and space harmonics (Sinusoidal POD).
- Distorted Operation- considering four levels (Equation 5-18) of time and space harmonics (Robust POD).

The main goal is to relocate the lightly-damped electromechanical modes into the desired region of the *s*-plane, which is specified by suitable limits for the real parts of the eigenvalues (σ^d=-1) and damping ratios (ζ^{min}=0.2). Table 5-3 shows computed optimal values for the POD controller parameters using the proposed hybrid Genetic-Fuzzy algorithm. The value of T_ω is set to 10seconds.

Table 5-3
SSSC based POD controller optimal parameters determined by proposed genetic-fuzzy algorithm

System Condition	K_s	T_1	T_2	T_3	T_4
Sinusoidal	0.95	0.30	0.19	0.32	0.74
Distorted	0.34	0.64	0.53	0.29	1.24

C. Simulation Results

The calculated open-loop and closed-loop system eigenvalues for sinusoidal operating condition are presented in Table 5-4. Table 5-5 shows results for the synchronous generator rotor angle, the open-loop system eigenvalues and the comparison between closed-loop system eigenvalues using the "Sinusoidal POD" and the "Robust POD" for all harmonic levels.

Table 5-4
System open-loop and closed-loop eigenvalues for sinusoidal operating condition and rotor angle=39.07°

	open-Loop	Closed-Loop (Sinusoidal POD)
Eigenvalues and Damping Ratio	$-0.11 \pm 5.71i,\ \ \zeta = 0.019$ -0.08 -0.016	$-12.31 \pm 51.99i,\ \zeta = 0.23$ -3.06 -1.75 -0.14 -0.0678 -0.0062

Table 5-5
Impact of time and space harmonics on the SG rotor angle, eigenvalues of the open-loop system and closed-loop system with "sinusoid POD" and "robust POD"

Harmonic Level (Eq.5-18)	**Rotor Angle (δ_o) [% Deviation]**	**Open-Loop Eigenvalues and Damping Ratios**	**Closed-Loop Eigenvalues and Damping Ratios**	
			Sinusoidal POD	**Robust POD**
1	38.81^o [-0.68%]	$-0.098 \pm 5.97i$ $(\zeta = 0.016)$ -0.09 -0.018	$-3.518 \pm 28.88i$ $(\zeta = 0.12)$ -3.045 -1.755 -0.137 -0.066 -0.007	$-4.214 \pm 12.16i$ $(\zeta = 0.32)$ $-1.537 \pm 1.09i$ -0.119 -0.071 -0.013
2	39.47^o [+1.0%]	$-0.137 \pm 5.31i$ $(\zeta = 0.025)$ $-0.038 \pm 0.01i$	$-0.755 \pm 13.21i$ $(\zeta = 0.057)$ -3.035 -1.757 -0.129 -0.062 -0.008	$-2.359 \pm 9.33i$ $(\zeta = 0.24)$ $-1.523 \pm 1.094i$ -0.112 -0.054 -0.020
3	38.76^o [-0.8%]	$-0.088 \pm 6.1i$ $(\zeta = 0.014)$ -0.104 -0.014	$-1.199 \pm 16.63i$ $(\zeta = 0.072)$ -3.051 -1.752 -0.140 -0.065 -0.006	$-2.988 \pm 10.25i$ $(\zeta = 0.28)$ $-1.552 \pm 1.08i$ -0.119 -0.067 -0.014
4	40.10^o [+2.6%]	$-0.218 \pm 4.20i$ $(\zeta = 0.051)$ $0.005 \pm 0.038i$	$-0.446 \pm 9.85i$ $(\zeta = 0.045)$ -3.033 -1.756 -0.127 -0.057 -0.009	$-1.657 \pm 7.81i$ $(\zeta = 0.21)$ $-1.527 \pm 1.08i$ -0.109 $-0.031 \pm 0.01i$

Figure 5.18 shows the system dynamic responses to a mechanical input power change of 0.1pu before and after installing the POD controller designed for sinusoidal and distorted operating conditions for all harmonic levels. Figure 5.19 illustrates the improvement of system electromechanical modes after installation of the proposed POD. Note that the "Sinusoidal POD" controller is unable to shift electromechanical modes into the desired region of the *s*-plane under harmonic conditions while the proposed "Robust POD" remains effective under all operating considerations.

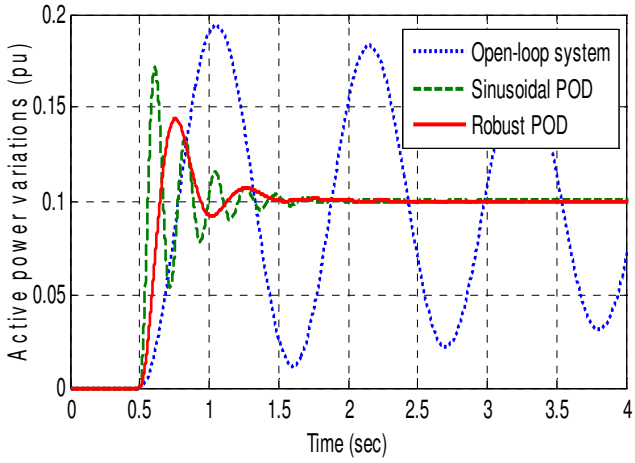

(a)

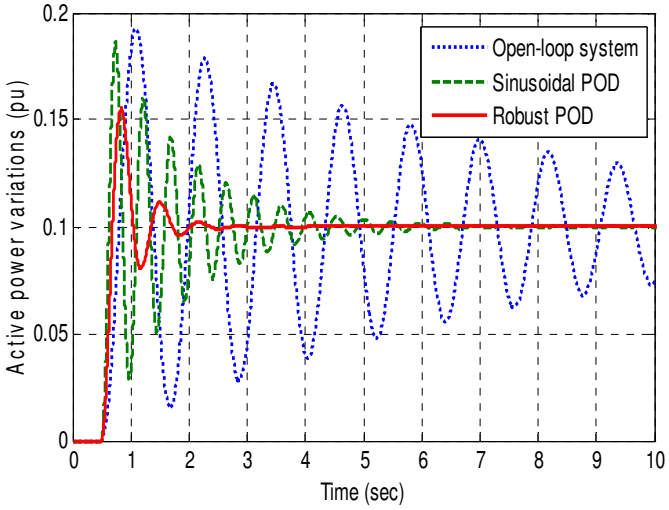

(b)

Figure 5.18 Time responses of open-loop and closed-loop systems (with "Sinusoidal POD" and the proposed "Robust POD") to a mechanical input change of 0.1pu for; (a) harmonic level 1, (b) harmonic level 2, (c) harmonic level 3, (d) harmonic level 4 (the selected harmonic levels are listed in Eq.5-18)

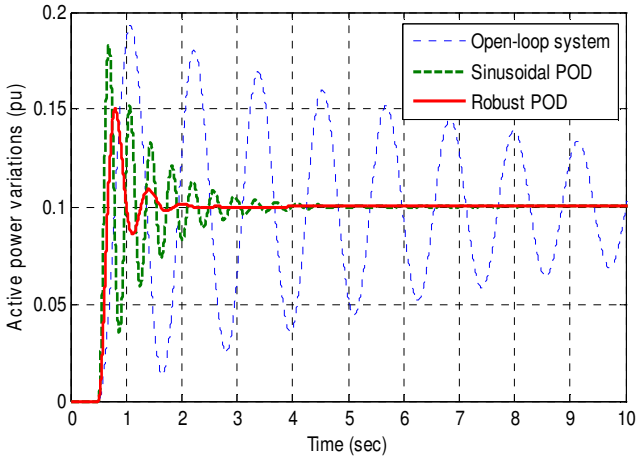

(c)

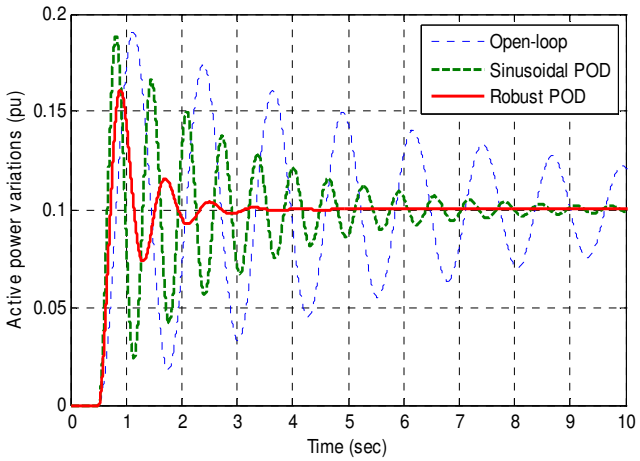

(d)

Figure 5.18 …continued

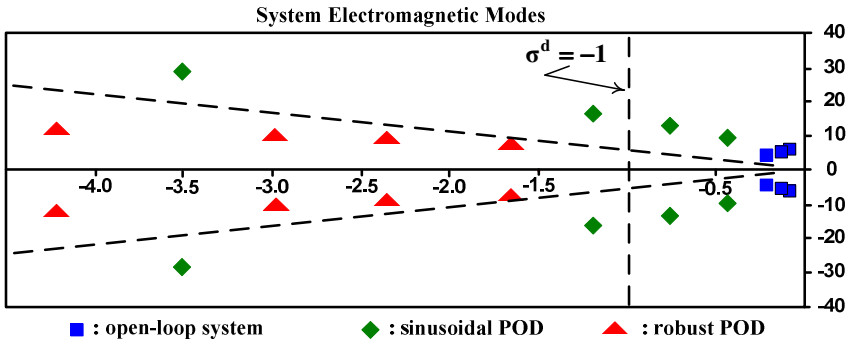

Figure 5.19 Locations of eigenvalues in *s*-plane for open- and closed-loop systems with "Sinusoidal POD" and "Robust POD" showing the effectiveness of the proposed controller (the selected desired region in *s*-plane is bounded by $\sigma^d = -1$ and $\zeta^{min} = 0.2$)

5.6. Conclusions

In this chapter, the influence of time and space harmonics on small-signal stability of distorted SMIB systems installed with an SSSC was investigated using eigenvalue analysis. The modified Heffron-Phillips model for this system was derived in the presence of harmonics. To increase the damping of electromechanical oscillations and improve the relative stability, a supplementary control action was applied to the SSSC through the auxiliary controller. The analysis of mode observability was used to select the effective feedback signal for the damping controller. The problem of optimal selection of SSSC based robust damping controller parameters has been formulated as a nonlinear constrained problem and was solved using a genetic-fuzzy algorithm in the presence of time and space harmonics. Fuzzy approximate reasoning was used to calculate the chromosome fitness values. Total penalties of the real parts and damping ratios of the eigenvalues were defined as the inputs to the fuzzy system. Outcomes from this chapter were:

- Time and space harmonics will change elements of the system state matrix and hence relocate system eigenvalues (equations 5-10 and 5-17, tables 5-2 and 5-5).
- Harmonic phase angles have considerable impact on the steady state and dynamic behaviour of the system and can cause power system instability (tables 5-2 and 5-5).
- Using the proposed hybrid genetic-fuzzy algorithm (Figure 5.12) and considering different levels of time harmonics (Equation 5-18), a robust POD controller for distorted operating conditions is designed and tested (tables 5-3, 5-5, figures 5.18 and 5.19).
- Tuning the POD controller based on sinusoidal conditions by ignoring time and space harmonics can cause undesired system dynamic behaviour under the influence of harmonics (figures 5.18 and 5.19 and Table 5-5: column 4).
- The proposed method is applicable for tuning other types of system stabilizers in order to keep them effective under non-sinusoidal operating conditions.

The outcomes make a significant contribution to the work in this area.

CHAPTER SIX

DYNAMIC BEHAVIOUR OF A MULTI MACHINE MULTI BUS DISTRIBUTED GENERATION SYSTEM IN THE PRESENCE OF HARMONICS

6.1. Introduction

In the previous chapters the impact of time and space harmonics on dynamic behaviour of a SMIB power system was studied in details. It was shown that the presence of harmonics introduces additional terms in the machine equations; this makes the stability study of the system very complex. The simplification of the power system as a SMIB system helps with the understanding and solving the problem of the small-signal stability by linearizing the equations around the operating point. However, to show the impact of harmonics on the behaviour of a more realistic power system, in this chapter an actual Multi Machine Multi Bus (MMMB) Distributed Generation (DG) system located in Western Australia is investigated under sinusoidal and distorted operating conditions.

DG systems include generators with low inertia and higher levels of harmonic distortions. Hence, the dynamic behaviour of these systems is more likely to be affected by the presence of harmonics. This can be of more concern if the systems are highly loaded and are marginally stable. The system under study is a 24-bus system including six distributed generators. The dynamic models of generation buses include the synchronous generators, exciter systems and turbine-governors.

In distorted conditions, nine nonlinear loads are connected in the system and a Decoupled Harmonic Power Flow (DHPF) algorithm is used to calculate the steady state parameters [70]. The nonlinear loads are modelled as decoupled harmonic current sources and the model of a synchronous generator in the harmonic domain, presented in chapter three, is used for distributed generators. The power system toolbox with the modified model of the synchronous generator is used for the

calculation of the system eigenvalues. The results are presented for sinusoidal and distorted conditions. Also the effectiveness of the PSSs designed for sinusoidal conditions is investigated under distorted conditions. The results show that the gain of the PSSs should be increased in distorted conditions in order to obtain sufficient and acceptable damping ratios.

6.2. Dynamic Stability of a Multi-Machine Multi-Bus System

The general procedure adapted in this chapter to study the small-signal stability of multi machine systems is similar to that taken for a SMIB system in the previous sections. However, representation of an extensive transmission network, loads, a variety of generators, excitation systems and prime mover models and others, makes the process very complex. The procedure can be summarised in the following steps:

1- Initialize all dynamic models at the initial conditions set by the power flow.

2- Form linearized models of all of the specified system components at the operating point.

3- Interconnect these models to obtain an overall state space model of the linearized system, including the power system network.

4- Form the full linearized model by eliminating the network variables.

In the distorted conditions, including the impact of harmonics in the synchronous generators models makes the analytical calculation of the system state equations even more complex. However, there are a number of small-signal stability programs which form the required models of the system components such as the generators and their controls. In this work, the MATLAB based Power System Toolbox is used. The generator models are modified to include the impact of harmonics. In this program, the linearization of the nonlinear equations is performed by numerically calculating the Jacobian. Starting from the states determined from model initialization, a small perturbation is applied to each state in turn. The change in the rates of change of all the states divided by the magnitude of the perturbation gives a column of the state matrix corresponding to the disturbed state. Following each rate of change of state

calculation, the perturbed state is returned to its equilibrium value and the intermediate variable values are reset to there initial values.

The input matrix B, the output matrix C and the feed forward matrix D can be determined in a similar manner [68].

6.3. Characteristics of the DG System under Investigation

In this section the steady-state operation and dynamic behaviour of a DG system is investigated. The study is done under sinusoidal and harmonically polluted conditions.

The modelled system is in the distributed level and is based on an existing system in Western Australia [69]. Figure 6.1 illustrates the single line diagram of the system.

6.3.1. Steady-State Model of the System

The DG system under study has 24 buses. Bus 9000 and buses below till bus 9109 are 22kV and the rest of buses, except bus 9020, are 33kV. Bus 9020 is the distributed generation plant and is 415V.

The system is connected to the grid, which is represented by a bus with a large generator and load connected to it. This bus is assumed as the swing bus for load flow studies (bus 9000).

This system includes a distributed generation plant that consists of six generators of 400kW each. These generators generate power at 415V and are connected to the 33kV system through a step up transformer.

There are four transformers in the system. The transformer connecting bus 9020 to bus 9120, steps up the voltage from 415V to 33kV. Tap changing transformers are connected between buses 9012 and 9011 and also between buses 9015 and 9113 for voltage regulation. A step down transformer connects bus 9011 to bus 9109 and reduces voltage from 33kV to 22kV.

The capacitance of the lightly loaded transmission lines are represented by shunt capacitor banks.

The system characteristics including all the data for the loads, transmission lines generators and transformers are presented in Table 6-1, Table 6-2, Table 6-3 and Table 6-4, respectively. Table 6-11 shows the active power produced by the generators.

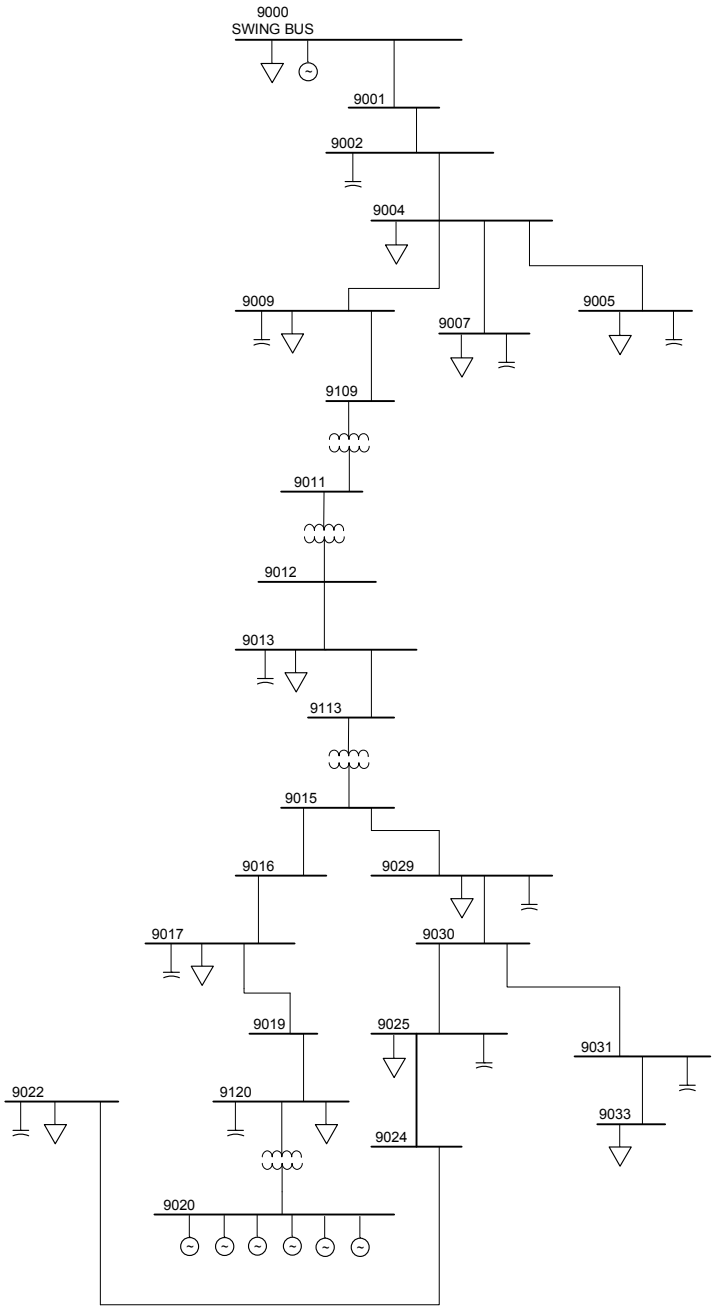

Figure 6.1. Single line diagram of the DG system under investigation located in Western Australia [69] (S_{Base}=100 MVA)

Table 6-1
System loads

Bus Number	P-Load (Mw)	Q-Load (Mvar)
9000	1913.5	942.6
9004	0.9	0.6
9005	0.3	0.2
9007	0.7	0.4
9009	0.3	0.2
9011	1	0.62
9013	0.2	0.1
9017	0.1	0.05
9019	0.7	0.4
9022	0.35	0.2
9025	0	0
9028	0.2	0.1
9031	0.1	0.05
9033	0.1	0
9120	0.956	0.853

Table 6-2
Capacitors used to model lightly loaded transmission lines

Bus Number	Capacitance (Mvar)
9002	0.03
9005	0.06
9007	0.03
9009	0.11
9013	0.31
9017	0.03
9022	0.12
9025	0.12
9028	0.19
9031	0.12
9120	0.91

Table 6-3
Machine characteristics

Bus Number	P-max (Mw)	P-min (Mw)	Q-max (Mvar)	Q-min (Mvar)	M-Base (MVA)
9000	2400	-9999	1800	-1307	3000
9020	0.4	-9999	0.28	-0.2	0.47
9020	0.4	-9999	0.28	-0.2	0.47
9020	0.4	-9999	0.28	-0.2	0.47
9020	0.4	-9999	0.28	-0.2	0.47
9020	0.4	-9999	0.28	-0.2	0.47
9020	0.4	-9999	0.28	-0.2	0.47

Table 6-4
Transformer characteristics

From Bus	To Bus	X (pu)	Winding 1 Ratio (pu)	Winding 2 Ratio (pu)
9011	9012	0.66667	1	1
9011	9109	1	1	1
9015	9113	1	0.95	1
9020	9120	3	1	1.08

6.3.2. Dynamic Model of the System

To study the small-signal stability of the system, dynamic models of the generator plants are required. The infinite bus is represented by a very large synchronous machine, and the distributed generation plant (bus 9020) has six small gas turbine synchronous generators. The dynamic characteristics of the system generation are presented in the following sections.

6.3.2.1. Dynamic Model of the Swing Bus

The swing bus includes a large synchronous generator, thermal turbine governor and an excitation system.

Synchronous Generator of the Swing Bus

The swing synchronous machine has a salient pole structure with three damper windings, one along *d*-axis and two along *q*-axis. The model used for the generators is in *dq* coordinates and is based on the real values of the generator inductances and resistances. However, these parameters, referred as fundamental or basic parameters, can not be directly determined from measured responses of the machine. Therefore, the traditional approach is adopted to express the generator data in terms of standard parameters which are related to the observed behaviour as viewed from the terminals under suitable test conditions [2]. The standard generator data is given in Table 6-5.

Table 6-5
Data used to model the synchronous machine for the swing bus

Bus Number	9000	**Xd (pu)**	2.43
T'd0	7.8 sec.	**Xq (pu)**	1.25
T "d0	0.03 sec.	**X'd (pu)**	0.348
T "q0	0.6 sec.	**X "d (pu)**	0.22
H (Inertia)	3.39 (MW.s/MVA)	**X "q (pu)**	0.22
D (Speed Damping)	0	**Xl (pu)**	0.18

Following equations are used to extract the fundamental parameters from the standard generator data [2].

$$
\begin{aligned}
&X_{ad} = X_d - X_l \\
&R_F = X_{ad}{}^2 / (X_d - X'_d)(\omega_0 T'_{d0}) \\
&X_F = X_{ad}(X'_d - X_l)/(X_d - X'_d) \\
&R_D = (X'_d - X_l)^2 / (X'_d - X''_d)(\omega_0 T''_{d0}) \\
&X_D = (X'_d - X_l)(X''_d - X_l)/(X'_d - X''_d) \\
&X_{aq} = X_q - X_l \\
&R_G = X_{aq}{}^2 / (X_q - X'_q)(\omega_0 T'_{q0}) \\
&X_G = X_{aq}(X'_q - X_l)/(X_q - X'_q) \\
&R_Q = (X'_q - X_l)^2 / (X'_q - X''_q)(\omega_0 T''_{q0}) \\
&X_Q = (X'_q - X_l)(X''_q - X_l)/(X'_q - X''_q)
\end{aligned}
\qquad (6\text{-}1)
$$

Using the above equations, the fundamental parameters of the swing generator are calculated as follows:

Stator Parameters: L_s=1.286, L_m=0.393, M_s=0.553 R_a =0.0.

Rotor Parameters: R_F =0.0008, R_D =0.0195, R_G =0.0108, R_Q =0.0018,

L_F = 2.4316, L_D = 2.3025, L_G = 1.6356, L_Q = 1.1148,

L_{GQ}=1.07, L_{FD}=2.25, L_{FG}= L_{FQ}= L_{DG}= L_{DQ}=0.

Stator Rotor Mutual Parameters: M_F =M_D= 2.25, M_G =M_Q=1.07.

Excitation System of the Swing Bus

The excitation system includes terminal voltage transducer, voltage regulator, exciter and a feedback. Figure 6.2 illustrates the general structure of an excitation system.

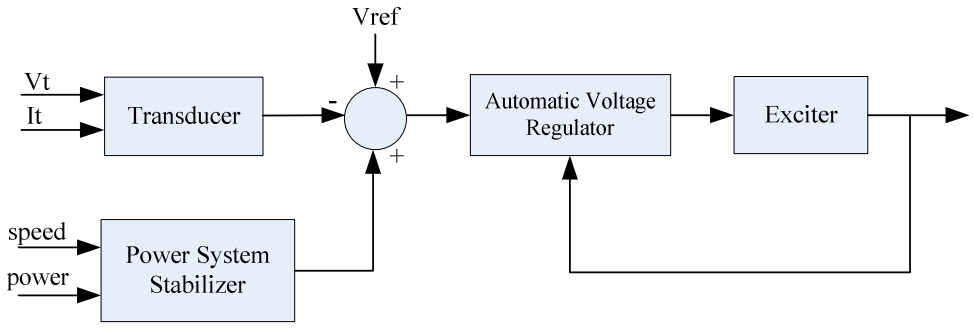

Figure 6.2. The excitation system [68]

The exciter used for the swing generator is a DC exciter. These types of exciters use direct current generators with shunt or series field connection to supply the field current to the synchronous generator. The same model structure is used for both types of generators but different data are used to represent the type of the field connection. The DC generators used here have series connected field configuration.

The corresponding block diagram is shown in Figure 6.3 and the exciter data used for the generator installed on the swing bus is presented in Table 6-6.

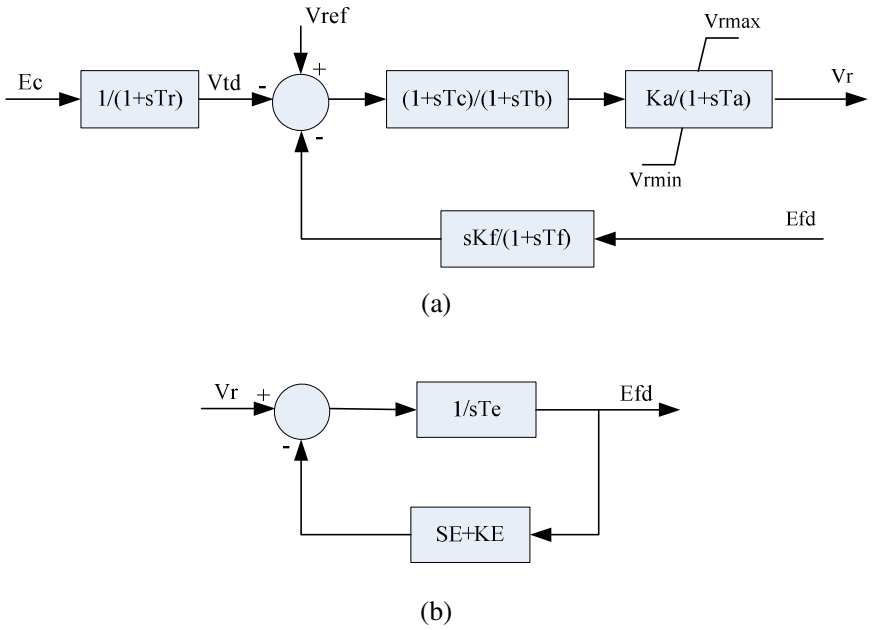

Figure 6.3. Swing generator excitation system; (a) voltage regulator, (b) DC exciter

Table 6-6
Data used to model the voltage regulator and the exciter for the swing bus

Tr	0.035 sec.	**V_{rmax}**	6
Ka	50	**Ke**	0.4
Ta	18.9 sec.	**Te**	0.2 sec.
Tb	0.01	**E1**	0.1
Tc	0.072	**SE(E1)**	0.4
Kf	0	**E2**	8
Tf	1	**SE(E2)**	0.05
V_{rmin}	0		

Turbine-Governor of the Swing Bus

A simplified model is used for turbine-governor as shown in Figure 6.4. This is a general purpose model and can be assumed as a thermal plant. The data used for this model is given in Table 6-7.

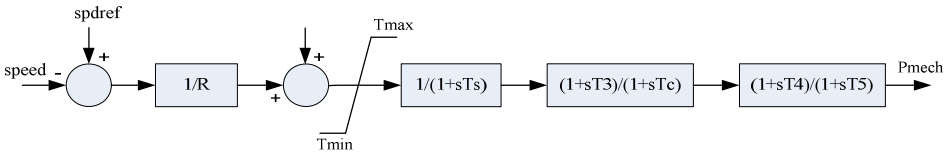

Figure 6.4. Simple turbine-governor model used for the swing bus

Table 6-7
Data used to model the turbine-governor for the swing bus

Bus Number	9000	**T4**	0
1/R	25pu	**T5**	0.01sec.
Ts	0.35 sec.	**spdref**	1
Tc	0.15 sec.	**Tmax**	0.81pu
T3	0	**Tmin**	0pu

6.3.2.2. Dynamic Model of the Distributed Generation Bus

The distributed generation plant includes six identical generators. Each generator has its own synchronous machine, exciter and governor.

Synchronous Generator of the DG Bus

Synchronous machines of the DG bus are salient pole with three damper windings, one along *d*-axis and two along *q*-axis. The data used for distributed generators is given in Table 6-8.

Table 6-8
Standard parameters used for the distributed generators

Bus Number	9020	**Xd (pu)**	2.19
T'd0	3.41 sec.	**Xq (pu)**	1.61
T "d0	0.03 sec.	**X'd (pu)**	0.2
T "q0	0.1748	**X "d (pu)**	0.22
H (Inertia)	0.74 (MW.s/MVA)	**X "q (pu)**	0.22
D (Speed Damping)	0	**Xl (pu)**	0.0055

Using Equation 6-1, the fundamental parameters of the distributed generators are calculated as:

Stator Parameters: L_s=1.316, L_m=0.193, M_s=0.583 R_a=0.0.

Rotor Parameters: R_F=0.0017, R_D=0.0249, R_G=0.0224, R_Q=0.0047,

L_F = 2.2019, L_D = 2.1713, L_G = 1.6917, L_Q = 1.5677,

L_{GQ}=1.46, L_{FD}=2.04, L_{FG}= L_{FQ}= L_{DG}= L_{DQ}=0.

Stator Rotor Mutual Parameters: M_F =M_D= 2.04, M_G =M_Q=1.46.

Excitation System of the DG Bus

Figure 6.5 shows the exciter used for the distributed synchronous machines with the parameters of Table 6-9.

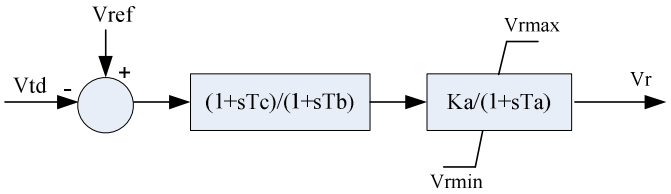

Figure 6.5. Excitation system used for the DG generators

Table 6-9
Data used to model the excitation system for the DG generators

Ka	200	**Tc**	0
Ta	0.1 seconds	$\mathbf{V_{rmax}}$	10
Tb	0.01 sec.	$\mathbf{V_{rmin}}$	0

Turbine-Governor of the DG Bus

For stability studies, the distributed generators prime movers are assumed to be gas turbines with the block diagram shown in Figure 6.6 and the data presented in Table 6-10.

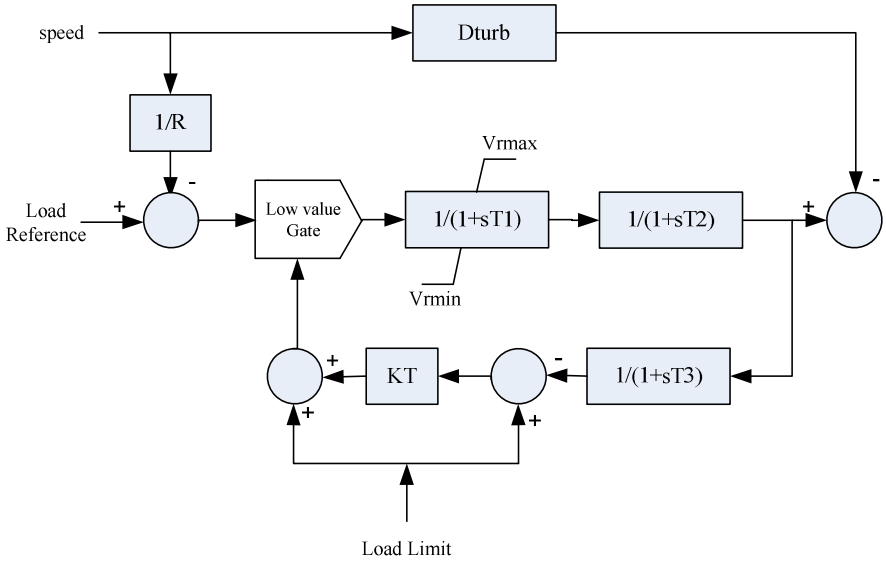

Figure 6.6. Model of the gas turbine used for distributed generators

Table 6-10
Data used to model the turbine-governor for the distributed generators [69]

R	0.05	**KT**	2.43
T1	0.4 sec.	**Mmax**	1.25
T2	0.1 sec.	**Vmin**	0.348
T3	3 sec.	**Dturb**	0
AT (Ambient Temperature Load limit)	1.0		

6.4. Operation of the DG System under Sinusoidal Conditions

The first step to study the dynamic behaviour of a system is to find the initial steady-state operating conditions. Later, to calculate the system eigenvalues, the machine and system equations will be linearized around this initial operating point.

6.4.1. System Steady-State Operation

To calculate the steady-state parameters of the system in sinusoidal conditions, a load flow program is applied to the system. The selected load flow program is based on the Newton-Raphson method and is coded in Matlab software. The system loading is presented in Section 6.3.1, and listed in Table 6-1.

The load flow outputs including the generators powers and the system steady-state bus voltages are summarized in Table 6-11 and Table 6-12, respectively.

Other system parameters including active and reactive powers and also line currents can be calculated from system characteristics and the bus voltages.

The steady-state rotor angle of the distributed generators is calculated as follows:

S_{base}=0.47 MVA, P=0.3 MW, Q=0.05 MVar, V=1pu → P=0.638 pu, Q=0.1064 pu

I_t =0.647 pu, PF=0.986, ψ_d=0.88pu, ψ_q=-0.64pu using Equation 3-28 → δ_0 = 41.19°.

Table 6-11
Load flow outputs for DG system under rated sinusoidal operating conditions: Generators powers

Generator Number	**Bus Number**	**Generated active power (MW)**	**Generated reactive power (Mvar)**
1	9000	1917.13	944.47
2	9020	0.3	0.05
3	9020	0.3	0.05
4	9020	0.3	0.05
5	9020	0.3	0.05
6	9020	0.3	0.05
7	9020	0.3	0.05

Table 6-12
Load flow outputs for DG system of Figure 6.1 under rated sinusoidal operating conditions: System bus voltages

Bus Number	**Voltage Magnitude (pu)**	**Voltage Angle (deg)**
9000	1.03	0
9001	1.0215	-0.3335
9002	1.013	-0.6726
9004	1.0045	-1.0152
9005	1.0038	-1.0385
9007	1.0028	-1.0661
9009	1.0004	-1.2223
9011	0.9893	-2.6782
9012	0.99	-3.1439
9013	0.9893	-3.2654
9015	0.9878	-3.8305
9016	0.9875	-3.8114
9017	0.9873	-3.7919
9019	0.9872	-3.7623
9020	1	-0.3699
9022	0.9849	-4.1169
9024	0.9855	-4.0827
9025	0.9862	-4.0483
9028	0.9871	-3.9327
9030	0.9866	-4.0048
9031	0.9864	-4.0335
9033	0.9863	-4.0451
9109	0.9969	-1.4035
9113	0.9884	-3.3474
9120	0.9889	-3.6835

6.4.2. System Dynamic Behaviour

System dynamic behaviour is studied under the sinusoidal operating conditions using the power system toolbox. The system eigenvalue are found in order to evaluate the system small-signal stability. Furthermore, PSSs are included to improve the stability

of the distributed generators. The phase compensation method is used for tuning the PSSs and the root locus is plotted to determine their optimum gain values.

There are 74 state variables in the DG system under investigation having no PSSs connected. It includes 10 variables for each distributed generator and 14 variables are related to the swing generator. Synchronous generators state variables are $\delta, \omega, \psi_{FD}, \psi_D, \psi_G$ and ψ_Q.

Table 6-13 summarizes the eigenvalues of the system, as well as the corresponding mode frequencies and damping ratios.

The first eigenvalue represents the zero eigenvalue due to the redundant state variables or in other words, the lack of uniqueness of absolute rotor angle [2]. According to Table 6-13, all system eigenvalues are in the left side of the *s*-plane and hence, the system is stable. Calculating the participation factors for the weakly damped modes shows that these are the interplant modes of rotor angle and speed variations in distorted generation bus. The normalized participation factors for the eigenvalues number 52 and 53 are shown in Figure 6.7.

It is observed that the rotor angle and speed of the distributed generator number 5 are the dominant state variables. The damping ratio of these modes is 0.09 which is less than the sufficient value of 0.2. Usually, the local plant and interplant modes have frequencies in the range of 0.7 to 2.0Hz. But in this system, having small distributed generators with very low inertia (H=0.7), the rotor oscillation frequencies has increased to 4.8Hz.

Table 6-13
DG system modes under sinusoidal conditions and without PSS

Eigenvalue Number	**Eigenvalue**	**Frequency (Hz)**	**Damping Ratio**
1	-4.81×10^{-8}	0	1
2,3	-0.23 ± 0.52i	0.0835	0.4118
4	-0.7378	0	1
5	-1	0	1
6,7,8,9,10	-1.426	0	1
11	-1.6803	0	1
12,13	-0.59 ± 2.84i	0.4521	0.2049
14,15,16,17,18	-3.0353	0	1
19	-3.3002	0	1
20	-3.8765	0	1
21	-7.8646	0	1
22	-8.3406	0	1
23,24,25,26,27	-9.0269	0	1
28,29,30, 31,32,33	-10	0	1
34,35,36,37,38	-10.2891	0	1
39	-10.5438	0	1
40	-11.8432	0	1
1,42,43,44,45	-13.4688	0	1
46	-24.618	0	1
47,48	-3.42 ± 24.50i	3.9003	0.1383
49	-28.5162	0	1
50,51,52,53,54,5 5,56,57,58,59	-2.72 ± 30.24i	4.8132	0.09
60,61,62,63,64	-31.133	0	1
65	-36.0473	0	1
66	-45.6384	0	1
67	-61.4144	0	1
68,69,70,71,72	-95.833	0	1
73,74	-99.9923	0	1

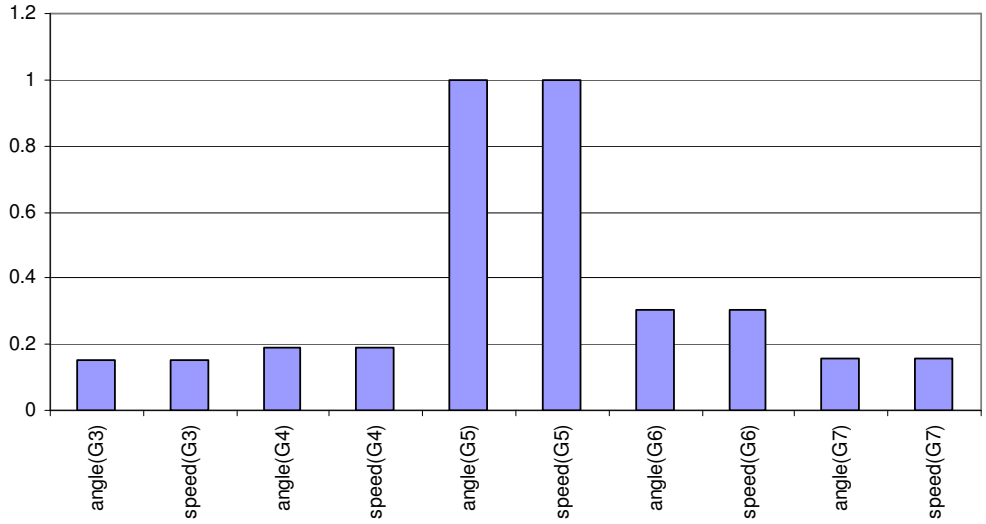

Figure 6.7. The participation factors for eigenvalues number 52 and 53

To increase the damping of distributed generators rotor oscillating modes, PSSs are connected to the exciter system as shown in Figure 6.2. The basic function of a PSS is to increase damping of the generator rotor oscillations by controlling its excitation using an auxiliary stabilizing signal.

Figure 6.8 shows structure of the connected PSSs. To increase the damping, the PSS should produce a signal in phase with the rotor speed deviations. Hence, the rotor speed deviation is selected as the input signal to the PSS.

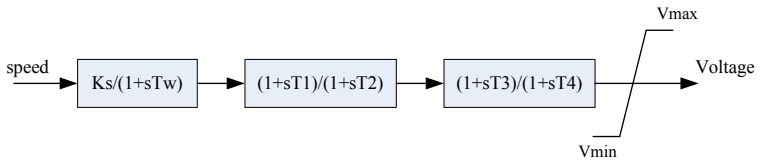

Figure 6.8. Structure of the PSS

The phase compensation method is used for tuning the PSSs. This method is widely used by industry to design the system stabilizers. Using this method and in the ideal case, the phase characteristic of the PSS is an exact inverse of the exciter and generator phase characteristics. Hence, the PSS would result in a pure damping torque.

Figure 6.9 shows the ideal and actual phase lead of the power system stabilizers connected on the distributed generators. The selected PSS parameters are:

$T_\omega = 10\text{sec.}$, $T_1 = 0.08\text{sec.}$, $T_2 = 0.03\text{sec.}$, $T_3 = 0.1\text{sec.}$, and $T_4 = 0.03\text{sec.}$

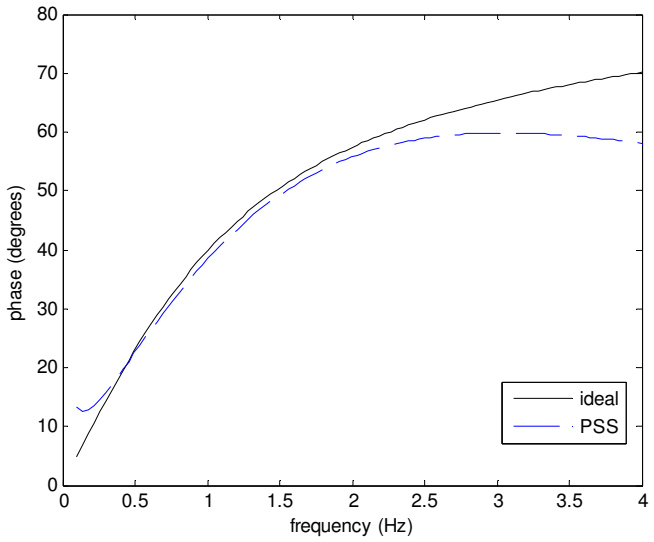

Figure 6.9. Ideal and actual PSS phase leads

A root locus with gain of the PSS is calculated and plotted in Figure 6.10. The star points indicate the eigenvalues with a PSS gain of 5. This figure shows that the PSS can increase the damping of the oscillating modes to the acceptable level of 0.2.

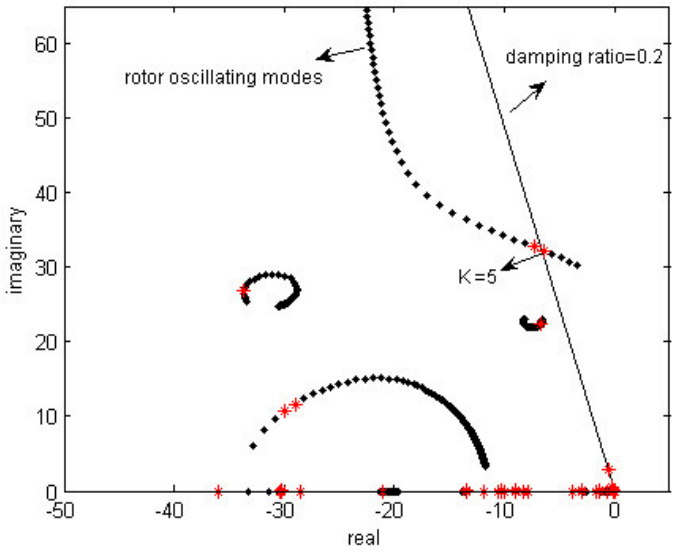

Figure 6.10. Root locus with PSS gain under sinusoidal conditions

Table 6-14 shows the system eigenvalues after installation of the PSSs on distributed generators with the following parameters:

$K = 5$, $T_\omega = 10\text{sec.}$, $T_1 = 0.08\text{sec.}$, $T_2 = 0.03\text{sec.}$, $T_3 = 0.1\text{sec.}$, and $T_4 = 0.03\text{sec.}$

Figure 6.11 demonstrates the eigenvalues damping ratios before and after the installation of PSSs. It is observed that the PSSs have increased the damping of poorly damped modes to the acceptable level of 0.2. It is also shown in Table 6-14 that the PSS installation has increased damping of the rotor oscillating modes from 0.09 to the acceptable level of 0.21.

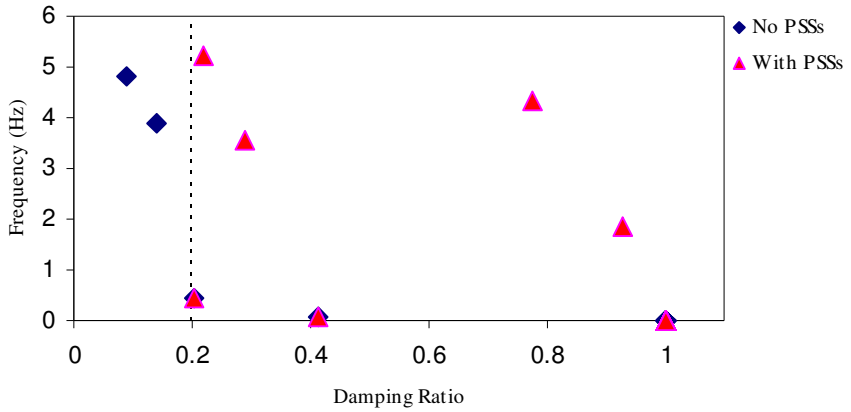

Figure 6.11. System eigenvalues before and after the installation of PSS under sinusoidal conditions

Table 6-14
DG system modes under sinusoidal conditions and with PSS, K=5

Eigenvalue Number	**Eigenvalue**	**Frequency (Hz)**	**Damping Ratio**
1	-4.81×10^{-8}	0	1
2	-0.1001	0	1
3,4,5,6,7	-0.1004	0	1
8,9	-0.23 ± 0.52i	0.0835	0.4118
10	-0.7378	0	1
11	-1	0	1
12,13,14,15,16	-1.371	0	1
17	-1.6693	0	1
18,19	-0.59 ± 2.84i	0.4521	0.2049
20,21,22,23,24	-2.994	0	1
25	-3.002	0	1
26	-3.8596	0	1
27	-7.8646	0	1
28	-8.3406	0	1
29,30,31,32,33	-9.026	0	1
34,35,36,37,38,39	-10	0	1
40,41,42,43,44	-10.2895	0	1
45	-10.5432	0	1
46	-11.8449	0	1
47,48,49,50,51	-13.4765	0	1
52	-21.0556	0	1
53,54	-6.75 ± 22.30i	3.5493	0.29
55	-28.5163	0	1
56,57,58,59,60	-30.2916	0	1
61	-30.3365	0	1
62,63,64,65,67,68,69,70,71	-29.02 ± 11.65i	1.8545	0.928
72,73,74,75,76,77,78,79,80,81	-7.30 ± 32.74i	5.2112	0.2179
82	-35.9812	0	1
83,84	-33.53 ± 27.26i	4.3398	0.7759
85	-73.2905	0	1
86,87,88,89,90	-96.2054	0	1
91,92	-99.9923	0	1

6.5. Operation of the DG System under Distorted Conditions

Actual DG systems include nonlinear loads that inject time current harmonics into the system and increase the level of voltage harmonic distortion at the buses. A synchronous generator operating under distorted conditions will inject current harmonics and hence deteriorates the power quality of the system. In this section, the nonlinear model of a synchronous generator considering the space harmonics, presented in Chapter three, is used to model the distributed generators. As the actual data of the system nonlinear loads is not provided in reference [69], it is assumed that some parts of the loads are of nonlinear type. The space harmonics of the generators are similar to those used in chapters 3, 4 and 5. Table 6-15 shows the power levels and types of the nonlinear loads.

In order to be able to compare the results with the sinusoidal conditions, the fundamental components of the loads are assumed to be equal to those used in Section 6.4. Hence in this section, the active and reactive components of the linear loads are equal to the values of Table 6-1 minus the power of nonlinear loads, as listed in Table 6-15.

The magnitudes (in percentage) and angles (in degrees) of the three types of nonlinear loads used in the DG system are presented in Table 6-16.

Table 6-15
Nonlinear load data for the DG system

Bus Number	Nonlinear load type	Active power (kW)	Reactive power (kVAR)
9004	six-pulse 2	0.45	0.3
9005	six-pulse 3	0.2	0.1
9007	six-pulse 3	0.35	0.2
9009	six-pulse 2	0.1	0.05
9011	six-pulse 2	0.05	0.03
9017	six-pulse 1	0.1	0.05
9019	six-pulse 2	0.1	0.05
9022	six-pulse 3	0.35	0.2
9031	six-pulse 1	0.1	0.05

Table 6-16
Harmonic spectra of nonlinear loads (Table 6-15)

Harmonic order	six-pulse 1		six-pulse 2		six-pulse 3	
	magnitude (%)	phase (deg)	magnitude (%)	phase (deg)	magnitude (%)	phase (deg)
1	100	0	100	0	100	0
5	20	0	19.1	0	42	0
7	14.3	0	13.1	0	14.3	0
11	9.1	0	7.2	0	7.9	0
13	7.7	0	5.6	0	3.2	0
17	5.9	0	3.3	0	3.7	0
19	5.3	0	2.4	0	2.3	0
23	4.3	0	1.2	0	2.3	0
25	4	0	0.8	0	1.4	0
29	3.4	0	0.2	0	0	0
31	3.2	0	0.2	0	0	0
35	2.8	0	0.4	0	0	0
37	2.7	0	0.5	0	0	0
41	2.4	0	0.5	0	0	0
43	2.3	0	0.5	0	0	0
47	2.1	0	0.4	0	0	0
49	2	0	0.4	0	0	0

6.5.1. System Steady-State Operation

A Decupled Harmonic Power Flow (DHPF) algorithm was used to calculate the system voltage harmonics for the steady-state operating conditions. This algorithm is based on the Newton-Raphson method and the nonlinear loads are modelled as decouple harmonic current sources. The harmonic domain model of a synchronous generator, Equation 3-19, is used for presenting the distributed generators.

Figure 6.12 shows a flowchart of the iterative method used for calculating the system steady-state voltage harmonics.

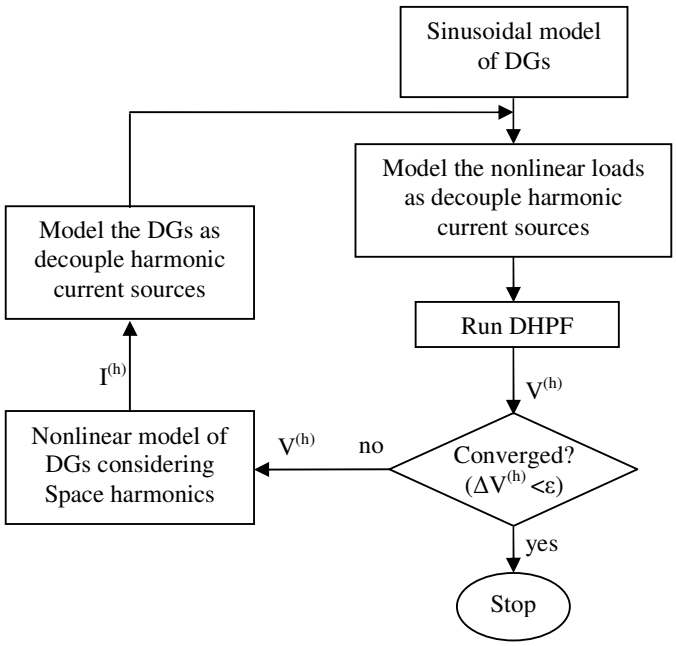

Figure 6.12. Flowchart for the harmonic voltage calculation of DG system for steady state operation

The harmonic components are considered up to order 11. As the fundamental components of the system active and reactive loads are the same as the sinusoidal conditions, the presence of nonlinear loads will not affect the system steady-state fundamental results. Hence, the fundamental active and reactive powers generated by the generators are similar to the sinusoidal conditions. However, the system losses increase from 0.103MW to 0.108MW due to the additional harmonic losses.

Table 6-17 shows the results of running the DHPF for the distorted DG system. Table 6-18 presents the voltage Total Harmonic Distortion (THDv) of the system buses.

Table 6-17
Steady-state bus voltages under distorted conditions

Harmonic Order	**1st**		**5th**		**7th**		**11th**	
Bus Number	**Mag. (pu)**	**Angle (deg)**	**Mag. (pu)**	**Angle (deg)**	**Mag. (pu)**	**Angle (deg)**	**Mag. (pu)**	**Angle (deg)**
9000	1.0300	0	0.0002	170.56	0.0001	-8.2283	0.0001	-36.55
9001	1.0215	-0.33	0.0037	-115.32	0.0018	70.3487	0.0022	46.14
9002	1.0130	-0.67	0.0073	-113.82	0.0036	71.4499	0.0044	46.85
9004	1.0044	-1.01	0.0109	-113.30	0.0054	71.8296	0.0066	47.11
9005	1.0038	-1.04	0.0104	-112.87	0.0059	70.5778	0.0071	47.67
9007	1.0028	-1.06	0.0101	-112.29	0.0062	69.1892	0.0074	47.56
9009	1.0004	-1.22	0.0167	-115.10	0.0051	81.1993	0.0065	46.02
9011	0.9892	-2.68	0.0578	-113.44	0.0068	159.1762	0.0040	31.64
9012	0.9899	-3.15	0.0842	-111.53	0.0112	179.9530	0.0023	11.14
9013	0.9891	-3.28	0.0904	-111.65	0.0124	-177.8594	0.0020	2.32
9015	0.9876	-3.85	0.1203	-109.37	0.0178	-164.8211	0.0028	-112.23
9016	0.9874	-3.83	0.1230	-109.15	0.0187	-161.1052	0.0043	-120.60
9017	0.9871	-3.81	0.1258	-108.94	0.0197	-157.7624	0.0059	-124.65
9019	0.9871	-3.78	0.1285	-108.76	0.0209	-154.4275	0.0077	-126.90
9020	1.0000	-0.39	0.0883	-75.25	0.0327	-80.8704	0.0075	-95.19
9022	0.9846	-4.14	0.1246	-109.37	0.0167	-176.3550	0.0023	24.92
9024	0.9853	-4.10	0.1246	-109.47	0.0170	-174.2695	0.0015	10.55
9025	0.9859	-4.07	0.1246	-109.56	0.0174	-172.2726	0.0010	-23.12
9028	0.9869	-3.95	0.1227	-109.59	0.0179	-167.6784	0.0019	-101.35
9030	0.9864	-4.02	0.1239	-109.61	0.0177	-170.2842	0.0011	-71.91
9031	0.9862	-4.05	0.1244	-109.69	0.0177	-170.9539	0.0010	-61.72
9033	0.9861	-4.06	0.1244	-109.74	0.0177	-171.0364	0.0010	-61.85
9109	0.9969	-1.40	0.0226	-115.95	0.0048	93.1712	0.0062	44.87
9113	0.9882	-3.36	0.0952	-111.54	0.0132	-175.6897	0.0016	-9.89
9120	0.9888	-3.70	0.1317	-108.29	0.0224	-150.7822	0.0096	-127.61

Table 6-18
THDv values of the DG system bus voltages

Bus Number	**9000**	**9001**	**9002**	**9004**	**9005**	**9007**	**9009**	**9011**	**9012**
THDv [%]	0.02	0.45	0.91	1.37	1.38	1.39	1.86	5.89	8.58
Bus Number	**9013**	**9015**	**9016**	**9017**	**9019**	**9020**	**9022**	**9024**	**9025**
THDv [%]	9.22	12.31	12.60	12.91	13.21	9.44	12.77	12.76	12.76
Bus Number	**9028**	**9030**	**9031**	**9033**	**9109**	**9113**	**9120**		
THDv [%]	12.56	12.68	12.74	12.74	2.39	9.72	13.54		

It should be mentioned that including the nonlinear model of the generators considerably increased the harmonic distortion level of the DG system. For example, using the sinusoidal model of the generators the highest voltage THD of the system will be 4.9% at bus 9120 while including the nonlinear model of the generators considering space harmonics increases the voltage THD to 13.5%.

The employed DHPF algorithm assumes balance three-phase conditions. It is shown in Chapter three that the nonlinear characteristics of the SG in the presence of harmonics will inject unbalance currents to the power system. However, the system is assumed to be balanced and the parameters of phase 'a' are considered for the system study. The injected harmonic components by the distributed generators are presented in Table 6-19.

Table 6-19
Harmonic currents injected to the system by each of the distributed generators

Harmonic order	**1st**	**3rd**	**5th**	**7th**	**9th**
Current (pu)	0.647	0.300	0.097	0.065	0.0376

These harmonics will affect the operating conditions of the distributed generators such as their rotor angle. The modified parameters and the new rotor angle of the generators under non-sinusoidal conditions are calculated using Equation 3-28:

ψ_d=0.76pu, ψ_q=-0.66, δ_0 = 40.42°.

Comparing these results with the sinusoidal conditions shows a decrease of 1.2% in the steady-state rotor angle of DGs.

6.5.2. System Dynamic Behaviour

In order to investigate the system dynamic stability under the distorted operating conditions, the modified model of a synchronous generator in the *dq*-frame of reference considering the impact of harmonics that has been proposed in Chapter three (Section 3.4.3) is used for the distributed generators. Table 6-20 shows the system eigenvalues calculated using the power system toolbox and the modified equation of the generators.

Table 6-20
DG system eigenvalues under distorted conditions and without PSS

Eigenvalue Number	Eigenvalue	Frequency (Hz)	Damping Ratio
1	-0.0004	0	1
2,3	-0.23 ± 0.52i	0.08	0.41
4	-0.73	0	1
5	-1	0	1
6	-2.26	0	1
7,8,9,10,11	-2.29	0	1
12,13	-0.59 ± 2.84i	0.45	0.20
14	-3.30	0	1
15,16,17,18,19	-5.25	0	1
20	-7.86	0	1
21	-8.34	0	1
22,23	-9.56 ± 0.49i	0.07	0.99
24,25,26,27,28,29	-10	0	1
30,31,32,33,34	-10.10	0	1
35,36,37,38,39	-12.46	0	1
40	-13.28	0	1
41,42,43,44,45	-18.99	0	1
46,47	-8.80 ± 23.83i	3.79	0.34
48	-28.51	0	1
49,50,51,52,53	-31.09	0	1
54	-36.00	0	1
55,56,57,58,59,60,61,62,63,64	-2.51 ± 41.86i	6.66	0.05
65	-55.87	0	1
66,67,68,69,70	-94.50	0	1
71,72	-99.99	0	1
73	-148.493	0	1
74	-212.32	0	1

The first eigenvalue is the theoretically zero eigenvalue. It is observed that harmonics can relocate the modes related to the DG bus including the rotor oscillating modes in the interplant and local modes that generate the oscillations between the distributed generators or between the swing bus and the DG bus. The real parts of the distributed

generators rotor oscillating modes are slightly pushed toward the right hand side of the *s*-plane, from -2.7 to -2.5, and their damping ratios is decreased from 0.09 to 0.05.

As the harmonics relocate the system modes, it is important to make sure the system stabilizers remain effective under distorted conditions.

To evaluate the effectiveness of the designed PSSs in Section 6.4.2 under distorted conditions, the system eigenvalues are re-calculated in the presence of the PSSs. The results show that under distorted conditions, these PSSs are not capable of moving the rotor oscillating modes to the desired level of damping ratio.

Figure 6.13 shows the system root locus with the PSS gain under the distorted conditions. The star and circle points show the system modes with the PSS gains of 5 and 10, respectively. It is shown that for having sufficient damping ratio of rotor oscillating modes under distorted conditions, a minimum PSS gain of 10 is required. Also the interplant eigenvalues follow different paths compared with the sinusoidal case of Figure 6.10.

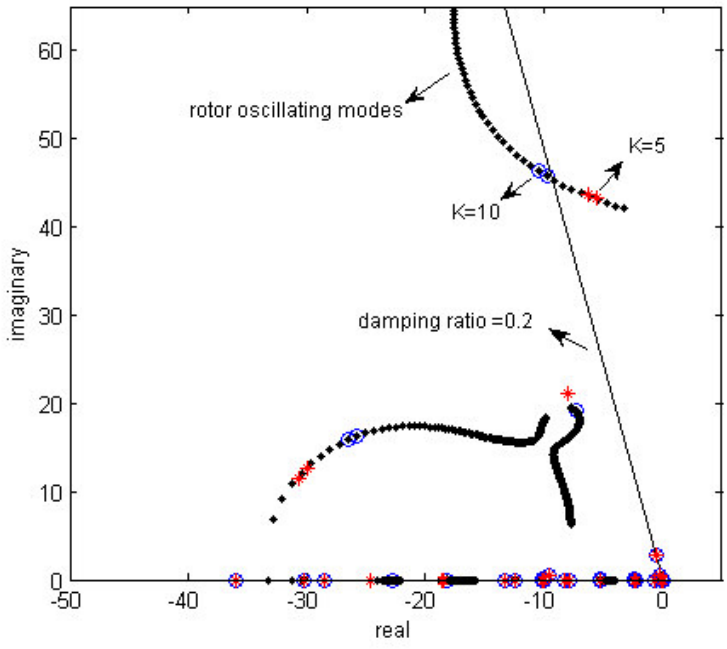

Figure 6.13. Root locus with PSS gains of 5 and 10 under distorted conditions

Table 6-21 shows the system eigenvalues with the PSSs gain of 10. It is observed that applying the PSSs with the modified gain of 10 will effectively improve the damping ratio of the distributed generators rotor oscillating modes to the acceptable level of 0.22. Furthermore, their real parts are shifted toward the left side of the *s*-plane, from -2.5 to -10.4.

Figure 6.14 demonstrates the damping ratios and frequencies of the system modes without PSSs and with PSSs gains of 5 and 10. This figure shows that considering the impact of harmonics in tuning the PSSs will keep them effective under distorted conditions. For proper operation of MMMB systems under distorted conditions, it is necessary to include the impacts of harmonics in the calculation and design of PSSs, as presented in this chapter.

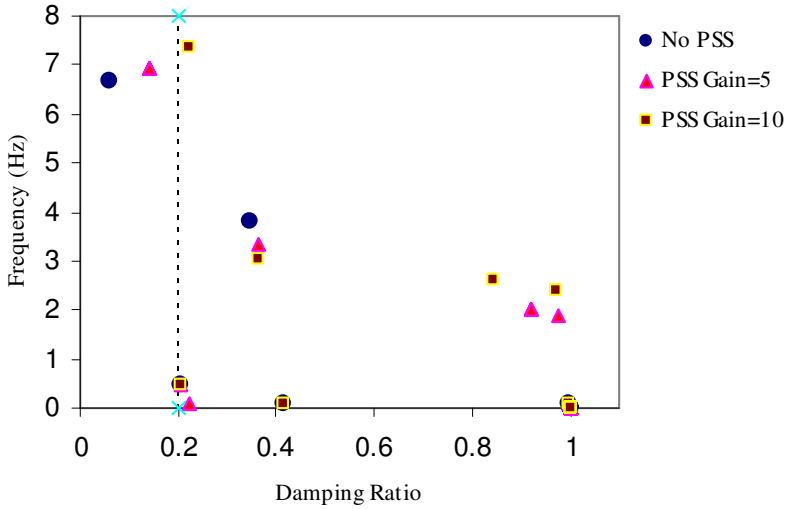

Figure 6.14. System eigenvalues under distorted conditions before and after the installation of PSS

Table 6-21
DG system eigenvalues under distorted conditions with PSS, K=10

Eigenvalue Number	**Eigenvalue**	**Frequency (Hz)**	**Damping Ratio**
1	-0.0004	0	1
2,3,4,5,6,7	-0.1001	0	1
8,9	-0.2388 - 0.5265i	0.0838	0.4131
10	-0.7364	0	1
11	-1	0	1
12	-2.2964	0	1
13,14,15,16,17	-2.3275	0	1
18,19	-0.5941 - 2.8422i	0.4523	0.2046
20	-3	0	1
21,22,23,24,25	-5.2168	0	1
26	-7.8645	0	1
27	-8.3406	0	1
28,29	-9.5595 - 0.4936i	0.0786	0.9987
30,31,32,33,34,35	-10	0	1
36,37,38,39,40	-10.1073	0	1
41,42,43,44,45	-12.4658	0	1
46	-13.2745	0	1
47,48,49,50,51	-18.216	0	1
52,53	-7.4841 - 19.0428i	3.0307	0.3658
54	-22.7396	0	1
55	-28.5163	0	1
56,57,58,59,60	-30.2524	0	1
61,62,63,64,65,66,67,68,69,70	-25.7496 - 16.2891i	2.5925	0.8451
71	-35.9883	0	1
72,73,74,75,76,77,78,79,80,81	-10.4721 - 46.2993i	7.3688	0.2206
82,83	-60.2265 - 15.0838i	2.4007	0.97
84,85,86,87,88	-95.4167	0	1
89,90	-99.9923	0	1
91	-162.738	0	1
92	-212.32	0	1

6.6. Conclusions

In this chapter the impact of harmonics on the steady state operation and dynamic behaviour of an actual distributed generation system was investigated. The system was studied under sinusoidal and distorted operating conditions. A decoupled harmonic power flow algorithm was used for steady state study and the power system toolbox with a modified model for generators was used for the calculation of system eigenvalues. The modified model of a synchronous generator in *dq*-frame of reference including the impact of time and space harmonics was used for dynamic modelling of the distributed generators. The following steps were performed for the system investigation.

At first, the system steady state parameters including the system bus voltages and generated powers were computed under sinusoidal conditions using the DHPF algorithm (Table 6-11 and Table 6-12). The results were used for the DGs rotor angle calculation.

Second step included finding the system eigenvalues using the power system toolbox. While at this stage the system was being studied under the sinusoidal conditions, a conventional model of a synchronous generator in *dq*-frame of reference was used to model the DGs. The results, Table 6-13, show that all of the eigenvalues were in the left side of the *s*-plane and hence the system was stable. However, the damping ratios of the DGs rotor oscillation modes were 0.09 which is less than the desired value of 0.2.

In the third step, power system stabilizers were designed and installed at the excitation system of the distributed generators to improve the damping of the rotor oscillation modes. A conventional structure was assumed for the PSSs and the phase compensation method along with the root locus were utilized for tuning the parameters of the phase compensator block and gain of the PSS. The results, Table 6-14 and Figure 6.11, show that a gain of 5 will improve the damping ratio of the rotor oscillating modes to 0.21.

The next steps were related to the system study under the distorted conditions.

In forth step, to include the impact of harmonics, some parts of the connected loads were assumed as nonlinear loads that inject current harmonics to the system. These nonlinear loads were modelled as decoupled harmonic current sources in the DHPF algorithm. To consider the impact of space harmonics, the model of a synchronous generator in the harmonic domain, Equation 3-19, was used. The generated harmonic currents by the distributed generators were applied to the system as harmonic current sources. It was shows that adding the model of DGs increased the level of voltage THD from %4.9 to %13.5 at the distributed generation bus. It should be reminded that there were 6 units of the DGs connected at this bus. In this step the DGs rotor angle was calculated and a difference of -1.7% was shown in compare with the sinusoidal conditions.

Step five was related to the calculation of the system eigenvalues under the distorted conditions. In this stage the model of distributed generators were modified using the steady state parameters of the time harmonics and rotor angle calculated in the previous step. The results showed relocations of rotor oscillating modes and interplant eigenvalues. Damping ratio of the rotor modes was decreased from 0.09 to 0.05 and their real parts were moved from -2.7 to -2.5. It was stated that if the system was marginally stable, such as highly loaded conditions, the harmonics could cause small-signal instability. However, in this case the system was relatively stable.

In the last step, the effectiveness of the installed PSSs was tested under distorted conditions. The root locus, Figure 6.13, show that to have sufficient damping ratio of the rotor oscillating modes, the PSSs gains should be increased to a minimum value of 10. Having these results show that in order to guarantee the effectiveness of a PSS in distorted conditions, it is necessary to consider the harmonics in tuning its parameters.

Suggested guidelines for tuning the PSS are as follows:

1- Calculate the system voltage and current harmonics.

1A- Use the Nonlinear model of SG considering space harmonics.

1B- Use a harmonic power flow, such as decoupled harmonic power flow.

2- For the PSS installed generators, calculate the additional terms of stator fluxes due to the presence of harmonics.

3- Use an optimization method such as GA-Fuzzy method, as proposed in chapter 5, to tune the PSS parameters.

4- If an optimization program is not available, use the phase compensation method considering the presence of harmonics.

CHAPTER SEVEN

SUMMARY AND CONCLUSIONS

In this thesis, the impact of time and space harmonics on the small-signal stability of the power systems was studied. The study was done on a distorted SMIB system. To show the impact on more realistic systems, an actual MMMB distributed generation system located in Western Australia was also modelled and its dynamic behaviour under the influence of harmonics was studied.

The method used for stability study was the eigenvalue analysis method. This method is based on linearizing the system differential equations around the operating point. Hence, the first step was finding the impact of harmonics on the system steady-state operating conditions. As synchronous generators are of the most important parts of the power systems, the operation of a synchronous generator was investigated in the presence of time and space harmonics in Chapter three. A synchronous generator was modelled in the harmonic domain and the *abc*-frame of reference. This model was used to calculate the harmonic components of the generator parameters such as stator fluxes and voltages. It was shown that the interaction between time and space harmonics will include additional terms to the fundamental components of generator parameters. These additional components are functions of time and space harmonics and also the rotor angle. They were calculated and used to modify the conventional model of the generator in the *dq*-frame of reference. This is done by applying the Park transformation on the modified fundamental components including the additional terms. This model was also used to calculate the steady-state operating point of the synchronous generator. The simulation results were presented for a sample synchronous generator working under three different operating conditions including sinusoidal, presence of space harmonics and presence of time and space harmonics. The characteristics of this generator were adopted form reference [2]. Hence, it was possible to confirm the sinusoidal results of the system steady-state and dynamic stability. The impact of

damper windings and the harmonic phase angles were also includes and the simulation results showed variations in the steady-state operating conditions of the synchronous generator in distorted conditions.

In Chapter four, the modified model of the synchronous generator was connected to a distorted infinite bus to find the impact of harmonics on the small-signal stability. As the system equations were very complicated in the presence of harmonics, a simplified model of generator and system was employed. This was in order to make it possible to solve the equations and show the impact of harmonics on the system state matrix. The system eigenvalues were calculated and it was shown that harmonics can move them toward the left side of the *s*-plane. The relocation of the eigenvalues depended on the phase angle and magnitude of the harmonics. Even though it is hard to predict the change in the system modes by harmonics, it is important to consider them in system study as they can cause instability in the marginally stable systems.

The next step of this work concentrates on improving the system small-signal stability in the presence of harmonics. As FACTS devices with auxiliary POD controllers have been widely used in the power systems, the effectiveness of these damping controllers in distorted conditions was investigated. In chapter five, an SSSC device was connected in the distorted SMIB system and the system state space equations were derived. A hybrid genetic-fuzzy approach was proposed for solving the nonlinear constrained problem of optimal selection of the POD parameters. The object of the method is moving the eigenvalues into the desired part of the *s*-plane and the constraints include the limits of the POD controller to avoid prolonged saturation in the SSSC actuators. The chromosomes fitness values were computed using the fuzzy approximate reasoning with the inputs of real parts and damping ratios of the electromechanical modes. The results showed that the POD controller designed for the sinusoidal conditions can not be effective under the influence of harmonics. However it was shown that considering different levels of time harmonics as well as sinusoidal conditions simultaneously, could result in design of a robust POD controller. This POD controller remained effective under the influence of harmonics. The proposed method is also applicable for tuning the other types of power system stabilizers.

The stability studies in chapters 4 and 5 were based on a distorted SMIB system and the impacts of exciter systems and turbine-governors were not considered. The reason for that was to simplify the calculation as the presence of harmonics made the calculations more complex. The SMIB system is the basic model for understanding and investigating the small-signal stability of the system. However, to expand the study to a more realistic system, an actual MMMB system was investigated in Chapter six. The system was a 24-bus distributed generation system in Western Australia. The steady-state and dynamic behaviour of this system was studied under sinusoidal and distorted conditions. A decupled harmonic power flow algorithm was used to calculate the system the steady-state parameters such as bus voltages and generator powers. The nonlinear loads were modelled as decoupled harmonic current sources in steady state conditions and the synchronous generators were modelled in harmonic domain of reference. The power system toolbox with modified model of the synchronous generators in *dq*-frame of reference was used for eigenvalue calculations. It was observed that the harmonics can affect the distributed generators rotor oscillating modes and the interplant modes. The excitation systems of the distributed generators include power system stabilizers to increase the damping of rotor oscillating modes. These PSSs were designed based on the phase compensation. The simulation results showed that these PSSs are not quite effective under the influence of harmonics. In distorted conditions it was necessary to apply more gain to the PSSs in order to have proper damping ratio of the oscillating modes. It was stated that in order to guarantee the effectiveness of a PSS in distorted conditions, it is necessary to consider the harmonics in tuning its parameters and properly modify its gain.

7.1. Thesis Contributions

The main contributions of this thesis are as follows:

- Analysis of distorted power systems and inclusion of auxiliary signals on the conventional PSS devices to guarantee stable operations in the presence of time and space harmonics.

- The conventional power system stabilizer might not work properly under distorted operating conditions enforced by nonlinear loads and/or nonlinearity of synchronous generators.

- A proposed modified model for the synchronous generator in the *dq*-frame of reference that considers the influences of time and space harmonics.

- The harmonics can change the steady state operating conditions of synchronous generators.

- The harmonics can relocate the system eigenvalues and cause instability in the marginally stable systems.

- The POD controllers might not remain effective in distorted conditions, hence the harmonics should be considered in their design.

- The distortion level of DG systems is considerable and their voltage THD level can be computed using the nonlinear model of the synchronous generators including space harmonics.

- The PSSs installed at the DG systems should be tuned considering the presence of harmonics.

7.2. Future Work

It was shown in this thesis that the presence of harmonics can change the dynamic behaviour of the power systems and might cause instability in marginally stable power systems. It is also necessary to consider the harmonics in tuning the power system stabilizers in order to keep them affective in distorted conditions.

However to continue the impact of power quality issues on the system stability, the following subjects are still to be investigated:

- The small-signal stability of the unbalanced systems.

- The possible interaction between harmonics and the POD controllers.

- The impact of sub-harmonics on the system dynamic stability.

- The impact of harmonics on transient and voltage stability.

REFERENCES

Every reasonable effort has been made to acknowledge the owners of copyright material. I would be pleased to hear from any copyright owner who has been omitted or incorrectly acknowledged.

1. Kundur, P., et al., *Definition and classification of power system stability IEEE/CIGRE joint task force on stability terms and definitions.* IEEE Transactions on Power Systems, 2004. **19**(3): p. 1387 - 1401.
2. Kundur, P., *Power System Stability and Control*. 1994, New York: McGraw-Hill.
3. Basler, M.J. and R.C. Schaefer. *Understanding power system stability*. in *58th Annual Conference for Protective Relay Engineers*. 2005.
4. Lyapunov, A.M., *Stability of Motion*. 1967: Academic Press, Inc.
5. Demello, F.P. and C. Concordia, *Concepts of synchronous machine stability as affected by excitation control.* IEEE Transactions on Power Apparatus and Systems, 1969. **88**(4): p. 316 - 329.
6. Xia, D. and G.T. Heydt, *Self-tuning controller for generator excitation control.* IEEE Transactions on Power Apparatus and Systems, 1983. **102**(6): p. 1877 - 1885.
7. Samarasinghe, V.G.D.C. and N.C. Pahalawaththa, *Damping of multimodal oscillations in power systems using variable structure control techniques.* Generation, Transmission and Distribution, IEE Proceedings-, 1997. **144**(3): p. 323 - 331.
8. Abido, M.A. and Y.L. Abdel-Magid, *Hybridizing rule-based power system stabilizers with genetic algorithms.* IEEE Transactions on Power Systems, 1999. **14**(2): p. 600 - 607.
9. Abido, M.A., *Robust design of multimachine power system stabilizers using simulated annealing.* IEEE Transactions on Energy Conversion, 2000. **15**(3): p. 297 - 304.

10. Zhou, E., O.P. Malik, and G.S. Hope, *Design of stabilizer for a multimachine power system based on the sensitivity of PSS effect.* IEEE Transactions on Energy Conversion, 1992. **7**(3): p. 606 - 613.

11. Hingorani, N. and L. Gyugyi, *Understanding FACTS*. 2000, New York: IEEE Press.

12. Tang, Y. and A.P.S. Meliopoulos, *Power system small signal stability analysis with FACTS elements.* IEEE Transactions on Power Delivery, 1997. **12**(3): p. 1352 - 1361.

13. Wang, H.F., *Phillips-Heffron model of power systems installed with STATCOM and applications.* Generation, Transmission and Distribution, IEE Proceedings, 1999. **146**(5): p. 521-527.

14. Farsangi, M.M., Y.H. Song, and K.Y. Lee, *Choice of FACTS device control inputs for damping interarea oscillations.* IEEE Transactions on Power Systems, 2004. **19**(2): p. 1135 - 1143.

15. Zhao, Q. and J. Jiang, *Robust SVC controller design for improving power system damping.* IEEE Transactions on Power Systems, 1995. **10**(4): p. 1927 - 1932.

16. Martins, N. and L.T.G. Lima, *Determination of suitable locations for power system stabilizers and static VAR compensators for damping electromechanical oscillations in large scale power systems.* IEEE Transactions on Power Systems, 1990. **5**(4): p. 1455 - 1469.

17. Oliveira, S.E.M.D., *Synchronizing and damping torque coefficients and power system steady-state stability as affected by static VAr compensators.* IEEE Transactions on Power Systems, 1994. **9**(1): p. 109 - 119.

18. Fang, D.Z., et al., *Adaptive fuzzy-logic SVC damping controller using strategy of oscillation energy descent.* IEEE Transactions on Power Systems, 2004. **19**(3): p. 1414 - 1421.

19. Rahim, A.H.M.A., S.A. Al-Baiyat, and F.M. Kandlawala. *A robust STATCOM controller for power system dynamic performance enhancement*. in *IEEE Power Engineering Society Summer Meeting*. 2001.

20. Ghazi, R., A. Azemi, and K.P. Badakhshan. *Adaptive fuzzy sliding mode control of SVC and TCSC for improving the dynamic performance of power systems.*

in *Seventh International Conference on AC-DC Power Transmission (Conf. Publ. No. 485)*. 2001.

21. Wang, H.F., *A unified model for the analysis of FACTS devices in damping power system oscillations III. unified power flow controller.* IEEE Transactions on Power Delivery, 2000. **15**(3): p. 978-983.

22. Faried, S.O. and A.A. Eldamaty. *Damping power system oscillations using a genetic algorithm based unified power flow controller*. in *Canadian Conference on Electrical and Computer Engineering*. 2004.

23. Wang, H.F., *Design of SSSC Damping Controller to Improve Power System Oscillation Stability*, in *IEEE AFRICON*. 1999. p. 495-500.

24. Chaudhuri, B. and B.C. Pal, *Robust damping of multiple swing modes employing global stabilizing signals with a TCSC.* IEEE Transactions on Power Systems, 2004. **19**(1): p. 499 - 506.

25. Zhang, P., et al. *Selection of locations and input signals for multiple SVC damping controllers in large scale power systems*. in *IEEE Power Engineering Society Winter Meeting*. 1999.

26. Kennedy, B.W., *Power Quality Primer*. 2000: McGraw-Hill.

27. Schlabbach, J., D. Blume, and T. Stephanblome, *Voltage Quality in Electrical Power Systems*. 2001, UK: Institution of Electrical Engineers.

28. Arrillaga, J., N.R. Watson, and S. Chen, *Power System Quality Assessment*. 2000: John Wiley & Sons.

29. Fuchs, E.F. and M.A.S. Masoum, *Power Quality in Power Systems and Electrical Machines*. 2008: Elsevier Academic Press.

30. *Standard IEEE-1159*.

31. Bommareddy, C. and E. Makram. *Power quality studies in the presence of DG*. in *Power Systems Conference: Advanced Metering, Protection, Control, Communication, and Distributed Resources*. 2006.

32. Dolezal, J., et al. *The effect of dispersed generation on power quality in distribution system*. in *Quality and Security of Electric Power Delivery Systems. CIGRE/IEEE PES International Symposium*. 2003.

33. Leva, S., *Dynamic stability of isolated system in the presence of PQ disturbances.* IEEE Transactions on Power Delivery, 2008. **23**(2): p. 831 - 840.

34. Leva, S., A.P. Morando, and D. Zaninelli. *Influence of PQ disturbances on dynamic stability of isolated system.* in *Power Engineering Society Summer Meeting, IEEE*. 2001.

35. Blondel, A., *The two-reaction method for study of oscillatory phenomena in coupled alternators.* Revue Générale de L'Electricité, 1923. **13**: p. 235-251.

36. Doherty, R.E. and C.A. Nickle, *Synchronous machine I and II.* AIEE Trans., 1926. **45**: p. 912-942.

37. Park, R.H., *Two-reaction theory of synchronous machines-generalized method of analysis-Part I.* Trans. AIEE, 1929. **48**: p. 716-727.

38. Park, R.H., *Two-reaction theory of synchronous machines II.* Trans. AIEE, 1933. **52**: p. 352-355.

39. Roark, J.D. and C.A. Fross. *Unbalanced synchronous machine analysis using frequency domain methods*. in *IEEE PES summer meeting*. 1978. Los Angeles, CA.

40. Medina, A., J. Arrillaga, and J.F. Eggleston. *A synchronous machine model in the harmonic domain*. in *International Conference on Electrical Machines*. 1992. Manchester, UK.

41. Hart, P.M. and W.J. Bonwick, *Harmonic modeling of synchronous machine.* IEE Proceedings on Electric Power Applications, 1988. **135**(2): p. 52-58.

42. CIGRE Working Group, *Harmonics, characteristic parameters, method of study, estimates of existing values in the network.* 1981. **77**: p. 35-54.

43. EGGLESTON, J.F., J. ARRILLAGA, and A. SEMLEY, *Harmanic Norton equivalent of the synchronous generator.* Electr. & Electron. Eng., 1986. **7**(1): p. 13-21.

44. Chen, H., Y. Long, and X.P. Zhang, *More sophisticated synchronous machine model and the relevant harmonic power flow study.* IEE Proceedings on Generation, Transmission and Distribution, 1999. **146**(3): p. 261-268.

45. Rodriguez, P. and A. Medina. *Fast periodic steady state solution of a synchronous machine model incorporating the effects of magnetic saturation and hysteresis*. in *IEEE PES Winter Meeting*. 2001.

46. Subramaniam, P. and P.P. Malik. *Digital simulation of a synchronous generator in direct-phase coordinates*. in *Inst. Electr. Eng.* . 1971.

47. Arrillaga, J., J.G. Campos-Barros, and H.J. Al-Kashali, *Dynamic modeling of single generators connected to HVDC converters.* IEEE Transaction on Power Apparatus and System, 1978. **4**: p. 1018-1029.

48. A Ramirez, A. Semlyen, and R. Iravani, *Harmonic domain characterization of the resonant interaction between generator and transmission line.* IEEE Transactions on Power Delivery, 2005. **2**(2): p. 1753-1762.

49. Corzine, K.A., et al., *An improved method for incorporating magnetic saturationin the q-d synchronous machine model.* IEEE Transactions on Energy Conversion, 1998. **13**(3): p. 270-275.

50. Arrillaga, J., et al., *The harmonic domain. A frame of reference for power system harmonic analysis.* IEEE Transactions on Power Delivery, 1995. **10**: p. 433-440.

51. Rico, J.J., M. Madrigal, and E. Acha, *Dynamic harmonic evolution using the extended harmonic domain.* IEEE Transactions on Power Delivery, 2003. **18**(2): p. 587-594.

52. Demerdash, N.A. and T.W. Nehl, *Electric machinery parameters and torques by current and energy perturbations from field computations. I. Theory and formulation.* IEEE Transaction on Energy Conversion, 1999. **14**(4): p. 1507 - 1513.

53. Escarela-Perez, R., et al., *Comparison of two techniques for two-dimensional finite-element inductance computation of electrical machines.* Electric Power Applications, IEE Proceedings, 2005. **152**(4): p. 855 - 861.

54. Demerdash, N.A.O. and P. Baldassari, *A combined finite element-state space modeling environment for induction motors in the ABC frame of reference: the no-load condition.* IEEE Transaction on Energy Conversion, 1992. **7**(4): p. 698 - 709.

55. Demerdash, N.A.O., R. Wang, and R.R. Secunde, *Three dimensional magnetic fields in extra high speed modified Lundell alternators computed by a combined vector-scalar magnetic potential finite element method.* IEEE Transaction on Energy Conversion, 1992. **7**(2): p. 353 - 366.

56. Demerdash, N.A., R. Wang, and M.A. Alhamadi, *An adaptive Newton-Raphson technique for combined vector-scalar potential solutions of large scale 3D magnetic field problems involving anisotropic materials.* IEEE Transactions on Magnetics, 1993. **29**(2): p. 1950 - 1957.

57. Chaudhry, S.R., S. Ahmed-Zaid, and N.A. Demerdash, *Coupled finite-element/state-space modeling of turbogenerators in the abc frame of reference-the no-load case.* IEEE Transactions on Energy Conversion, 1995. **10**(1): p. 56 - 62.

58. Deng, E. and N.A.O. Demerdash, *A coupled finite-element state-space approach for synchronous generators. I. model development.* IEEE Transactions on Aerospace and Electronic Systems, 1996. **32**(2): p. 775 - 784.

59. Wang, R. and N.A. Demerdash, *A combined vector potential-scalar potential method for FE computation of 3D magnetic fields in electrical devices with iron cores.* IEEE Transactions on Magnetics, 1991. **27**(5): p. 3971 - 3977.

60. Toliyat, H.A. and N.A. Al-Nuaim, *Simulation and detection of dynamic air-gap eccentricity in salient-pole synchronous machines.* IEEE Transaction on Industrial Applications, 1999. **35**: p. 86-93.

61. Wakileh, G.J., *Power Systems Harmonics: Fundamentals, Analysis and Filter Design*. 2001, Berlin: Springer.

62. Hingorani, N.G., *High power electronics and flexible AC transmission system.* IEEE Power Engineering review, 1988.

63. Swift, F.J. and H.F. Wang, *Application of the controllable series compensator in damping power system oscillations.* Generation, Transmission and Distribution, IEE Proceedings, 1996. **143**(4): p. 359-364.

64. Wang, H.F., *Damping function of unified power flow controller.* Generation, Transmission and Distribution, IEE Proceedings, 1999. **146**(1): p. 81-87.

65. Wang, H.F. and F.J. Swift, *A unified model for the analysis of FACTS devices in damping power system oscillations. I. Single-machine infinite-bus power systems.* IEEE Transactions on Power Delivery, 1997. **12**(2): p. 941-946.

66. Wang, H.F., F.J. Swift, and M. Li, *A unified model for the analysis of FACTS devices in damping power system oscillations. II. Multi-machine power systems.* IEEE Transactions on Power Delivery, 1998. **13**(4): p. 1355-1362.

67. Gyugyi, L., C.D. Schauder, and K.K. Sen, *Static synchronous series compensator: A solid-state approach to the series compensation of transmission lines.* IEEE Transaction on Power Delivery, 1997. **12**(1): p. 406-417.

68. Rogers, G., *Power System Toolbox, Dynamic Tutorial and Functions*. 2007: Ontario, Canada.

69. Malhi, E.S., *Stability enhancement of distributed power systems with embedded low inertia generators*, in *Department of Electrical & Computer Engineering*. 2006, Curtin University of Technology: Perth, WA.

70. Ulinuha A., *Optimal Dispatch of LTC and Switched Shunt Capacitors for Distribution Networks in the Presence of Harmonics*, in *Department of Electrical & Computer Engineering*. PhD Thesis 2007, Curtin University of Technology: Perth, WA.

APPENDIX A

LIST OF THE SUPPORTING PAPERS

1. M. Ladjevardi, M.A.S. Masoum, S.M. Islam, *"Operation of Synchronous Generator under the Influence of Time and Space Harmonics",* Australian Journal of Electrical & Electronics Engineering, AJEEE, Vol.4, No.2, Page(s): 179-189, 2008.

2. M. Ladjevardi, M.A.S. Masoum, S.M. Islam, *"GA-Based Damping Control of Distributed SMIB Systems Using Static Synchronous Series Compensator",* Submitted to Australian Journal of Electrical & Electronics Engineering, 2008.

3. M. Ladjavardi, M.A.S. Masoum, "*Impact of Time and Space Harmonics on Optimal Parameter Selection of SSSC Based Power Oscillations Damping Controller Using Hybrid Genetic-Fuzzy Algorithm*", Submitted to IEEE Trans. on Power Delivery.

4. A. Kazemi, M. Ladjevardi, M.A.S. Masoum, "*Optimal Selection of SSSC Based Damping Controller Parameters for Improving Power System Dynamic Stability using Genetic Algorithms"*, Iranian Journal of Science & Technology, Vol.29, No.B1, pp.1-10, 2005.

5. M. Ladjevardi, M.A.S. Masoum, S.M. Islam, *"Impact of a SG Nonlinear Model on the Harmonic Distortion of a Distributed Generation System",* Submitted to Australian Universities Power Engineering Conference, Australia, AUPEC2008.

6. M. Ladjevardi, M.A.S. Masoum, S.M. Islam, "*Impact of SG Damper Windings on Small-Signal Stability of Distorted SMIB Including Time and Space Harmonics*", Submitted to North American Power Symposium, NAPS 2008, Calgary, Canada.

7. M. Ladjevardi, M.A.S. Masoum, S.M. Islam, *"Small-Signal Stability Analysis of Distorted Power Systems installed with SSSC",* Power Engineering Society, General Meeting 24-28 June 2007, Tampa, USA, Page(s):1 - 6.

8. M. Ladjevardi, M.A.S. Masoum, S.M. Islam, *"Time Domain Analysis of Synchronous Generator in Distorted Power System",* Australian Universities Power

Engineering Conference, Australia, AUPEC2007 (Winner of the Best Student Paper Award).

9. M. Ladjevardi, M.A.S. Masoum, S.M. Islam, "Impact of Time and Space Harmonics on Small-Signal Stability of Power System", Australian Universities Power Engineering Conference, Australia, AUPEC2006.

10. M. Ladjevardi, M.A.S. Masoum, *"Application of Multi-Objective Genetic Algorithm for Optimal Design of SSSC Based Robust Damping Controllers to Improve Small Signal Stability",* Power Systems Conference and Exposition, PSCE '06. 2006 IEEE PES, 2006.

11. M. Ladjevardi, M.A.S. Masoum, *"Impact of Time and Space Harmonics on Synchronous Generator Load Angle",* Power Systems Conference and Exposition, PSCE '06. 2006 IEEE PES, 2006.

APPENDIX B

LINIEARIZING THE SYSTEM PARAMETERS

A. No damper windings:

Equation 4-14 shows the deviations of the stator currents in *dq*-frame as follows:

$$\begin{cases} \Delta i_d^{(1)} = m_1 \Delta \psi_{Fd} + m_2 \Delta\delta + m_3 \Delta \psi_d^{due\ to\ harm} + m_4 \Delta \psi_q^{due\ to\ harm} \\ \Delta i_q^{(1)} = n_1 \Delta \psi_{Fd} + n_2 \Delta\delta + n_3 \Delta \psi_d^{due\ to\ harm} + n_4 \Delta \psi_q^{due\ to\ harm} \end{cases} \tag{B2}$$

The stator additional fluxes are also obtained in equation 4-17:

$$\begin{cases} \Delta \psi_d^{due\ to\ harm} = \dfrac{N}{\mathrm{P}_0^2 + 1}[A\,\Delta\delta + B\,\Delta i_d^{(1)} + C\,\Delta i_q^{(1)}] \\ \Delta \psi_q^{due\ to\ harm} = \dfrac{M}{\mathrm{P}_0^2 + 1}[A\,\Delta\delta + B\,\Delta i_d^{(1)} + C\,\Delta i_q^{(1)}] \end{cases} \tag{B-3}$$

To calculate the stator currents and voltages as functions of state variables, the above equations have been solved as follows:

$$\begin{aligned} \Delta i_d^{(1)} &= \frac{E_2}{E_1}\Delta\psi_{Fd} + \frac{E_3}{E_1}\Delta\delta + \frac{E_4}{E_1}\Delta i_q^{(1)} \\ \Delta i_q^{(1)} &= \frac{F_2}{F_1}\Delta\psi_{Fd} + \frac{F_3}{F_1}\Delta\delta + \frac{F_4}{F_1}\Delta i_d^{(1)} \end{aligned} \tag{B-4}$$

Where,

$$E_1 = 1 - \frac{BNm_3 + BMm_4}{\mathrm{P}_0^2 + 1},\quad E_2 = m_1,\ E_3 = m_2 + \frac{ANm_3 + AMm_4}{\mathrm{P}_0^2 + 1},\ E_4 = \frac{CNm_3 + CMm_4}{\mathrm{P}_0^2 + 1}$$

$$F_1 = 1 - \frac{CNn_3 + CMn_4}{\mathrm{P}_0^2 + 1},\quad F_2 = n_1,\ F_3 = n_2 + \frac{ANn_3 + AMn_4}{\mathrm{P}_0^2 + 1},\ F_4 = \frac{BNn_3 + BMn_4}{\mathrm{P}_0^2 + 1}$$

Hence,

$$\begin{cases} \Delta i_d^{(1)} = g_{d1}\Delta\psi_{Fd} + g_{d2}\Delta\delta \\ \Delta i_q^{(1)} = g_{q1}\Delta\psi_{Fd} + g_{q2}\Delta\delta \end{cases}, \qquad \begin{cases} g_{d1} = \dfrac{F_1E_2 + F_2E_4}{F_1E_1 - F_4E_4},\ g_{d2} = \dfrac{F_1E_3 + F_3E_4}{F_1E_1 - F_4E_4} \\ g_{q1} = \dfrac{F_4E_2 + F_2E_1}{F_1E_1 - F_4E_4},\ g_{q2} = \dfrac{F_4E_3 + F_3E_1}{F_1E_1 - F_4E_4} \end{cases} \tag{B-5}$$

And

$$\begin{cases} \Delta \psi_d^{due\ to\ harm} = k_1\Delta\delta + k_2\Delta\psi_{Fd} \\ \Delta \psi_q^{due\ to\ harm} = l_1\Delta\delta + l_2\Delta\psi_{Fd} \end{cases} \tag{B-6}$$

Where,

$$k_1 = \frac{NA + NBm_1 + NCn_1}{P_0^2 + 1}, \quad k_2 = \frac{NBm_2 + NCn_2}{P_0^2 + 1}$$
$$l_1 = \frac{MA + MBm_1 + MCn_1}{P_0^2 + 1}, \quad l_2 = \frac{MCn_2 + MBm_2}{P_0^2 + 1} \tag{B-7}$$

Now, using equation 4-18, the deviations of stator fluxes can be calculated as:

$$\begin{cases} \Delta\psi_d^{(1)} = f_{d1}\,\Delta\psi_{Fd} + f_{d2}\Delta\delta \\ \Delta\psi_q^{(1)} = f_{q1}\Delta\psi_{Fd} + f_{q2}\Delta\delta \end{cases}, \quad \begin{cases} f_{d1} = k_2 - L_d m_2 + \dfrac{M_F^{(1)}}{L_F} + \dfrac{(M_F^{(1)})^2 m_2}{L_F} \\ f_{d2} = k_1 - L_d m_1 + \dfrac{(M_F^{(1)})^2 m_1}{L_F} \\ f_{q1} = l_2 - L_q n_2 \\ f_{q2} = l_1 - L_q n_1 \end{cases} \tag{B-8}$$

B. With damper windings:

Using Equation 4-26,

$$\begin{cases} I_F = \psi_D(\underbrace{\dfrac{L_{FD}}{L_{FD}^2 - L_F L_D}}_{f_1}) + \psi_F(\underbrace{\dfrac{-L_D}{L_{FD}^2 - L_F L_D}}_{f_2}) + I_d(\underbrace{\dfrac{L_{FD}M_D - M_F L_D}{L_{FD}^2 - L_F L_D}}_{f_3}) \\ I_D = \psi_D(\underbrace{\dfrac{-L_F}{L_{FD}^2 - L_F L_D}}_{d_1}) + \psi_F(\underbrace{\dfrac{L_{FD}}{L_{FD}^2 - L_F L_D}}_{d_2}) + I_d(\underbrace{\dfrac{L_{FD}M_F - M_D L_F}{L_{FD}^2 - L_F L_D}}_{d_3}) \\ I_G = \psi_Q(\underbrace{\dfrac{L_{GQ}}{L_{GQ}^2 - L_G L_Q}}_{g_1}) + \psi_G(\underbrace{\dfrac{-L_Q}{L_{GQ}^2 - L_G L_Q}}_{g_2}) + I_q(\underbrace{\dfrac{L_{GQ}M_Q - M_G L_Q}{L_{GQ}^2 - L_G L_Q}}_{g_3}) \\ I_Q = \psi_Q(\underbrace{\dfrac{-L_G}{L_{GQ}^2 - L_G L_Q}}_{q_1}) + \psi_G(\underbrace{\dfrac{L_{GQ}}{L_{GQ}^2 - L_G L_Q}}_{q_2}) + I_q(\underbrace{\dfrac{L_{GQ}M_G - M_Q L_G}{L_{GQ}^2 - L_G L_Q}}_{q_3}) \end{cases} \tag{B-8}$$

Substituting the above values in Equation (4-25):

$$\Delta\psi_d^{(1)} = \Delta\psi_F(\underbrace{M_F f_2 + M_D d_2}_{K_1}) + \Delta\psi_D(\underbrace{M_F f_1 + M_D d_1}_{K_2})$$
$$+ \Delta i_d^{(1)}(\underbrace{M_F f_3 + M_D d_3 - L_d + \frac{BN}{(P_0)^2 + 1}}_{T_1}) + \Delta\delta(\underbrace{\frac{AN}{(P_0)^2 + 1}}_{T_2})$$
$$+ \Delta i_q^{(1)}(\underbrace{\frac{CN}{(P_0)^2 + 1}}_{T_3})$$

$$\begin{aligned}\Delta\psi_q^{(1)} &= \Delta\psi_G\underbrace{(M_G g_2 + M_Q q_2)}_{K_4} + \Delta\psi_Q\underbrace{(M_G g_1 + M_Q q_1)}_{K_5} \\ &+ \Delta i_q^{(1)}\underbrace{(M_G g_3 + M_Q q_3 - L_q + \frac{CM}{(P_0)^2+1})}_{T_4} + \Delta\delta\underbrace{(\frac{AM}{(P_0)^2+1})}_{T_5} \\ &+ \Delta i_d^{(1)}\underbrace{(\frac{BM}{(P_0)^2+1})}_{T_6}\end{aligned} \tag{B-9}$$

The following coefficients are defined to simplify the equations:

$$\begin{aligned}&kh = (R_a + T_6 + R_E)(R_a + R_E - T_3) + (X_E - T_1)(X_E - T_4) \\ &rr_1 = \frac{K_1(R_a + T_6 + R_E)}{kh},\quad rr_2 = \frac{K_2(R_a + T_6 + R_E)}{kh}, rr_3 = \frac{K_4(X_E - T_1)}{kh}, \\ &rr_4 = \frac{K_5(X_E - T_1)}{kh},\quad rr_5 = \frac{X_E - T_1}{kh}, rr_6 = \frac{R_a - T_6 - R_E)}{kh},\quad rr_7 = T_5(X_E - T_1) + T_2(R_a + T_6 + R_E) \\ &ss_1 = \frac{rr_1(X_E - T_4)}{R_a + T_6 + R_E},\quad ss_2 = \frac{rr_2(X_E - T_4)}{R_a + T_6 + R_E},\quad ss_3 = \frac{rr_3(X_E - T_4) - K_4}{R_a + T_6 + R_E} \\ &ss_4 = \frac{rr_4(X_E - T_4) - K_5}{R_a + T_6 + R_E},\quad ss_5 = \frac{rr_5(X_E - T_4) - 1}{R_a + T_6 + R_E},\quad ss_6 = \frac{rr_6(X_E - T_4)}{R_a + T_6 + R_E},\quad ss_7 = \frac{rr_7(X_E - T_4) - T_5}{R_a + T_6 + R_E}\end{aligned} \tag{B-10}$$

Using the above coefficients, the deviations of stator currents are derived:

$$\Delta i_d^{(1)} = \Delta\delta\underbrace{(E_B ss_5 \cos\delta_0 - E_B ss_6 \sin\delta_0 + ss_7)}_{m_1} + \Delta\psi_F\underbrace{ss_1}_{m_2} + \Delta\psi_D\underbrace{ss_2}_{m_3} + \Delta\psi_G\underbrace{ss_3}_{m_4} + \Delta\psi_Q\underbrace{ss_4}_{m_5}$$

$$\Delta i_q^{(1)} = \Delta\delta\underbrace{(E_B rr_5 \cos\delta_0 - E_B rr_6 \sin\delta_0 + rr_7)}_{n_1} + \Delta\psi_F\underbrace{rr_1}_{n_2} + \Delta\psi_D\underbrace{rr_2}_{n_3} + \Delta\psi_G\underbrace{rr_3}_{n_4} + \Delta\psi_Q\underbrace{rr_4}_{n_5} \tag{B-11}$$

And the deviations of the rotor currents are calculated.

$$\begin{aligned}\Delta I_F &= \Delta\delta\underbrace{(m_1 f_3)}_{F_1} + \Delta\psi_F\underbrace{(m_2 f_3 + f_2)}_{F_2} + \Delta\psi_D\underbrace{(m_3 f_3 + f_1)}_{F_3} + \Delta\psi_G\underbrace{(m_4 f_3)}_{F_4} + \Delta\psi_Q\underbrace{(m_5 f_3)}_{F_5} \\ \Delta I_D &= \Delta\delta\underbrace{(m_1 d_3)}_{D_1} + \Delta\psi_F\underbrace{(m_2 d_3 + D_2)}_{D_2} + \Delta\psi_D\underbrace{(m_3 d_3 + d_1)}_{D_3} + \Delta\psi_G\underbrace{(m_4 d_3)}_{D_4} + \Delta\psi_Q\underbrace{(m_5 d_3)}_{D_5} \\ \Delta I_G &= \Delta\delta\underbrace{(n_1 g_3)}_{G_1} + \Delta\psi_F\underbrace{(n_2 g_3)}_{G_2} + \Delta\psi_D\underbrace{(n_3 g_3)}_{G_3} + \Delta\psi_G\underbrace{(n_4 g_3 + g_2)}_{G_4} + \Delta\psi_Q\underbrace{(n_5 g_3 + g_1)}_{G_5} \\ \Delta I_Q &= \Delta\delta\underbrace{(n_1 q_3)}_{Q_1} + \Delta\psi_F\underbrace{(n_2 q_3)}_{Q_2} + \Delta\psi_D\underbrace{(n_3 q_3)}_{Q_3} + \Delta\psi_G\underbrace{(n_4 q_3 + q_2)}_{Q_4} + \Delta\psi_Q\underbrace{(n_5 q_3 + q_1)}_{Q_5}\end{aligned} \tag{B-12}$$

In order to linearize the torque equation around the operating point, the deviations of stator fluxes as functions of the state variables are needed. These equations are expressed in Equation B13.

$$
\begin{aligned}
\Delta\psi_d^{(1)} &= \Delta\delta\underbrace{\left(m_1\left(\frac{BN}{(P_0)^2+1}-L_d\right)+M_F F_1+M_D D_1+\frac{n_1 NC}{(P_0)^2+1}+\frac{AN}{(P_0)^2+1}\right)}_{s_1}\\
&+\Delta\psi_F\underbrace{\left(m_2\left(\frac{BN}{(P_0)^2+1}-L_d\right)+M_F F_2+M_D D_2+\frac{n_2 NC}{(P_0)^2+1}\right)}_{s_2}\\
&+\Delta\psi_D\underbrace{\left(m_3\left(\frac{BN}{(P_0)^2+1}-L_d\right)+M_F F_3+M_D D_3+\frac{n_3 NC}{(P_0)^2+1}\right)}_{s_3}\\
&+\Delta\psi_G\underbrace{\left(m_4\left(\frac{BN}{(P_0)^2+1}-L_d\right)+M_F F_4+M_D D_4+\frac{n_4 NC}{(P_0)^2+1}\right)}_{s_4}\\
&+\Delta\psi_Q\underbrace{\left(m_5\left(\frac{BN}{(P_0)^2+1}-L_d\right)+M_F F_5+M_D D_5+\frac{n_5 NC}{(P_0)^2+1}\right)}_{s_5}
\end{aligned}
$$

$$
\begin{aligned}
\Delta\psi_q^{(1)} &= \Delta\delta\underbrace{\left(n_1\left(\frac{CM}{(P_0)^2+1}-L_q\right)+M_G G_1+M_Q Q_1+\frac{m_1 MB}{(P_0)^2+1}+\frac{AM}{(P_0)^2+1}\right)}_{t_1}\\
&+\Delta\psi_F\underbrace{\left(n_2\left(\frac{CM}{(P_0)^2+1}-L_q\right)+M_G G_2+M_Q Q_2+\frac{m_2 MB}{(P_0)^2+1}\right)}_{t_2}\\
&+\Delta\psi_D\underbrace{\left(n_3\left(\frac{CM}{(P_0)^2+1}-L_q\right)+M_G G_3+M_Q Q_3+\frac{m_3 MB}{(P_0)^2+1}\right)}_{t_3}\\
&+\Delta\psi_G\underbrace{\left(n_4\left(\frac{CM}{(P_0)^2+1}-L_q\right)+M_G G_4+M_Q Q_4+\frac{m_4 MB}{(P_0)^2+1}\right)}_{t_4}\\
&+\Delta\psi_Q\underbrace{\left(n_5\left(\frac{CM}{(P_0)^2+1}-L_q\right)+M_G G_{51}+M_Q Q_5+\frac{m_5 MB}{(P_0)^2+1}\right)}_{t_5}
\end{aligned}
\qquad \text{(B-13)}
$$

APPENDIX C

LINEARIZING THE SYSTEM PARAMETERS INSTALLED WITH SSSC

To calculate the state matrix components, a similar method to Chapter four is followed.

The deviations of current components are computed as:

$$\begin{cases} \Delta f = a_{1f}\Delta\psi_{Fd} + a_{2f}\Delta\delta + a_{3f}\Delta\psi_d^{due\ to\ harm} + a_{4f}\Delta\psi_q^{due\ to\ harm} + a_{5f}\Delta V_{DC} + a_{6f}\Delta m \\ f = i_d, i_q, \psi_d, \psi_q \end{cases}$$

$$\Delta i_d^{(1)} = a_{1i_d}\Delta\psi_{Fd} + a_{2i_d}\Delta\delta + a_{3i_d}\Delta\psi_d^{due\ to\ harm} + a_{4i_d}\Delta\psi_q^{due\ to\ harm} + a_{5i_d}\Delta V_{DC} + a_{6i_d}\Delta m$$
$$\Delta i_q^{(1)} = a_{1i_q}\Delta\psi_{Fd} + a_{2i_q}\Delta\delta + a_{3i_q}\Delta\psi_d^{due\ to\ harm} + a_{4i_q}\Delta\psi_q^{due\ to\ harm} + a_{5i_q}\Delta V_{DC} + a_{6i_q}\Delta m$$

$$a_{1i_d} = \frac{X_{Tq}M_F^{(1)}}{L_F D},\quad a_{2i_d} = \frac{X_{Tq}E_B^{(1)}\sin(\delta_0) - R_T E_B^{(1)}\cos(\delta_0) - mkV_{DC}\cos(\beta)X_{Tq} + mkV_{DC}\sin(\beta)R_T}{D},$$
$$a_{3i_d} = \frac{X_{Tq}}{D},\quad a_{4i_d} = \frac{-R_T}{D},\quad a_{5i_d} = \frac{-mk\sin(\beta)X_{Tq} - mk\cos(\beta)R_T}{D},$$
$$a_{6i_d} = \frac{-kV_{DC}\sin(\beta)X_{Tq} - kV_{DC}\cos(\beta)R_T}{D}$$

$$a_{1i_q} = \frac{R_T M_F^{(1)}}{L_F D},\quad a_{2i_q} = \frac{R_T E_B^{(1)}\sin(\delta_0) + X_{Td}E_B^{(1)}\cos(\delta_0) - mkV_{DC}\cos(\beta)R_T - mkV_{DC}\sin(\beta)X_{Td}}{D},$$
$$a_{3i_q} = \frac{R_T}{D},\quad a_{4i_q} = \frac{X_{Td}}{D},\quad a_{5i_q} = \frac{-mk\sin(\beta)R_T + mk\cos(\beta)X_{Td}}{D},$$
$$a_{6i_q} = \frac{-kV_{DC}\sin(\beta)R_T + kV_{DC}\cos(\beta)X_{Td}}{D}$$

$$D = X_{Tq}X_{Td} + R_T^2 \tag{C-1}$$

Also having the following equations:

$$\begin{aligned} \Delta\psi_d^{due\ to\ harm} &= \frac{N}{P_0^2 + 1}[A\Delta\delta + B\Delta i_d^{(1)} + C\Delta i_q^{(1)} + D\Delta V_{DC} + E\Delta m] \\ \Delta\psi_q^{due\ to\ harm} &= \frac{M}{P_0^2 + 1}[A\Delta\delta + B\Delta i_d^{(1)} + C\Delta i_q^{(1)} + D\Delta V_{DC} + E\Delta m] \end{aligned} \tag{C-2}$$

The deviations of current and flux component are derived as follows:

$$\Delta i_d^{(1)} = \underbrace{\left(\frac{1}{\left(E_1 - \frac{F_4}{F_1}E_4\right)}\right)\left(E_3 + \frac{E_4F_3}{F_1}\right)}_{m_1}\Delta\delta + \underbrace{\left(\frac{1}{\left(E_1 - \frac{F_4}{F_1}E_4\right)}\right)\left(E_2 + \frac{E_4F_2}{F_1}\right)}_{m_2}\Delta\psi_{Fd}$$
$$+ \underbrace{\left(\frac{1}{\left(E_1 - \frac{F_4}{F_1}E_4\right)}\right)\left(E_5 + \frac{E_4F_5}{F_1}\right)}_{m_3}\Delta V_{DC} + \underbrace{\left(\frac{1}{\left(E_1 - \frac{F_4}{F_1}E_4\right)}\right)\left(E_6 + \frac{E_4F_6}{F_1}\right)}_{m_4}\Delta m$$

$$E_1 = 1 - \frac{BNa_{3i_d} + BMa_{4i_d}}{P_0^2 + 1}, \quad E_2 = a_{1i_d}, \quad E_3 = a_{2i_d} + \frac{ANa_{3i_d} + AMa_{4i_d}}{P_0^2 + 1},$$
$$E_4 = \frac{CNa_{3i_d} + CMa_{4i_d}}{P_0^2 + 1}, \quad E_5 = a_{5i_d} + \frac{DNa_{3i_d} + DMa_{4i_d}}{P_0^2 + 1}, \quad E_6 = a_{6i_d} + \frac{ENa_{3i_d} + EMa_{4i_d}}{P_0^2 + 1}$$

$$F_1 = 1 - \frac{CNa_{3i_q} + CMa_{4i_q}}{P_0^2 + 1}, \quad F_2 = a_{1i_q}, \quad F_3 = a_{2i_q} + \frac{ANa_{3i_q} + AMa_{4i_q}}{P_0^2 + 1},$$
$$F_4 = \frac{BNa_{3i_q} + BMa_{4i_q}}{P_0^2 + 1}, \quad F_5 = a_{5i_d} + \frac{DNa_{3i_q} + DMa_{4i_q}}{P_0^2 + 1}, \quad F_6 = a_{6i_d} + \frac{ENa_{3i_q} + EMa_{4i_q}}{P_0^2 + 1}$$

and:

$$\Delta i_q^{(1)} = \underbrace{\left(\frac{1}{F_1}\right)\left(F_3 + m_1F_4\right)}_{n_1}\Delta\delta + \underbrace{\left(\frac{1}{F_1}\right)\left(F_2 + m_2F_4\right)}_{n_2}\Delta\psi_{Fd}$$
$$+ \underbrace{\left(\frac{1}{F_1}\right)\left(F_5 + m_3F_4\right)}_{n_3}\Delta V_{DC} + \underbrace{\left(\frac{1}{F_1}\right)\left(F_6 + m_4F_4\right)}_{n_4}\Delta m \qquad \text{(C-3)}$$

The following coefficients are defined to simplify the equations:

$$P_1 = \frac{NA + NBm_1 + NCn_1}{P_0^2 + 1}, \quad P_2 = \frac{NBm_2 + NCn_2}{P_0^2 + 1},$$
$$P_3 = \frac{ND + NBm_3 + NCn_3}{P_0^2 + 1}, \quad P_4 = \frac{NE + NBm_4 + NCn_4}{P_0^2 + 1}$$

$$J_1 = \frac{MA + MBm_1 + MCn_1}{P_0^2 + 1}, \quad J_2 = \frac{MBm_2 + MCn_2}{P_0^2 + 1},$$
$$J_3 = \frac{MD + MBm_3 + MCn_3}{P_0^2 + 1}, \quad J_4 = \frac{ME + MBm_4 + MCn_4}{P_0^2 + 1} \qquad \text{(C-4)}$$

Using the above coefficients, the deviations of stator fluxes as calculated as:

$$\Delta\psi_d^{(1)} = \underbrace{(P_1 - L_d m_1 + \frac{(M_F^{(1)})^2 m_1}{L_F})}_{H_1}\Delta\delta + \underbrace{(P_2 - L_d m_2 + \frac{M_F^{(1)}}{L_F} + \frac{(M_F^{(1)})^2 m_2}{L_F})}_{H_2}\Delta\psi_{Fd}$$
$$+ \underbrace{(P_3 - L_d m_3 + \frac{(M_F^{(1)})^2 m_3}{L_F})}_{H_3}\Delta V_{DC} + \underbrace{(P_4 - L_d m_4 + \frac{(M_F^{(1)})^2 m_4}{L_F})}_{H_4}\Delta m$$

$$\Delta\psi_q^{(1)} = \underbrace{(J_1 - L_q n_1)}_{S_1}\Delta\delta + \underbrace{(J_2 - L_q n_2)}_{S_2}\Delta\psi_{Fd}$$
$$+ \underbrace{(J_3 - L_q n_3)}_{S_3}\Delta V_{DC} + \underbrace{(J_4 - L_q n_4)}_{S_4}\Delta m \qquad \text{(C-5)}$$

Using the above formulations, the coefficients of the electromechanical torque deviation are obtained in the following form:

$$\Delta T_e^{(1)} = K_1^{(harm)}\Delta\delta + K_2^{(harm)}\Delta\psi_{Fd} + K_{pDC}^{(harm)}\Delta V_{DC} + K_{pm}^{(harm)}\Delta m$$

$$K_1^{(harm)} = H_1 i_{q0} + n_1\psi_{d0} - S_1 i_{d0}\Delta\delta - m_1\psi_{q0}$$
$$K_2^{(harm)} = H_2 i_{q0} + n_2\psi_{d0} - S_2 i_{d0}\Delta\delta - m_2\psi_{q0}$$

$$K_{pDC}^{(harm)} = H_3 i_{q0} + n_3\psi_{d0} - S_3 i_{d0}\Delta\delta - m_3\psi_{q0}$$
$$K_{pm}^{(harm)} = H_4 i_{q0} + n_4\psi_{d0} - S_4 i_{d0}\Delta\delta - m_4\psi_{q0} \qquad \text{(C-6)}$$

Equation 5-9 shows the derivatives of DC capacitor voltage and field flux are as,

$$\Delta\dot{\psi}_{fd} = K_{f\delta}^{(harm)}\Delta\delta + K_{f\psi}^{(harm)}\Delta\psi_{Fd} + K_{fDC}^{(harm)}\Delta V_{DC} + K_{fE}\Delta E_{fd} + K_{fm}^{(harm)}\Delta m$$
$$\Delta\dot{V}_{DC} = K_{d\delta}^{(harm)}\Delta\delta + K_{d\psi}^{(harm)}\Delta\psi_{Fd} + K_{dDC}^{(harm)}\Delta V_{DC} + K_{dm}^{(harm)}\Delta m \qquad \text{(C-7)}$$

The coefficients in the above equation are defined as follows:

$$K_{f\delta}^{(harm)} = \frac{-\omega_0 R_{Fd} M_F^{(1)} m_1}{L_F},\ K_{f\psi}^{(harm)} = \frac{-\omega_0 R_{Fd}(1 + M_F^{(1)} m_2)}{L_F}$$
$$K_{fDC}^{(harm)} = \frac{-\omega_0 R_{Fd} M_F^{(1)} m_3}{L_F},\ K_{fE} = \frac{\omega_0 R_{Fd}}{M_F^{(1)}},\ K_{fm}^{(harm)} = \frac{-\omega_0 R_{Fd} M_F^{(1)} m_4}{L_F}$$

$$K_{d\delta}^{(harm)} = \frac{km_0}{C_{DC}}(m_1\cos\beta + n_1\sin\beta),\ K_{d\psi}^{(harm)} = \frac{km_0}{C_{DC}}(m_2\cos\beta + n_2\sin\beta)$$
$$K_{dDC}^{(harm)} = \frac{km_0}{C_{DC}}(m_3\cos\beta + n_3\sin\beta), \qquad \text{(C-8)}$$
$$K_{dm}^{(harm)} = \frac{k}{C_{DC}}(i_{d0}\cos\beta + i_{q0}\sin\beta + m_0\cos\beta m_4 + m_0\sin\beta n_4)$$